UNIVERSITY OF CALIFORNIA, SAN DIEGO

Infection strategies of related *Nematocida* microsporidian species in their natural host, *Caenorhabditis elegans*

A dissertation submitted in partial satisfaction

of the requirements for the degree

Doctor of Philosophy

in

Biology

by

Robert James Luallen

Committee in charge:

Professor Emily Troemel, Chair
Professor Sreekanth Chalasani
Professor William McGinnis
Professor Victor Nizet
Professor Steve Wasserman

2016

The Dissertation of Robert James Luallen is approved, and it is acceptable in quality and form for publication on microfilm and electronically:

_____

_____

_____

_____

_____
Chair

University of California, San Diego

2016

Dedication

This dissertation is dedicated to my parents, Robert Lee Luallen and Nam Suk Park, who have always supported me in my academic endeavors.

Table of Contents

Signature Page iii

Dedication iv

Table of Contents v

List of Figures and Tables viii

Acknowledgements xi

Vita xiii

Abstract of the Dissertation xv

1. Introduction: Evolution of natural host/pathogen interaction in *Caenorhabditis elegans* 1

1.1 Summary 2
1.2 Microsporidia in *C. elegans* as a model system 2
1.3 Polar tube length and tissue tropism 4
1.4 Microsporidia spreading within a host 7
1.5 References 10

2. Characterization of microsporidia-induced developmental arrest and a transmembrane leucine-rich repeat protein in *Caenorhabditis elegans* 12

2.1 Supplemental Figures 31
2.2 Additional Acknowledgements 37

3. Discovery of a natural microsporidian pathogen with a broad tissue tropism in *Caenorhabditis elegans* 38

3.1 Taxonomic Summary of *N. displodere* 67
3.2 Supplemental Figures and Tables 69
3.3 Additional Acknowledgements 84

4. Cell-to-cell spread of microsporidia causes *C. elegans* organs to form syncytia 85

4.1 Summary 86
4.2 Introduction 86
4.3 Results 90
4.3.1 Intracellular infection by a single microsporidian cell grows to occupy most of the *C. elegans* intestine 90
4.3.2 *N. parisii* infection spreads across host cell boundaries by fusing neighboring intestinal cells 93

4.3.3 Infection by different *Nematocida* species causes syncytia formation within distinct host tissue 95
4.3.4 Microsporidia species vary in their intestinal growth dynamics and effects on host fitness 97
4.3.5 Host body size and infection density affect the timing of microsporidia sporulation 99
4.4 Discussion 101
4.5 Materials and methods 106
4.5.1 *C. elegans* and *Nematocida* strains 106
4.5.2 Single microsporidia cell infections 107
4.5.3 Measuring microsporidia growth by microscopy 107
4.5.4 Analysis of microsporidia growth across host intestinal cells 108
4.5.5 Comparing *Nematocida* growth across different host tissues 109
4.5.6 Measuring microsporidia growth by qPCR 110
4.5.7 Measuring animal size, egg number, and microsporidia spores 110
4.6 Supplemental Figures and Tables 112
4.7 Acknowledgements 116
4.8 References 117

5. *N. displodere* displays a broad host tropism but limited temperature range compared to other *Nematocida* species 121

5.1 Summary 122
5.2 Introduction 123
5.3 Results 126
5.3.1 *N. displodere* proliferates at 15°C but fails to grow at a higher temperature 126
5.3.2 *N. displodere* meronts are cleared at higher temperatures 128
5.3.3 *N. displodere* displays a broad host range 129
5.3.4 *N. displodere* infected animals show a minor cryophilic behavior phenotype 130
5.4 Discussion 133
5.5 Materials and methods 135
5.5.1 *N. displodere* infection at 15°C and 25°C. 135
5.5.2 *N. displodere* clearance at higher temperatures 135
5.5.3 *N. displodere* infection at higher temperatures 136
5.5.4 Comparison of *N. displodere* infection in several nematode species 136
5.5.5 *Nematocida* host range for spore production 137
5.5.6 Thermotaxis assay 137
5.6 Acknowledgements 139
5.7 References 140

6. Appendix 142

6.1 *C. elegans* growth in axenic media 143
6.2 Making polyclonal antibodies to *N. parisii* spores 144
6.3 Pulldown of RAB-11 associates proteins after *N. parisii* infection 146

6.4 References..152

List of Figures and Tables

Figure 2-1. RNAi screen for host genes that regulate *N. parisii*-induced larval arrest of *C. elegans* 19

Figure 2-2. *F56A8.3* RNAi clone reduces the level of *N. parisii* infection at several stages of infection 20

Figure 2-3. *F56A8.3* RNAi clone acts in the intestine, and the F56A8.3 protein localizes to lysosome-related organelles in the intestine 22

Figure 2-4. Mutation of *F56A8.3a* does not recapitulate the larval arrest phenotype of *F56A8.3* RNAi 23

Figure 2-5. A complete deletion of the *F56A8.3* locus does not recapitulate the larval arrest phenotype of *F56A8.3* RNAi 25

Figure 2-S1. *F56A8.3* RNAi clone reduces the level of *N. parisii* beta-tubulin transcript in animals at the L2/L3 stage 31

Figure 2-S2. *F56A8.3* RNAi reduces the number of *N. parisii* spores produced in *C. elegans* infected as L1s 32

Figure 2-S3. *N. parisii* pathogen load is inversely correlated with *C. elegans* animal size 33

Figure 2-S4. F56A8.3 protein colocalizes with GLO-3::GFP 34

Figure 2-S5. *F56A8.3* RNAi clone reduces the amount of *F56A8.3* transcript 35

Figure 2-S6. DNA sequence for *F56A8.3* RNAi clone 36

Figure 3-1. A new microsporidian species that infects *C. elegans* 42

Figure 3-2. Transmission electron micrographs of *N. displodere*-infected *C. elegans* . 44

Figure 3-3. *N. displodere* infects multiple tissues but shows preferential proliferation in non-intestinal tissues 45

Figure 3-4. *N. displodere* induces an intestinal response, and host feeding is required for infection 47

Figure 3-5. *N. displodere* likely accesses non-intestinal tissues from the intestinal lumen 49

Figure 3-6. *N. displodere* spores exit through a bursting route 51

Figure 3-7. Analysis and comparison of *N. displodere*, *N. parisii*, and *N.* sp. 1 genomes 52

Figure 3-S1. Identification of microsporidia infection in the body wall of a wild *C. elegans* 69

Figure 3-S2. *N. displodere* proliferation in seam cells and coelomocytes 70

Figure 3-S3 *N. displodere* proliferation and differentiation is occasionally observed in the intestine..... 71

Figure 3-S4. *N. displodere* infection of *C. elegans* intestinal and epidermal reporter strains 72

Figure 3-S5. *N. displodere* spores are observed in the intestinal lumen 73

Figure 3-S6. Pharyngeal pumping of *eat-2* mutants 74

Figure 3-S7. Infection comparison between N2 and *dyn-1(ts)* at the permissive temperature..... 75

Figure 3-S8. *N. displodere* invasion events are seen in close proximity to the intestine 76

Figure 3-S9. Measurement *N. displodere* spore size..... 77

Figure 3-S10. *N. displodere* invasion events are seen in non-intestinal tissues as early as 2 minutes post-infection 78

Figure 3-S11. Non-intestinal *N. displodere* infection remains unchanged over time after a pulse infection 79

Figure 3-S12. *N. displodere*-infected *C. elegans* with a burst vulva 80

Figure 3-S13. *N. displodere*-infected animals with a burst vulva can transmit the infection to uninfected animals..... 81

Figure 3-S14. Phylogenetic trees of putative cases of horizontal gene transfer..... 82

Table 3-S1. Summary of genome assembly statistics 83

Figure 4-1 . A single *N. parisii* cell can grow to fill most of the *C. elegans* intestine. 92

Figure 4-2. *N. parisii* can spread across and fuse intestinal cells into a syncytia 94

Figure 4-3. Spreading is a conserved microsporidia growth strategy with distinct host cell fusion patterns caused by different *Nematocida* species 96

Figure 4-4. *Nematocida* sp. 1 completes its lifecycle faster and impairs fitness of *C. elegans* more than *N. parisii* 98

Figure 4-5. *N. parisii* forms spores faster in denser growth environments..... 100

Figure 4-S1. Quantification of *N. parisii* spreading across host intestinal cells over time 112

Figure 4-S2. *N. displodere* causes syncytia formation in the anterior hypodermal cells of *C. elegans*..... 113

Figure 4-S3. Quantification of *N. parisii* growth rate in size mutants and at high multiplicity of infection 114

Table 4-S1. Quantification of infection distributions..... 115

Figure 5-1 *N. displodere* proliferates at 15°C but fails to proliferate at 25°C 127

Figure 5-2 *N. displodere* meronts are cleared at 25°C 128

Figure 5-3 *N. displodere* growth is restricted to lower temperature in every host species tested 130

Figure 5-4 *N. displodere* infection leads to a cryophilic thermotaxis by L1 larvae 132

Figure 6-1. Confocal image of *N. parisii*-infected *C. elegans* intestine stained with anti-*Np* spore antibody..... 145

Figure 6-2. Flag-RAB-11 colocalizes with *N. parisii* spores 147

Figure 6-3. SDS-PAGE of Flag-RAB-11 pulldowns 149

Table 6-1 Mass spectrometry hits of putative RAB-11 interactors in uninfected conditions. 150

Table 6-2 Mass spectrometry hits of putative RAB-11 interactors after infection with *N. parisii*..... 151

Acknowledgements

Thank you to all my friends, family, and lab members for their support throughout my graduate career. Emily has been a very supportive advisor and Marie-Anne has been a very generous collaborator. The Troemel lab during these years has been such a great group of intelligent people, and a large amount of my growth and training has been due to them. So thank you to the peak ping pong member: Keir Balla (my twin), Aaron Reinke, Kirthi Reddy, Malina Bakowski, Lianne Cohen, Michael Botts, Tal Dror, and Suzy Szumowski. And thank you to those who came before or after: Linda Tong, Tiffany Dunbar, Erin Daniels, and Johan Panek. Thanks to my committee members who have been steady supporters throughout: Steve Wasserman, Sreekanth Chalasani, Bill McGinnis, and Victor Nizet.

Chapter 2, in full, is reprinted from Luallen RJ, Bakowski MA, Troemel ER (2015) Characterization of Microsporidia-Induced Developmental Arrest and a Transmembrane Leucine-Rich Repeat Protein in *Caenorhabditis elegans*, PLoS One 10(4): e0124065, doi:10.1371/journal.pone.0124065 with permission from Public Library of Science (PLoS). The dissertation author was the primary investigator and author of this material. Author contributions to manuscript are as follows: Luallen, R contributed all research for Figures 1-5 and all Supplemental Figures; Bakowski, M conducted the initially RNAi screen that originally identified the hits represented in Figure 1A prior to re-testing.

Chapter 3, in full, is reprinted from Luallen RJ, Reinke AW, Tong L, Botts MR, Félix M-A, Troemel ER (2016) Discovery of a Natural Microsporidian Pathogen with a Broad Tissue Tropism in *Caenorhabditis elegans*, PLoS Pathogens 12(6): e1005724, doi:10.1371/journal.ppat.1005724 with permission from Public Library of Science

(PLoS). The dissertation author was the primary investigator and author of this material. Author contributions to manuscript are as follows: Luallen, R contributed the research for Figures 1-6, except Figure 5b, and the supplemental information in S1-S13 Figures; Reinke, A contributed the genome sequencing and analysis of *N. displodere* represented in Figure 7 and supplemental information in S14 Figure and S1-S3 Tables, Tong, L in conjunction with Luallen, R contributed to Figure 1d and S9 Figure; Botts, M contributed Figure 5b. Félix, M-A co-discovered the new species *N. displodere* and initial work with this new species was conducted in her laboratory at École Normale Supérieure, Institut de Biologie de l'ENS (IBENS), Paris, France thanks to NSF Graduate Research Opportunities Worldwide Fellowship to Luallen, R.

Chapter 4, in full, has currently been resubmitted and accepted for publication, Balla KM, Luallen RJ, Bakowski MA, Troemel ER (2016) Cell-to-cell spread of microsporidia causes *C. elegans* organs to form syncytia, Nature Microbiology (*accepted*) with permission from Nature Publishing Group. The dissertation author was the second author of this material. Author contributions to manuscript are as follows: Luallen, R contributed to the data for Figure 4-3c-e and Figure 4-S2, Balla, K contributed to the data for all remaining figures and tables, and Bakowski, M generated the ERT147 transgenic strain.

The dissertation author was the primary investigator and author of the material in Chapter 5. Author contributions to the manuscript are as follows: Luallen, R contributed the research for Figures 5-1, 5-2, 5-3a, and 5-4. Thank you to Aaron Reinke for allowing use of his data in Figure 5-3b.

Vita

2016	Doctor of Philosophy, University of California, San Diego
2010-2016	Graduate Research Assistant, University of California, San Diego
2005-2010	Research Scientist, ProSci Incorporated, Poway, CA
2000-2005	Research Associate, ProSci Incorporated, Poway, CA
1999	Bachelor of Arts, University of California at Berkeley

Publications

Balla KM, **Luallen RJ**, Bakowski MA, and Troemel ER. Cell-to-cell spread of microsporidia causes *C. elegans* organs to form syncytia. Nat. Microbio. (*accepted*).

Luallen RJ, Reinke AW, Tong L, Botts M, Felix M-A, and Troemel ER. Discovery of a natural microsporidian pathogen with broad tissue tropism in *C. elegans.* PLoS Pathogens 2016 **12**: e1005724

Zhang H, Fu H, **Luallen RJ**, Liu B, Lee FH, Doms RW, and Geng Y. Antibodies elicited by yeast glycoproteins recognize HIV-1 virions and potently neutralize virions with high mannose N-glycans. Vaccine. 2015 **33**: 5140-7

Luallen RJ, Bakowski MA, and Troemel ER. Characterization of microsporidia-induced developmental arrest and a transmembrane leucine-rich repeat protein in *Caenorhabditis elegans*. PLoS One 2015 **10**: e0124065

Luallen RJ and Troemel ER. Breaking barriers: a GPCR triggers immunity in nematodes. Nat. Immunol. 2014 **15**: 826-8

Bakowski MA, **Luallen RJ**, Troemel ER. Microsporidia infection in *Caenorhabditis elegans* and other nematodes. In: L. Weiss & J. Becnel (Eds.) *Microsporidia: Pathogens of Opportunity* (Wiley, IA), 2014. p 341-56

Geng, Y. and **Luallen, R.J.** U.S. Patent 8,202,523, issued June 12, 2012; International patent application no. PCT/US2006/037302 (filed on Sep. 22, 2006). "Glycosylated polypeptides produced in yeast mutants and methods of use thereof."

Agrawal-Gamse C, **Luallen RJ**, Liu B, Fu H, Lee FH, Geng Y, and Doms RW. Yeast-elicited cross-reactive antibodies to HIV Env glycans efficiently neutralize

virions expressing exclusively high-mannose N-linked glycans. J. Virol. 2011 **85**: 470-80

Luallen RJ, Agrawal-Gamse C, Fu H, Smith D, Doms RW, and Geng Y. Antibodies against Manα1,2-Manα1,2-Man oligosaccharide structures recognize envelope glycoproteins from HIV-1 and SIV. Glycobiology. 2010 **20**: 280-6

Luallen RJ, Fu H, Agrawal-Gamse C, Mboudjeka I, Huang W, Lee F-H, Wang L-X, Doms RW, and Geng Y. A yeast glycoprotein shows high affinity binding to the broadly neutralizing HIV antibody 2G12 and effectively inhibits gp120 interactions with 2G12 and DC-SIGN. J. Virol. 2009 **83**: 4861-70

Luallen RJ, Lin J, Fu H, Cai KK, Agrawal C, Mboudjeka I, Lee F-H, Montefiori D, Smith DF, Doms RW, and Geng Y. An engineered *Saccharomyces cerevisiae* strain binds the broadly neutralizing HIV-1 antibody 2G12 and elicits mannose-specific, gp120-binding antibodies. J. Virol. 2008 **82**:6447-57

Fellowships and Awards

2015	NSF Graduate Research Opportunities Worldwide Fellowship
2013	Best Graduate Student Poster Award, UCSD Biology Divisional Retreat
2012	Best Talk Award, Southern California Eukaryotic Pathogen Symposium
2012	Excellence in Teaching Award as a Graduate Student TA
2012-2015	NSF Graduate Research Fellowship
2010	BD Biosciences Fellowship in Molecular Biology

ABSTRACT OF THE DISSERTATION

Infection strategies of related *Nematocida* microsporidian species in their natural host, *Caenorhabditis elegans*

by

Robert James Luallen

Doctor of Philosophy in Biology

University of California, San Diego, 2016

Professor Emily Troemel, Chair

Obligate intracellular pathogens evolve under selective pressure from their host organisms to successfully infect and replicate in host cells. Microsporidia are obligate intracellular pathogens that display evidence of this selective pressure, including severely reduced genomes, loss of true mitochondria, and loss of conserved metabolic pathways. Wild isolates of *Caenorhabditis elegans* are regularly found with

microsporidia infection, allowing for the investigation of natural microsporidia infection processes using a genetic model host. Two such microsporidian species *Nematocida parisii* and *N.* sp. 1 exclusively infect and replicate in the intestine of *C. elegans* leading to phenotypic consequences on the host, including developmental arrest and premature death. Through a targeted RNAi screen, we found several host genes that control infection-induced developmental arrest by *N. parisii*. We also discovered a new species of microsporidia inside a wild *C. elegans* isolated near Paris, France with a distinct tissue tropism from *N. parisii* and *N.* sp. 1, despite being in the *Nematocida* genus. This new species infects via host feeding, replicates in multiple tissues, and exits via vulva bursting, leading us to name it *N. displodere*. This new pathogen displays an complementary tissue tropism to other *Nematocida* species, as *N. displodere* is able to infect and proliferate in a broad array of tissues and cells but displays a reduced ability to replicate in the intestine. We found that during infection, *Nematocida* species can spread from a single host cell across numerous neighboring cells in a tissue, with *N. parisii* and *N.* sp. 1 limited to the intestine, and *N. displodere* capable of spreading in the muscle and epidermis, but mostly limited to a single cell in the intestine. Additionally, we found that *N. displodere* displays a broader host range than *N. parisii* but narrower temperature range, with efficient replication for *N. displodere* limited to temperatures lower than 20°C in all tested host species. Altogether, we characterize a new species of microsporidia, *Nematocida displodere*, and compare this pathogen to other *Nematocida* species identified to date, providing a powerful system to study the mechanistic and evolutionary bases of tissue tropism, temperature restriction, and host range of microsporidia.

1. Introduction: Evolution of natural host/pathogen interaction in *Caenorhabditis elegans*.

1.1 Summary

Hosts and pathogens impose strong evolutionary pressure on each other resulting in a rapid and noticeable arms race in molecular evolution. Host/pathogen interactions have also been implicated to play a strong role in the evolution of larger macroscopic mechanisms, like adaptive immunity and sexual reproduction (1-2). Obligate intracellular pathogens require a host cell for all replicative stages of infection, and therefore evolve under minimal environmental pressure and maximal host pressure. Microsporidia represent a large phylum of obligate intracellular pathogens that display hallmarks of host-induced evolutionary pressure, including severely reduced genomes, loss of true mitochondria, and loss of conserved metabolic pathways. The genetic model organism *C. elegans* has recently been discovered to regularly harbor microsporidia infections when isolated from rotting plant substrates in the wild. To date, three published species of microsporidia have been found infecting wild *C. elegans*, *Nematocida parisii* and *N.* sp. 1 which infect the intestine of the animal, and *N. displodere* which displays a broad tissue tropism. The discovery of these related *Nematocida* species infecting the same tractable, simple host *C. elegans* has enabled us to identify complex mechanisms of microsporidia infection, including a role for polar tube length in tissue tropism and a conserved capacity for a single proliferating pathogen to spread within a tissue.

1.2 Microsporidia in *C. elegans* as a model system

Microsporidia represent a large phylum of successful eukaryotic pathogens comprised of over 1400 species that infect a broad array of animal and protist species (3). To date, fourteen species of microsporidia have been discovered to infect humans,

often causing little to no noticeable pathology, as one study found that up to 56% of immunocompetent individual in the population shed microsporidian spores (4). Microsporidia infection can however become invasive, or even lethal, when host immunity has declined, for example in AIDS patients or patients on immunosuppression therapy (5). Despite their ubiquity in the animal kingdom, microsporidia infection is relatively understudied compared to other pathogens. This is especially true for complex mechanisms like tissue tropism and pathogen spreading which are difficult to study in tissue culture models or hosts with complex body plans.

The genetic model organism *C. elegans* has proven to be a convenient and tractable system to study infection in a whole animal. The majority of pathogens studied in *C. elegans* are clinically relevant bacteria and yeast that are artificially exposed to animals in the laboratory. However, recent samplings of wild *Caenorhabditis* nematodes from the environment have revealed that they are regularly infected by and harbor microbes, including microsporidia. In fact, microsporidia infection is very common in wild-isolated *Caenorhabditis* nematodes (6-7, personal observations). To date, three species of microsporidia have been described, and all of them are in the new genus *Nematocida* (or nematode-killer). These are *N. parisii* and *N.* sp. 1 that infect and proliferate in the intestine of *C. elegans*, and *N. displodere* that infects and proliferates in multiple tissues. However, another four new species of microsporidia have recently been discovered in wild nematodes and placed in the *Nematocida* genus, currently named *N. major*, *N. minor*, *N. ciargi*, and *N. homosporus* (8). Interestingly, like *N. parisii* and *N.* sp. 1, all these new species appear to infect and proliferate only in the intestine, making *N. displodere* an unusual species in this genus. These natural microsporidian pathogens that can infect and proliferate in the genetic

model organism *C. elegans* allows for a convenient system to study complex mechanisms for microsporidia infection.

1.3 Polar tube length and tissue tropism

One of the most unique aspects of microsporidia infection is the means through which the pathogen is able to invade a host cell. Microsporidia use an infection apparatus called the polar tube for entry into host cells (9). The polar tube comprises a collection of polar tube proteins that assemble inside spores and form coils that are observable by transmission electron microscopy (TEM) (10). Five known polar tube proteins (PTP1-5) have been identified and biochemically described for several microsporidian species, although genomic analyses have shown that many species lack some of these known PTPs (10). An external stimulus, like pH or solute change, is thought to prime the polar tube for firing by allowing for the uptake of water, which causes the spore to swell. This results in osmotic pressure that is thought to be the driving force for the firing of the polar tube (10). Once fired, the polar tube is thought to penetrate the host cell so that the intracellular contents of the spore (called the sporoplasm) can be extruded through the polar tube and injected into the host cell, although it is equally possible that some microsporidian species rely on host cellular processes (like endocytosis) for the uptake of the polar tube tip, or even the sporoplasm for productive infection (10-11). While the polar tube width shows little variation between species of microsporidia (at 0.1-0.2 μm), polar tube lengths can vary widely, from as short a 4 μm to as long as 50 μm (10, 12). Generally, the evolutionary pressure occurring on the polar tube is unknown, although given that it is used for

invasion a large part of this pressure likely comes from the target for invasion (the host).

Our recent discovery of *N. displodere* in a wild-isolated *C. elegans* nematode provided an opportunity to look into the role that polar tube length might play in microsporidia tissue tropism (12). *N. displodere* was notable for its unique tissue tropism in *C. elegans* compared to all other *Nematocida* species identified to date. It was found to invade multiple tissues in the animal, including the epidermis, muscle, intestine, and neurons, while *N. parisii* and *N.* sp. 1, were only found to infect the intestine of *C. elegans* (6, 13-14). In fact, the capacity for *N. displodere* to invade multiple tissues occurred despite similar means for entry into the host, as all three species enter *C. elegans* through host feeding of spores. Thus, the initial location for host cellular invasion is the lumen of the intestine, with *N. displodere* being the only species with the proven capacity to reach multiple tissues other than intestinal cells. This capacity of *N. displodere* to reach non-intestinal tissues of *C. elegans* was found to be associated with its polar tube length, as *N. displodere* polar tubes were approximately 3-fold longer than similarly sized *N. parisii* spores, at 12 μm and 4 μm (12), respectively, which matched TEM images showing more polar tube coils in *N. displodere* spores compared to *N. parisii* (6). In fact, the capacity for *N. displodere* to reach non-intestinal tissues decreased as the intestinal cell width increased with host growth and maturation, further supporting the idea that the length of the polar tube is the limiting factor for *N. displodere* access to host tissues.

This new data on *N. displodere* raises the question of whether polar tube length is a general feature used by microsporidia to limit or expand access to animal host tissues from the origin of pathogen exposure to the host. Different species of

microsporidia diverge widely in their range of tissue tropism. Some species infect strictly one tissue type like *Nosema apis* in the hindgut of honeybees or *Enterocytozoon bieneusi* in the enterocytes of the small intestine of humans (15-16). While other species lead to more systemic infections in their host, like *Edhazardia aedis* infection of mosquitoes or *Encephalitozoon cuniculi* infection in humans (15-16). However, there has not been any systematic comparison of the polar tube length and distances from spore sites to target tissues/cells. This is likely due to numerous difficulties in studying microsporidia infection in higher animals, including knowing which host cells are initially invaded, knowing the general location from which a spore fires its polar tube, and knowing the distances from the spore to the invaded cells in potentially complex and convoluted tissues. Many of these issues were solved using *Nematocida* infection in its relatively simple host *C. elegans* (12). Now, there are an additional four new *Nematocida* species that appear to only infect the intestine of their hosts (8). It would be interesting to measure the polar tube of these other *Nematocida* species to see if they are limited to 2-5 *μ*m in length like *N. parisii*. In fact, TEM images of *N.* sp. 1 showed that small spores (similar in size to *N. parisii* small spores) had only 1 polar tube coil like *N. parisii* (6, 8), suggesting a short polar tube. Both of these species also form large spores with longer polar tubes (five coils by TEM), but it is unknown if large spores are sufficient for *C. elegans* infection, while small *N. parisii* spores are sufficient (6). The availability of multiple related microsporidian species infecting the same host allows for a more systematic investigation of the evolution of the polar tube. *N. displodere* appears to be the earliest diverging member of the *Nematocida* group, and it is likely that *N. displodere* evolved a longer polar tube and broad tissue tropism after divergence from the last common ancestor for the group.

1.4 Microsporidia spreading within a host

Once a microsporidian spore has successfully invaded a host cell, the pathogen will undergo a series of generalized stages of proliferation and differentiation that are common to multiple species of microsporidia. The invasive sporoplasm will divide into multinucleate meront stage which spreads and divides in the host cell. At some point these meronts will commit to differentiation and cellularize into sporonts, which can potentially undergo further divisions, followed by sporoblasts that cannot divide further and will eventually mature into spores. However, despite these generalized hallmarks of the phenotypic stages of microsporidian growth in hosts there can be a divergence in the timing and location of these events among different species. Most species of microsporidia lead to a slow chronic infection that can spread to multiple cells and tissues of the host, but how this spreading occurs can vary dramatically between species (15).

In many microsporidia species that infect insects, invasion of other tissues requires proliferation and differentiation of the pathogen at the initial tissue of infection to produce a set of internal secondary spores that can infect and invade neighboring tissues (15). For example, many *Nosema* species of microsporidia initially reproduce in gut tissues, where internally produced spores will then invade and replicate in the neighboring alimentary tract, neurons, fat body, muscle, epidermis, and other cells (17-18). However, the use of a full round of the lifecycle to form new spores and infect new tissues does not appear to be a common feature used by microsporidia in order to spread within a tissue or between tissues. The actively proliferating stages of the pathogen (for example the meront stage) appear to have the capacity to spread. Initial observations of microsporidia-infected insects and fish have revealed the presence if

large host xenomas, or hypertrophic host cells with single or multiple host nuclei infected with various microsporidian stages (19). In fact, xenoma formation appears to be a widespread feature used by 9 of the 14 known microsporidia genera that infect fish (20). These large multinucleate host syncitia may have been formed as a result of the proliferative stages of microsporidia spreading into and fusing neighboring cells. However, it is equally possible that microsporidia infection and growth in a single cell can cause the host cell to become hypertrophic with multiple nuclear divisions without cellularization (perhaps by activating the cell cycle to facilitate pathogen growth). The complex tissue organization of many higher animals makes it difficult to parse between these two scenarios. Large formation of syncytial cells were seen in cell culture infection of green monkey kidney (E6) cells by *Vittaforma cornea*. However, even using monolayers of a single cell type in culture the authors were unable to determine if syncytial cells were formed due to nuclear division without cytokinesis or fusion of neighboring cells (21).

The discovery of *Nematocida* microsporidia that infect *C. elegans* has afforded the opportunity to look at pathogen spreading in intact animals with distinct, differentiated tissues in a relatively simple body plan. Single spore dose infection of *N. parisii* and *N.* sp. 1 showed that a single sporoplasm in the *C. elegans* intestine can grow and spread throughout the entire organ of the animal, but without spreading to other tissues (22). This spreading led to shared cytoplasmic material between the host intestinal cells, suggesting the formation of a syncitia. However, this occurred before new spores had differentiated, indicating that the proliferative meront stage was spreading between and fusing host cells. Similar experiments with *N. displodere* showed that this pathogen would also spread from a single sporoplasm across multiple

muscle cells or epidermal cells before differentiation (22). By contrast, however, *N. displodere* infection remained largely restricted to a single intestinal cell and failed to spread the majority of the time. Thus, it appears that at least for *Nematocida* that cell-to-cell spreading by the proliferative forms of the pathogen is a shared phenomenon and suggest that this could be a feature of some species of microsporidia, which otherwise do not have normal organelles associated with movement (like cilia or flagella) (15, 23). However, the capacity for spreading by these *Nematocida* organisms appeared to be restricted to the tissues capable of regularly supporting pathogen growth, as *N. parisii* and *N.* sp. 1 infection is restricted to the intestine and there was no evidence for spreading out of the intestine to other tissues, and *N. displodere* rarely showed spreading in the intestine, a tissue that rarely showed proliferative stages of the pathogen despite its capacity to regularly invade it.

1.5 References

1. Morran LT, Schmidt OG, Gelarden IA, Parrish R, Raymond C, Lively CM (2011) Running with the Red Queen: Host-Parasite Coevolution Selects for Biparental Sex. Science. 333: 216–218.

2. Hedrick SM (2004) The acquired immune system: a vantage from beneath. Immunity 21: 607-15.

3. Keeling PJ, Fast NM (2002) Microsporidia: biology and evolution of highly reduced intracellular parasites. Annual review of microbiology 56: 93-116.

4. Didier ES, Weiss LM (2011) Microsporidiosis: not just in AIDS patients. Curr Opin Infect Dis 24: 490-495.

5. Didier ES, Weiss LM (2006) Microsporidiosis: current status. Curr Opin Infect Dis 19: 485-492.

6. Troemel ER, Felix MA, Whiteman NK, Barriere A, Ausubel FM (2008) Microsporidia are natural intracellular parasites of the nematode *Caenorhabditis elegans*. PLoS Biol 6: 2736-2752.

7. Félix MA, Ashe A, Piffaretti J, Wu G, Nuez I, Belicard T, Jiang Y, Zhao G, Franz CJ, Goldstein LD, Sanroman M, Miska EA, Wang D (2011) Natural and experimental infection of *Caenorhabditis* nematodes by novel viruses related to nodaviruses. PLoS Biology 9: e1000586.

8. Zhang G, Sachse M, Prevost MC, Luallen RJ, Troemel ER, Félix MA, Microsporidian infection diversity and specificity among wild rhabditid nematodes (manuscript in preparation).

9. Xu Y, Weiss LM (2005) The microsporidian polar tube: a highly specialised invasion organelle. Int J Parasitol 35: 941-953.

10. Weiss LM, Delbac F, Hayman JR, Pan G, Xiaoqun D, Zhou Z. The Microsporidian Polar Tube and Spore Wall. In: Weiss LM, Becnel JJ, editors. Microsporidia: Pathogens of Opportunity. Ames, IA: Wiley-Blackwell; 2014. p. 261–306.

11. Foucault C, Drancourt M (2000) Actin mediates *Encephalitozoon intestinalis* entry into the human enterocyte-like cell line, Caco-2. Microb Pathog 28: 51-8.

12. Luallen RJ, Reinke AW, Tong L, Botts MR, Felix M-A, Troemel, ER. (2016) Discovery of a Natural Microsporidian Pathogen with a Broad Tissue Tropism in *Caenorhabditis elegans*. PLoS Pathog 12: e1005724.

13. Bakowski MA, Desjardins CA, Smelkinson MG, Dunbar TL, Lopez-Moyado IF, Rifkin SA, Cuomo CA, Troemel ER. (2014) Ubiquitin-mediated response to microsporidia and virus infection in *C. elegans*. PLoS Pathog 10: e1004200.

14. Szumowski SC, Botts MR, Popovich JJ, Smelkinson MG, Troemel ER (2014) The small GTPase RAB-11 directs polarized exocytosis of the intracellular pathogen *N. parisii* for fecal-oral transmission from *C. elegans*. Proc Natl Acad Sci U S A 10.1073/pnas.1400696111.

15. Solter, L. F. in *Microsporidia: Pathogens of Opportunity* (eds L. M. Weiss & J. J. Becnel) Ch. 4, 165-194 (Wiley-Blackwell, 2014).

16. Didier, E. S. & Khan, I. A. in *Microsporidia: Pathogens of Opportunity* (eds L. M. Weiss & J. J. Becnel) Ch. 11, 307-325 (Wiley-Blackwell, 2014).

17. Iwano H, Ishihara R (1989) Intracellular germination of spores of a *Nosema* sp. immediately after their formation in cultured cell. J Invertr. Pathol 54: 125-7.

18. Fries I, Feng F, DaSilva F, Slemenda SB, Pieniazek NJ (1996) *Nosema ceranae* n. sp. (Microspora, Nosematidae), morphological and molecular characterization of a microsporidian parasite of the Asian honey bee *Apis cerana* (Hymenoptera, Apidae). Eur J Protisol 32: 356-65.

19. Lom, J., and Dykova, I. (2005). Microsporidian xenomas in fish seen in wider perspective. Folia Parasitol (Praha) 52: 69-81.

20. Morsy, K., Bashtar, A.R., Abdel-Ghaffar, F. and Al-Quraishy, S. (2013). Morphological and phylogenetic description of a new xenoma-inducing microsporidian, *Microsporidium aurata* nov. sp., parasite of the gilthead seabream *Sparus aurata* from the Red Sea. Parasitology Research 112: 3905-15.

21. Leitch GJ, Shaw AP, Colden-Stanfield M, Scanlon M, Visvesvara GS (2005) Multinucleate host cells induced by *Vittaforma corneae* (Microsporidia). Folia Parasitol (Praha) 52:103-10.

22. Balla KM, Luallen RJ, Bakowski MA, Troemel ER (2016) Cell-to-cell spread of microsporidia causes *C. elegans* organs to form syncytia, Nature Microbiology (*accepted*).

23. Vavra J, Lukes (2013) Microsporidia and 'the art of living together'. Adv Parasitol 82: 253-319.

2. Characterization of microsporidia-induced developmental arrest and a transmembrane leucine-rich repeat protein in *Caenorhabditis elegans*

PLOS | ONE

RESEARCH ARTICLE

Characterization of Microsporidia-Induced Developmental Arrest and a Transmembrane Leucine-Rich Repeat Protein in *Caenorhabditis elegans*

Robert J. Luallen, Malina A. Bakowski, Emily R. Troemel*

Division of Biological Sciences, Section of Cell and Developmental Biology, University of California San Diego, La Jolla, California, United States of America

* etroemel@ucsd.edu

Abstract

Microsporidia comprise a highly diverged phylum of intracellular, eukaryotic pathogens, with some species able to cause life-threatening illnesses in immunocompromised patients. To better understand microsporidian infection in animals, we study infection of the genetic model organism *Caenorhabditis elegans* and a species of microsporidia, *Nematocida parisii*, which infects *Caenorhabditis* nematodes in the wild. We conducted a targeted RNAi screen for host *C. elegans* genes important for infection and growth of *N. parisii*, using nematode larval arrest as an assay for infection. Here, we present the results of this RNAi screen, and our analyses on one of the RNAi hits from the screen that was ultimately not corroborated by loss of function mutants. This hit was an RNAi clone against *F56A8.3*, a conserved gene that encodes a transmembrane protein containing leucine-rich repeats (LRRs), a domain found in numerous pathogen receptors from other systems. This RNAi clone caused *C. elegans* to be resistant to infection by *N. parisii*, leading to reduced larval arrest and lower pathogen load. Characterization of the endogenous F56A8.3 protein revealed that it is expressed in the intestine, localized to the membrane around lysosome-related organelles (LROs), and exists in two different protein isoforms in *C. elegans*. We used the CRISPR-Cas9 system to edit the *F56A8.3* locus and created both a frameshift mutant resulting in a truncated protein and a complete knockout mutant. Neither of these mutants was able to recapitulate the infection phenotypes of the RNAi clone, indicating that the RNAi-mediated phenotypes are due to an off-target effect of the RNAi clone. Nevertheless, this study describes microsporidia-induced developmental arrest in *C. elegans*, presents results from an RNAi screen for host genes important for microsporidian infection, and characterizes aspects of the conserved *F56A8.3* gene and its protein product.

OPEN ACCESS

Citation: Luallen RJ, Bakowski MA, Troemel ER (2015) Characterization of Microsporidia-Induced Developmental Arrest and a Transmembrane Leucine-Rich Repeat Protein in *Caenorhabditis elegans*. PLoS ONE 10(4): e0124065. doi:10.1371/journal.pone.0124065

Academic Editor: Rui Lu, Louisiana State University, UNITED STATES

Received: January 23, 2015

Accepted: March 10, 2015

Published: April 13, 2015

Data Availability Statement: All relevant data are within the paper and its Supporting Information files.

Funding: This work was supported by the National Science Foundation Graduate Research Fellowship to RJL, (https://www.nsfgrfp.org), the National Institutes of Health Cell and Molecular Genetics Training Grant (T32 GM008666) to RJL, (http://www.nih.gov), by NIAID R01 AI087528 (http://www.niaid.nih.gov/), the Searle Scholars Program (http://www.searlescholars.net/), Packard Foundation (http://www.packard.org/) and Burroughs Wellcome Fund (http://www.bwfund.org/grant-programs/infectious-diseases/

investigators-in-pathogenesis-of-infectious-disease) to ERT. The funders had no role in study design, data collection and analysis, decision to publish, or preparation of the manuscript.

Competing Interests: The authors have declared that no competing interests exist.

Introduction

Microsporidia represent a large phylum of obligate intracellular pathogens that are related to fungi, with significantly reduced genomes compared to true fungi and other eukaryotes [1–4]. There are 14 species of microsporidia that can infect humans, and this can lead to an invasive infection that is sometimes lethal when host immunity has declined, as in patients with AIDS or those on immunosuppressant therapy [5]. Microsporidia can also be isolated from asymptomatic immunocompetent people, with reports finding up to 56% of this population shedding microsporidian spores [6]. Most species found in humans infect the intestine, including *Enterocytozoon bieneusi*, *Encephalitozoon cuniculi*, and *Encephalitozoon intestinalis* [7]. Very little is known about microsporidian mechanisms of pathogenesis due to the difficulties of culturing these microbes.

We use the nematode *Caenorhabditis elegans* as a convenient, whole-animal system to study microsporidian infection. In its natural environment, *Caenorhabditis* nematodes are regularly infected by microsporidia, and we focus on a microsporidian species isolated from wild-caught *C. elegans* found in a compost pit near Paris [8–10]. This organism, named *Nematocida parisii*, infects *C. elegans* intestinal cells where it undergoes extensive replication that eventually leads to death of the host. Due to the many genetic tools available in *C. elegans*, we use *N. parisii* infection of *C. elegans* as a model for discovery-based genetic screens to find host genes important for microsporidian infection and progression.

Here, we present the results of a screen for host genes important for infection. We also present our analysis of the gene corresponding to an RNAi hit from the screen that was ultimately not corroborated by loss of function mutations in that gene. This screen involved searching for *C. elegans* RNAi clones that block infection, measured as a reduction in the severity of *N. parisii*-induced larval arrest. We chose to focus on one RNAi clone discovered in this screen based on its robust and specific inhibition of infection-induced larval arrest, and the identity of its target gene, *F56A8.3*, which encodes a predicted transmembrane domain protein with leucine-rich repeats (LRRs), which are found in many pathogen receptors. We found that feeding *C. elegans* the *F56A8.3* RNAi clone resulted in lower *N. parisii* pathogen load at various stages of infection, and that endogenous F56A8.3 protein localized to the membranes around lysosome-related organelles (LROs). However, after mutating *F56A8.3* using targeted genome editing with the CRISPR-Cas9 system, we found that mutations in *F56A8.3* did not recapitulate the infection phenotypes of the RNAi clone, indicating that these phenotypes are due to an off-target effect of the clone. The results described here provide new information about a microsporidian infection-induced phenotype in *C. elegans*, and the characterization of a LRR protein in *C. elegans* that shows conservation in other animals.

Materials and Methods

C. elegans and *N. parisii* culture conditions

All *C. elegans* strains were maintained on nematode growth media (NGM) and fed with *E. coli* strain OP50-1, as described [11]. *N. parisii* spores were prepared as previously described [12]. Briefly, *N. parisii* isolate ERTm1 was cultured by infecting large-scale cultures of *C. elegans*, followed by mechanical disruption of the nematodes and then filtering to isolate spores away from animal debris. The RNAi-sensitive sterile strain GR1373 *eri-1(mg366)* was used for the larval arrest screen and subsequent RNAi experiments [13]. The tissue-specific RNAi strains MGH167 *sid-1(qt9); alxIs9 [VHA-6p::SID-1::SL2::GFP]* and SPC272 *sid-1(qt9); Is[myo-3::sid-1]* were kind gifts from Drs. Gary Ruvkun, Justine Melo, Sean Curran, Antony Jose, and Alex Soukas [14, 15], WU1236 *cdf-2(tm788); amIs4[cdf-2::GFP::unc-119(+))]* was a kind gift from

Dr. Kerry Kornfeld, and GH351 *glo-3(zu446) X; kxEx41[glo-3p::glo-3::GFP; rol-6]* was a kind gift from Greg Herman [16, 17]. Two *F56A8.3* promoter strains ERT173 *jyEx77[pF56A8.3a::mCherry::unc54 3'UTR]* and ERT174 *jyEx78[pF56A8.3a::mCherry::unc54 3'UTR]* were generated for this study (see cloning details below). *F56A8.3* mutant strains ERT327 *F56A8.3(jy4)* and ERT425 *F56A8.3(jy8[LoxP Prps-0::HygR-CeOpt::gpd-2::GFP::unc-54 3'UTR LoxP)* were generated by CRISPR-Cas9 and backcrossed three times to N2, and these strains were crossed to GR1373 *eri-1(mg366)* to make ERT360 *F56A8.3(jy4); eri-1(mg366)* and ERT430 *F56A8.3(jy8 [LoxP Prps-0::HygR-CeOpt::gpd-2::GFP::unc-54 3'UTR LoxP); eri-1(mg366)*, respectively.

Larval arrest experiments

For the larval arrest screen, cherry-picked RNAi libraries derived from the *C. elegans* Ahringer feeding RNAi library were used, which included approximately 345 RNAi clones for predicted transcription factors and 91 RNAi clones for LRR genes [18]. Conditions for the screen were modified from published procedures [19]. Specifically, RNAi clones were amplified and plated on RNAi plates (6-well format) in duplicate overnight at 25°C. Five synchronized L1 *eri-1* animals were hand-picked onto each RNAi clone and grown for 65–66 hours at 20°C until hundreds of F1 generation L1s and eggs were observed. Wells were infected with *N. parisii* spores at 5.5 x 10^6 spores in 200 μl M9 per well and shifted to 25°C, which causes sterility in *eri-1* mutants and prevents further reproduction. At 2 days post-infection (dpi), the infected F1 generation animals in each well were visually scored together by overall size on a 1–4 scale. Completely unarrested animals that reached the young adult stage were scored as a 4, similar to uninfected *eri-1* grown on L4440 (control RNAi). Wells with partially arrested animals where the majority of animals reached the L4 larval stage were scored as a 3. Wells with more severely arrested animals, with the majority of animals in the L2 or L3 larval stage were scored as a 2. Fully arrested wells where the majority of animals were still at the L1 larval stage were scored as a 1. Because *eri-1* mutants are sterile at 25°C, there were no F2 generation animals to affect the assay. Larval arrest assays performed on hits involved scoring 100 animals per replicate (conducted in triplicate per experiment) that reached the L4 or adult stage at 2 or 3 dpi, respectively, using strains *eri-1*, MGH167, SPC272, ERT360, and ERT430.

For larval arrest experiments on *P. aeruginosa* (PA14), synchronized *eri-1* mutants were grown for one generation on RNAi from L1 to adulthood, and then bleached to obtain F1 eggs. SK plates were seeded with 20 μL of overnight cultures of PA14 and incubated at 37°C for 24 hours, followed by 25°C for 24 hours. A total of 100 RNAi-treated F1 eggs obtained from bleach were plated in duplicate on PA14 plates at 25°C, and the number of hatched animals reaching the L4 stage at 2 dpi was recorded.

Pathogen load measurement

For pathogen load measurements by quantitative RT-PCR (qRT-PCR), *eri-1* mutants were treated with RNAi for two generations. Specifically, gravid *eri-1* adults were bleached to obtain starved L1s. These synchronized P0 L1s were then grown to gravid adults on RNAi bacteria and bleached again to obtain synchronized F1 progeny, which were plated on fresh RNAi bacteria. These F1 L1 progeny were infected with a two-fold serial dilution of *N. parisii* starting at 5.76 x 10^6 spores per 10 cm plate at 25°C. At 30 hours post infection (hpi), animals were harvested and RNA was isolated by extraction with Tri-Reagent and bromochloropropane (BCP) (Molecular Research Center). cDNA was synthesized from 250–500 ng of RNA with the RETROscript kit (Ambion) and quantified with iQ SYBR Green Supermix (Bio-Rad) on a CFX Connect Real-time PCR Detection System (Bio-Rad). Pathogen load was measured as the relative abundance of an *N. parisii* ribosomal DNA (rDNA) transcript normalized to a *C. elegans*

rDNA transcript with the following primer sets: Np_rDNAF1: aaaaggcaccaggttgattc, Np_rDNAR1: agctctctgacgcttccttc, Ce18S_F1: ttgcgtacggctcattagag, Ce18S_R1: agctccagtatttccgcagt. Primer efficiencies were measured, and fold difference was calculated with using the Pfaffl method [20].

For pathogen load measurement by fluorescence in situ hybridization (FISH) experiments were performed essentially as described [21]. Specifically, *eri-1* animals were treated on duplicate plates with RNAi as above, but F1 progeny were grown for 24 hrs at 20°C before infection with 2.9 x 10^6 spores per 10 cm plate for 8 hours at 25°C. Harvested animals were fixed in 1 mL acetone at -20°C overnight (ON), washed with PBS + 0.1% Tween-20 (PBS-T), and stained with MicroB FISH probe against *N. parisii* rRNA as previously described [1, 9]. Stained samples were blinded and mounted on glass slides in Vectashield with DAPI (Vector Laboratories). FISH stained parasite sporoplasms, an early, single nucleated stage of the parasite, were counted in 16–24 animals per sample using a Zeiss AxioImager microscope with a 10X objective.

The spore production assay was performed as described with modifications [22]. Synchronized *eri-1* L1s were plated on 6 cm RNAi plates with RNAi bacteria in triplicate and grown 24 hours at 20°C, then transferred to fresh RNAi culture plates containing 2.0 x 10^6 spores and infected at 25°C for 40 hours, with a transfer to a fresh RNAi plate at 24 hpi to prevent starvation. Animals were fixed in 1 mL acetone at -20°C ON, washed with PBS-T, and loaded onto the COPAS Biosort (Union Biometrica) to dispense 50 animals per well of a 96-well plate. Animals in each well were lysed and stained ON in 100 μL PBS with 1% sodium dodecyl sulfate (SDS), 1% 2-mercaptoethanol (2ME), 1 mg/mL direct yellow 96. The number of spores was counted twice per sample on a hemocytometer with the AxioImager microscope at 10X. After COPAS Biosort dispensing of animals into wells, each well was spot-counted to verify the number of animals per well, and this number was used in the final calculation of spores produced per animal.

Generation of transgenic *C. elegans* strains

The *F56A8.3* promoter-mCherry fusion strains ERT173 and ERT174 were made by Gateway cloning (Life Technologies). Briefly, 1755 nucleotides of genomic DNA upstream of the *F56A8.3* start codon was amplified by PCR and cloned into the pDONR P4-P1r vector. This DNA was then recombined into the destination vector pSS-5 generously provided by Dr. Supriya Srinivasan, containing in frame mCherry with the *unc-54* 3' UTR (plasmid pET336). This promoter-mCherry fusion was co-injected with the dominant marker *rol-6* to allow selection of transgenic animals with a roller (*rol*) phenotype. Three independent lines were verified for similar mCherry expression. Two of these transgenic strains are ERT173 *jyEx77[pF56A8.3a::mCherry::unc54 3'UTR]* and ERT174 *jyEx78[pF56A8.3a::mCherry::unc54 3'UTR]*

Antibody production and immunological techniques

A recombinant F56A8.3 protein consisting of the entire N-terminal domain (F56A8.3-NT) (AA 1–243) was used for antibody production at ProSci, Inc (Poway, CA). Briefly, the 729 bp of DNA downstream of the start codon was cloned from cDNA by Gateway cloning into the pDONR221 vector and recombined into the destination vector pET-DEST42 with a C-terminal V5 and 6xHis tags. F56A8.3 protein was induced and purified from *E. coli* BL21(DE3) pr1952 [23], with Ni-NTA matrix (Qiagen) as described [24]. Two rabbits were immunized with 200 mg of purified F56A8.3-NT in complete Freund's adjuvant (Sigma) at week 0 and boosted with 100 mg of antigen in incomplete Freund's adjuvant (Sigma) at weeks 2 and 4 and thereafter every 4 weeks by ProSci Inc. The resulting sera, collected 1 week after each boost, were pooled, and the IgG was purified with protein A-agarose (Invitrogen).

For immunohistochemistry, N2, WU1236, and GH351 animals were anesthetized with 10 mM levamisole, their intestines dissected out, and fixed for 1 hour in 4% paraformaldehyde (PFA). For N2, dissected intestines were stained with anti-F56A8.3-NT diluted to 10 mg/mL in block buffer (PBS, 0.5% Triton X-100, 1 mM EDTA, 5% BSA, 0.05% NaN_3) for 1 hour, followed by Cy3-conjugated goat anti-rabbit (Jackson Immunoresearch) at 2 mg/mL in block. For WU1236 and GH351, intestines were stained as above with anti-F56A8.3-NT, together with the mouse primary antibody anti-GFP (Roche) at 10 mg/mL and the secondary antibody FITC-conjugated goat anti-mouse (Life Technologies) at 2 mg/mL.

CRISPR-Cas9 Targeted Genome Editing

For CRISPR disruption of *F56A8.3*, we used the technique previously described using the plasmids generously donated by Dr. John Calarco, *Peft-3*::cas9-SV40_NLS::*tbb-2* 3'UTR (Addgene plasmid 46168) and PU6::*klp-12*-sgRNA (Addgene plasmid 46170) [25]. Briefly, an sgRNA targeting the 5' end of *F56A8.3* was created using round-the-horn cloning for site directed mutagenesis of PU6::*klp-12*-sgRNA, replacing the *klp-12* sgRNA sequence with the *F56A8.3* sequence ATCGCATAAATATAGTCTGA [26]. N2 animals were injected with 112.5 ng/μL total DNA, with *Peft-3*::cas9 at 50 ng/μL, *F56A8.3* sgRNA at 45 ng/μL, and the dominant mCherry markers pGH8 at 10 ng/μL, pCFJ104 at 5 ng/μL, and pCFJ90 at 2.5 ng/μL. Transgenic F1 progeny were screened for mCherry expression and plated individually. After F2 progeny production, F1 animals were screened by single animal PCR using primers to amplify an 80 bp product spanning the Cas9 cut site. PCR products were run on 10% TBE gels (BioRad) to identify heterozygote mutants that had a wild-type 80 base pair (bp) PCR product, together with a larger or smaller PCR product, presumably generated by non-homologous repair after Cas9 cleavage. From these experiments we generated strain ERT325 *F56A8.3(jy4)*.

For CRISPR-mediated deletion of the *F56A8.3* region, a homologous recombination (HR) donor template was PCR cloned from genomic DNA to contain the 1796 bp upstream and 1790 bp downstream of the *F56A8.3* start and stop codons, respectively. These recombination arms were cloned into the Gateway donor vectors pDONR P4-P1r and pDONR P2r-P3, respectively, and the gene *Prps-0*::*HygR*::*gpd-2*::*GFP*::*unc-54 3'UTR* was cloned from the IR99 plasmid (generously donated by Dr. Jason Chin) into pDONR221, flanked by LoxP sites [27]. These three vectors were recombined into the destination vector pDEST R4-R3. N2 animals were injected with a 200 ng/μL total DNA mix, with *Peft-3*::cas9 at 50 ng/μL, *F56A8.3* sgRNA at 50 ng/μL, *F56A8.3* HR donor template at 50 ng/μL, and pRF4 (*rol-6)* at 50 ng/μL. Transgenic F1 progeny were screened by GFP and *rol-6* expression and plated individually. After F2 progeny production, plates were screened for 75% segregation of GFP among the F2s to indicate an HR event. A *F56A8.3* knockout was verified by PCR for loss of *F56A8.3* with internal primers, and for gain of the *Prps-0*::*HygR*::*gpd-2*::*GFP*::*unc-54 3'UTR* into the *F56A8.3* locus by junction PCR. From these experiments we generated the strain ERT424 *F56A8.3(jy8)*.

Results

An RNAi screen identifies genes important for *C. elegans* larval arrest induced by *N. parisii* infection

Previously, we described that *N. parisii* is a natural microsporidian pathogen of *C. elegans* that causes a lethal intestinal infection [9]. Here we report the finding that infection of first larval stage (L1) *C. elegans* animals with very high doses of *N. parisii* spores leads to an arrest in larval development (see Fig 1A–1C). By contrast, L1s infected with a high dose of killed, non-infectious spores develop normally, indicating that larval arrest after *N. parisii* exposure is

a host response to an active *N. parisii* infection, and not simply a response to the presence of a high does of *N. parisii* spores (data not shown). We used the easily scored, visual phenotype of larval arrest to conduct an RNAi screen for host genes required for *N. parisii* infection/development, using libraries of predicted transcription factors and LRR proteins. The initial screen included approximately 436 genes, and 12 genes were initially scored as hits. We repeated the larval arrest assay with these twelve hits and found that five of them consistently blocked larval arrest after infection, with a visual score of greater than 2.5 (Fig 1A). An interesting hit from this screen was the RNAi clone against a gene coding for a predicted transmembrane LRR protein *F56A8.3* (Gene ID: 176740). There is conservation of the LRR-containing, N-terminal region of F56A8.3 with a protein found in numerous animal species, including leucine-rich repeat-containing protein 59 (LRRC59) in humans. RNAi against this gene in *C. elegans* caused a significant inhibition of arrest at 2 days post-infection (dpi) when compared to the L4440 RNAi control (Fig 1B). These results were consistent across seven independent experiments with approximately 70% of infected *F56A8.3* RNAi-treated animals reaching the L4 stage at 2 dpi, compared to approximately 13% of infected control RNAi animals (Fig 1C). Under these conditions almost 100% of uninfected wild-type animals reached the L4 stage. The sequence for the *F56A8.3* RNAi clone is provided (S1 Text).

A defect in *C. elegans* larval development occurs after exposure to a number of pathogens, including the Gram-negative bacterial pathogen *Pseudomonas aeruginosa* [28]. In order to test for the specificity of this effect, four of the strongest RNAi hits from the *N. parisii* screen were tested for their effect on larval development after infection with *P. aeruginosa*. We found that RNAi of some genes, like *unc-55* and *fkh-10*, also inhibited arrest on *P. aeruginosa*, suggesting they are important for a general larval arrest response, or slowing of development upon infection (Fig 1D) [29, 30]. However, RNAi of *F56A8.3* failed to prevent larval arrest on *P. aeruginosa*, suggesting specificity of this RNAi clone to *N. parisii* infection (Fig 1D). Therefore, we chose to focus on *F56A8.3* because of this strong, consistent larval arrest inhibition by the *F56A8.3* RNAi clone after *N. parisii* infection but not after *P. aeruginosa* infection.

RNAi against *F56A8.3* results in lower *N. parisii* pathogen load

The lack of larval arrest seen on *F56A8.3* RNAi could be due to lower pathogen load or due to disruption of the pathways that mediate arrest upon *N. parisii* infection. To test if the *F56A8.3* RNAi clone affected pathogen load, we performed a series of experiments to quantify the *N. parisii* parasites at various time points after infection, which represent different stages of the parasite life cycle. *N. parisii* appears to have a life cycle similar to most microsporidia. Briefly, microsporidian spores fire an infection apparatus called a polar tube to inject their contents directly into host cells, where they replicate and ultimately differentiate back into infectious spores that exit hosts to infect other individuals [4, 9]. At 8 hours post infection (hpi) in *C. elegans*, we can use FISH-staining to visualize the early, single nucleated stage of the parasite called a 'sporoplasm' [1]. Here, we found that there were about 40% fewer *N. parisii* sporoplasms after *F56A8.3* RNAi compared to empty RNAi vector controls when measured by FISH against *N. parisii* rRNA (Fig 2A). At 30 hpi, *N. parisii* has replicated as multi-nucleate meronts throughout the intestine, but mature spores are not yet visible [1, 12]. Here, we found an approximately 50% reduction in pathogen load after *F56A8.3* RNAi across five different spore doses as measured by qRT-PCR for *N. parisii* rRNA (Fig 2B). Similar results were seen with qPCR for *N. parisii* β-tubulin transcript at the same doses and time point (S1 Fig). At 40 hpi, when the parasitic meronts have differentiated back into spores, we found that *F56A8.3* RNAi resulted in approximately 40% reduction in the number of spores produced per animal compared to RNAi controls (Fig 2C). The experiments described above were performed with

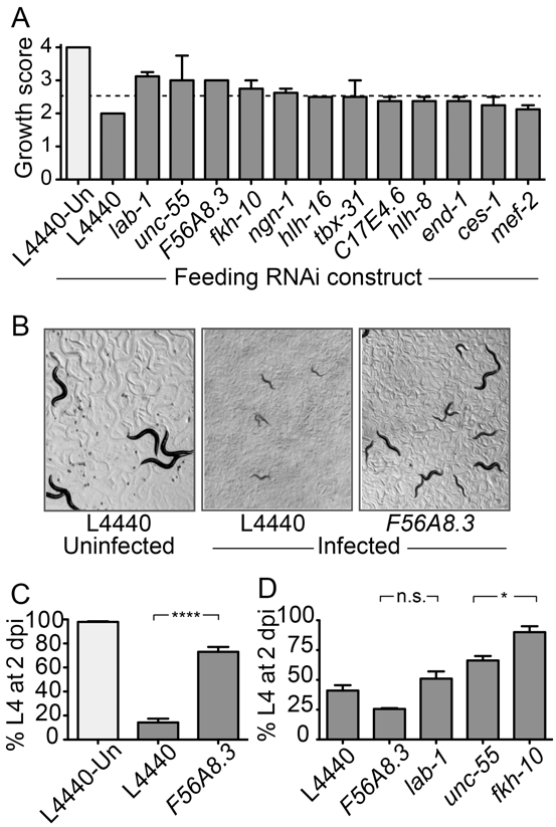

Fig 1. RNAi screen for host genes that regulate *N. parisii*-induced larval arrest of *C. elegans*. (A) Twelve RNAi clones that were originally scored as hits in the screen were retested, using a semi-quantitative visual score of *C. elegans eri-1* strain growth on feeding RNAi at 2 days post-infection (dpi). Uninfected animals grown on L4440 (control RNAi, light gray) provided the baseline for fully developed worms and were scored as a four, while fully arrested worms were scored as a one. Re-tested RNAi clones were scored under infected conditions (dark gray). Twelve hits are shown, consisting of 10 transcription factors, one LRR gene (*F56A8.3*), and one contaminant (gene identity different from what was listed in the library) belonging to neither gene class (*lab-1*). Data are represented as mean values with standard error of the mean (SEM) from biological duplicates in two independent screens. (B) Representative images of larval arrest upon *N. parisii* infection, and inhibition of arrest after *F56A8.3* RNAi. (C) Larval arrest on control or *F56A8.3* RNAi after *N. parisii* infection (dark gray) measured as the percent of animals reaching the L4 larval stage at 2 dpi. Uninfected animals grown on L4440 (control RNAi, light gray) are shown for comparison. Data are represented as mean values with SEM from seven independent experiments (****p<0.0001, unpaired two-tailed t-test). (D) Larval arrest on feeding RNAi after *P. aeruginosa* infection, quantified as the percent of animals reaching the L4 larval stage at 2 dpi. Data are representative of two independent experiments, with the mean and SEM from biological duplicates shown (n.s. is not significant and * is p<0.05 compared to L4440 in one-way analysis of variance with Dunnett's multiple comparison test).

doi:10.1371/journal.pone.0124065.g001

C. elegans infected after the L1 stage (see Materials and Methods), while the larval arrest experiments infected *C. elegans* at the L1 stage. Indeed, similar results were seen when the animals were infected at the L1 stages, with *F56A8.3* RNAi resulting in lower spore load (S2 Fig). Together, these results show that RNAi against *F56A8.3* results in lower *N. parisii* pathogen load

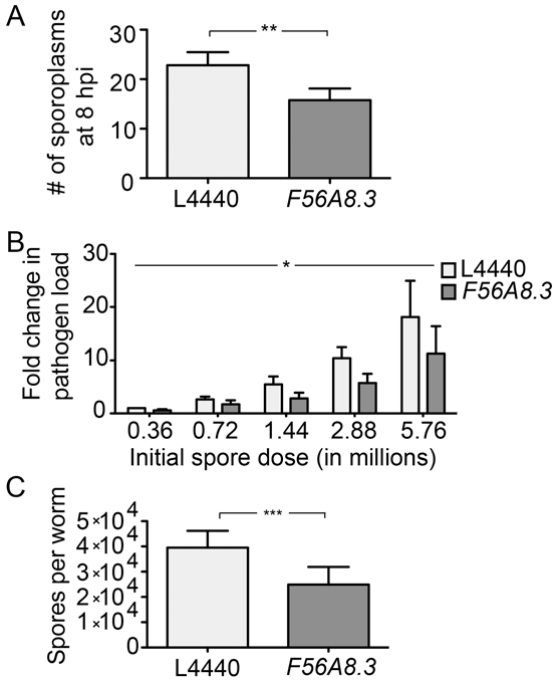

Fig 2. *F56A8.3* RNAi clone reduces the level of *N. parisii* infection at several stages of infection. (A) Pathogen load at 8 hpi on control or *F56A8.3* RNAi measured as the number of FISH-stained sporoplasms seen in intact *C. elegans* intestines. Data are represented as mean values with SEM from three independent, blinded experiments (**p = 0.002, paired two-tailed t-test). (B) Pathogen load at 30 hpi on control or *F56A8.3* RNAi measured as the fold change in *N. parisii* rDNA transcript by qRT-PCR relative to L4440 infected at the lowest dose. Data are represented as mean values with SEM from three independent experiments (*p = 0.033, two-way analysis of variation, testing RNAi treatment effecting pathogen load at all doses). (C) Pathogen load at 40 hpi with *C. elegans* infected at the L2 stage on control or *F56A8.3* RNAi measured as the average number of spores produced per animal. Data are represented as mean values with SEM from three independent experiments (***p = 0.0005, paired two-tailed t-test).

doi:10.1371/journal.pone.0124065.g002

across the majority of stages in the parasite life cycle. This lesser pathogen burden could explain the inhibition of larval arrest caused by this RNAi clone, as we show that increasing *N. parisii* pathogen load results in decreasing worm size (S3 Fig). We concluded from these results that the *F56A8.3* RNAi clone was reducing the expression of a protein required for *N. parisii* infection.

F56A8.3 protein is found on lysosome related organelles (LROs) in the *C. elegans* intestine

Before we learned that the *F56A8.3* RNAi clone was likely acting off-target to affect *N. parisii* infection (see results below), we studied the *F56A8.3* target gene further. *F56A8.3* encodes a single-pass transmembrane protein with five leucine-rich repeats (LRRs). Since LRR domains are found in numerous proteins that play a role in host-pathogen interactions, such as Toll-like and NOD-like receptors (TLRs and NLRs, respectively) [31, 32], we sought to further

characterize the role of *F56A8.3* in *N. parisii* infection. First, we investigated the tissue expression of *F56A8.3* by creating a transgenic strain that expressed mCherry under control of the putative *F56A8.3* promoter. This promoter drove mCherry expression in the intestine, pharynx, and some anterior and posterior neurons (Fig 3A). Given that *N. parisii* infection occurs exclusively in the intestine of *C. elegans*, we conducted tissue-specific RNAi to investigate if *F56A8.3* was acting in the intestine to facilitate infection. Using the intestinal-specific RNAi strain MGH167, we found that *F56A8.3* RNAi resulted in significant inhibition of larval arrest compared to the RNAi control (Fig 3B). By contrast, there was no significant effect of this RNAi clone on larval arrest in the muscle-specific RNAi strain SPC272. These results suggest that the *F56A8.3* RNAi clone acts in the intestine to inhibit *N. parisii* infection.

We next investigated the subcellular localization of the endogenous F56A8.3 protein in *C. elegans* intestinal cells. We generated rabbit anti-F56A8.3 polyclonal antibodies using an N-terminal domain of F56A8.3 (from the initial methionine to the beginning of the transmembrane domain) expressed and purified from *E. coli*. This antibody recognized a protein band of the correct size on Western blots (see below). With immunohistochemistry of dissected *C. elegans* intestines, we found that anti-F56A8.3 localized to the membrane surrounding large circular structures in the intestine generically called "gut granules" (Fig 3C, left) [33]. This antibody signal was noticeably reduced in wild type animals treated with *F56A8.3* RNAi (Fig 3C, right), further confirming the specificity of the antibody and indicating that this RNAi clone does indeed reduce expression of endogenous *F56A8.3* protein. In addition, we found that F56A8.3 colocalized with the zinc transporter CDF-2, which is found on a subset of gut granules called lysosome-related organelles (LROs) (Fig 3D) [17]. Similarly, F56A8.3 colocalized with another LRO membrane marker in the intestine, GLO-3 (S4 Fig) [16].

Mutation of the *F56A8.3* gene does not recapitulate the phenotype of the RNAi clone

The *N. parisii* infection phenotypes we saw with the *F56A8.3* gene were all conducted using RNAi. We confirmed that the *F56A8.3* transcript was knocked down by the RNAi clone (S5 Fig), and that levels of the endogenous protein were reduced (Fig 3C). However, we wanted to confirm that inhibition of larval arrest and reduced pathogen load from the RNAi clone was due to this *F56A8.3* knockdown and not due to an off-target effect. Since there were no existing null mutants for *F56A8.3*, we created a null mutant using the CRISPR-Cas9 system for targeted genome editing. The *F56A8.3* genomic region is predicted to encode two separate proteins, a full length protein called isoform a (F56A8.3a), and a truncated protein called isoform b (F56A8.3b), which lacks approximately 79% of the N-terminal region upstream of the TM domain, including the entire LRR domain (Fig 4A, bottom). The *F56A8.3a* transcripts encompass the entire coding region, while the *F56A8.3b* transcripts vary dramatically in length, with some containing only the downstream coding regions and other covering the entire coding region (Fig 4A, top). The *F56A8.3* RNAi clone targets the 5' coding region of the *F56A8.3* (indicated with a dotted line at the top of Fig 4A), which would be predicted to knockdown all transcript isoforms from the *F56A8.3a* gene. Therefore, we created an *F56A8.3a* mutant by designing a single-guide RNA (sgRNA) targeting the 5' coding region of *F56A8.3a* gene (Fig 4B). Using the protocol developed by Friedland *et al.* [25], we isolated a 5 bp deletion in the early *F56A8.3* coding region, which is predicted to cause a frameshift and early stop codon (Fig 4B). This frameshift mutant *F56A8.3 (jy4)*, showed a complete loss of *F56A8.3a* protein as detected by Western blot (Fig 4D, right). However, when the *F56A8.3(jy4)* mutant was infected with *N. parisii*, we saw no inhibition of larval arrest compared to the control (Fig 4C). Furthermore, *F56A8.3* RNAi treatment of *F56A8.3(jy4)* mutants caused an inhibition of arrest similar to

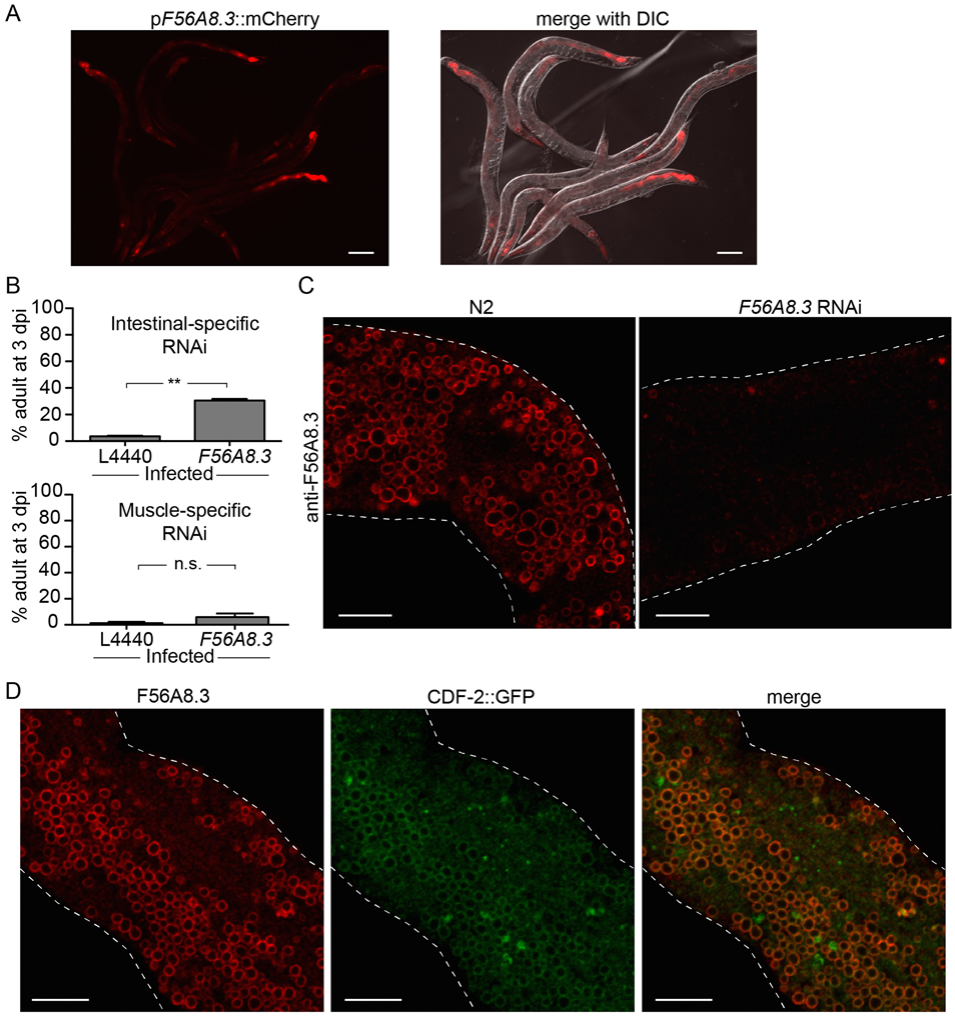

Fig 3. *F56A8.3* RNAi clone acts in the intestine, and the F56A8.3 protein localizes to lysosome-related organelles in the intestine. (A) Representative image of transgenic *C. elegans* expressing intestinal mCherry under control of the putative *F56A8.3* promoter. Scale bar = 100 μm. (B) Larval arrest of tissue-specific RNAi strains MGH167 (left, intestinal-specific) and SPC272 (right, muscle-specific) after *N. parisii* infection, measured as the percent animals reaching the adult stage at 3 dpi. Data are represented as mean values with SEM from two independent experiments (**p = 0.002; n.s. p = 0.26, unpaired two-tailed t-test). (C) Representative image of endogenous F56A8.3 localization in dissected intestines from wild-type N2 *C. elegans* (left) or from N2 treated with *F56A8.3* RNAi (right). F56A8.3 was detected with anti-F56A8.3 followed by goat anti-rabbit IgG conjugated to Cy3. Scale bar = 10 μm. (D) Representative image of endogenous F56A8.3 colocalization relative to CDF-2::GFP in the WU1236 transgenic strain. F56A8.3 was detected as in C; CDF-2 GFP was detected with anti-GFP followed by anti-mouse IgG conjugated to FITC. Scale bar = 10 μm.

doi:10.1371/journal.pone.0124065.g003

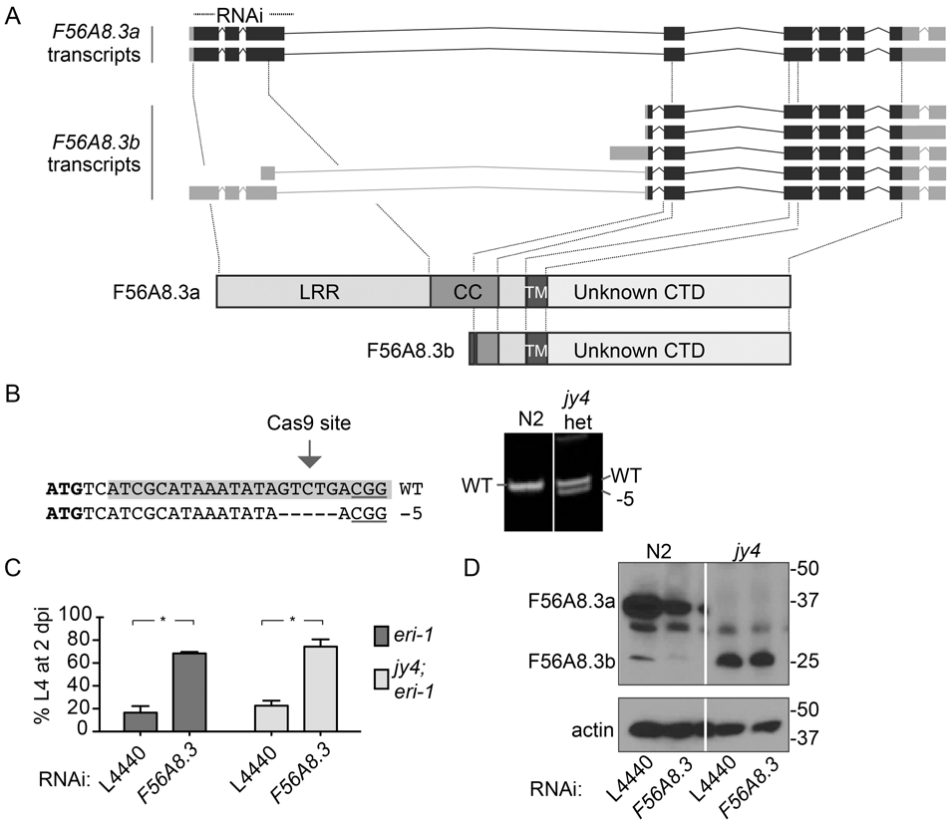

Fig 4. Mutation of *F56A8.3a* does not recapitulate the larval arrest phenotype of *F56A8.3* RNAi. (A) *Top*: Schematic representation of the *F56A8.3a* and *F56A8.3b* pre-mRNA transcripts, with exons represented as black and gray blocks, indicated coding and non-coding sequences, respectively, and solid lines representing introns. The sequence covered by *F56A8.3* RNAi clone is indicated at the top as a dotted line. Image adapted from WormBase and based on EST data (WBGene00010139). *Bottom*: Schematic representation of F56A8.3a and F56A8.3b protein, with dotted lines showing the relative locations on the coding exons from which the main protein domains are derived (LRR is the leucine-rich repeat domain, CC is the coiled coil domain, TM is the transmembrane domain, and CTD is the C-terminal domain). (B) Representation of CRISPR-Cas9 genome editing of the 5'-most exon of the *F56A8.3* gene, with the *F56A8.3* start codon in bold, the sgRNA targeting sequence highlighted, and the protospacer adjacent motif (PAM) underlined (left). WT is the wild-type sequence found in N2, and -5 is a 5 bp deletion found in the mutant ERT327 (*jy4*), with representative 80 bp and 75 bp PCR products from the F1 screen shown (right). (C) Larval arrest of *eri-1* and *F56A8.3* frameshift mutant ERT360 *F56A8.3(jy4)* (in an *eri-1* background) on control or *F56A8.3* RNAi after *N. parisii* infection, measured as the percent animals reaching the L4 at 2 dpi. Data are represented as mean values with SEM from two independent experiments (*p = 0.013 (left), *p = 0.022 (right), unpaired two-tailed t-test). (D) F56A8.3 protein in N2 and *F56A8.3* frameshift mutation ERT327 *F56A8.3(jy4)* on either control (L4440) or *F56A8.3* RNAi. The top picture represents a single blot probed with anti-F56A8.3 antibodies, while the bottom represents a single blot probed with anti-actin. Indicated molecular weight markers are in kilodaltons (kD).

doi:10.1371/journal.pone.0124065.g004

control animals on *F56A8.3* RNAi (Fig 4C). These experiments were performed in an *eri-1* mutant background, because *eri-1* mutants exhibited more robust larval arrest than wild-type N2 animals. Altogether, these data suggest that the larval arrest and pathogen load phenotypes seen on *F56A8.3* RNAi are not due to knockdown of F56A8.3a protein.

A complete deletion of the *F56A8.3* genomic region does not recapitulate the infection phenotypes seen with *F56A8.3* RNAi

We next sought to determine whether the truncated F56A8.3b protein was playing a role in *N. parisii* infection, because there are some *F56A8.3b* transcripts that could be targeted by the *F56A8.3* RNAi clone (Fig 4A). In support of this idea, we found that wild-type animals treated with *F56A8.3* RNAi showed a reduction in F56A8.3b protein, as well as F56A8.3a protein, although the decrease of F56A8.3b protein was not noticeable in *F56A8.3(jy4)* animals (Fig 4D). In fact, the amount of F56A8.3b protein appears to increase in the F56A8.3a null mutant *F56A8.3(jy4)* compared to N2 wild-type animals (Fig 4D, comparing left panel to right panel) which may represent a compensatory mechanism by the mutant. Thus, it was possible that the several-fold increase in F58A8.3b protein seen in *F56A8.3(jy4)* was rescuing these animals to WT infection levels. To determine if *F56A8.3b* plays a role in *N. parisii* infection, we knocked out the entire *F56A8.3* locus and replaced it with a GFP transgene. This editing was done using the same CRISPR-Cas9 technique described earlier, but included a donor vector containing a GFP transgene driven flanked by 1796 bp and 1790 bp upstream and downstream of the *F56A8.3* coding region, respectively (Fig 5A). This donor vector was designed to completely remove the *F56A8.3* gene, which includes the entire sequence homologous to the *F56A8.3* RNAi clone. We screened for successfully engineered genomes via GFP expression in the F1 progeny of the injected animals, and verified with PCR to span the upstream and downstream insertion sites (Fig 5A, *right*). We isolated and homozygosed one knockout *F56A8.3* mutant *F56A8.3 (jy8)*. This mutant completely lacked both F56A8.3a and F56A8.3b protein, as detected by Western blot analysis (Fig 5B). However, the *F56A8.3(jy8)* mutants exhibited no inhibition of larval arrest compared to the control animals after infection with *N. parisii* (Fig 5C), and treatment of *F56A8.3(jy8)* animals with *F56A8.3* RNAi showed an inhibition of arrest similar to control animals on *F56A8.3* RNAi. We also analyzed spore production and found that *F56A8.3 (jy8)* mutants had no difference in spore production at 40 hpi when compared to control animals, yet showed a similar reduction after *F56A8.3* RNAi (Fig 5D). Altogether, these results indicate that the infection phenotypes seen on the *F56A8.3* RNAi clone are likely due to an off-target RNAi effect of the *F56A8.3* RNAi clone.

Discussion

Here, we report *N. parisii*-induced larval arrest in *C. elegans* and the results of an RNAi screen to identify host genes that conferred susceptibility to microsporidian infection. We chose to focus on the *F56A8.3* because its RNAi clone was one of the strongest and most robust hits in this screen, and because this gene encodes a conserved transmembrane protein containing an LRR domain, which we hypothesized was being hijacked by *N. parisii* for infection. While we were able to characterize an effect of *F56A8.3* RNAi on infection and show that the F56A8.3 target is knocked-down by the RNAi clone, we ultimately found that the *F56A8.3* gene is not responsible for the larval arrest phenotype. These findings provide a cautionary tale about relying solely on an RNAi clone to assess the functional relevance of a gene. However, our description of larval arrest upon infection, results from an RNAi screen for host genes important for microsporidian infection, and characterization of the expression and localization of the F56A8.3 protein provide information and tools useful for further study of this phenotype and protein.

Microsporidian infection induces larval arrest in *C. elegans*

Larval arrest is among a range of phenotypes induced by microsporidian infection. These phenotypes can vary from benign to lethal depending on the species of pathogen and host

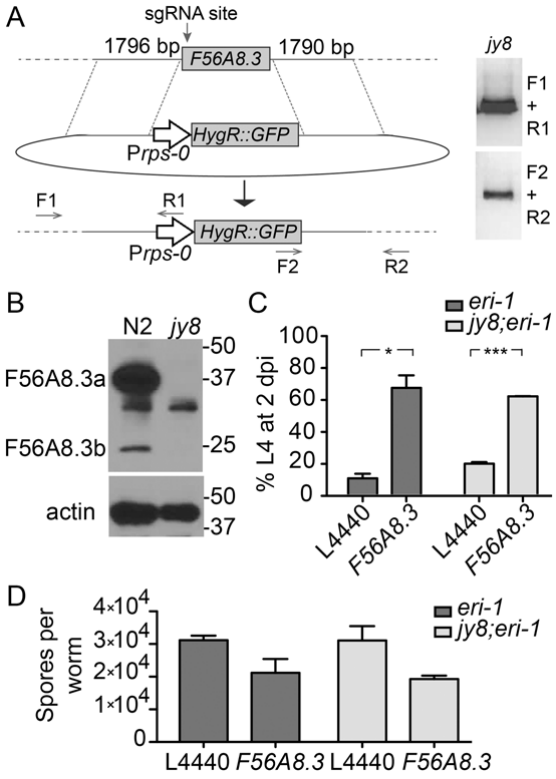

Fig 5. A complete deletion of the *F56A8.3* locus does not recapitulate the larval arrest phenotype of *F56A8.3* RNAi. (A) Schematic representation of donor homologous repair template and predicted recombinant product after CRISPR-Cas9 mediated cutting of *F56A8.3* (at the indicated sgRNA site). The donor template (middle) contains homologous regions of 1796 bp upstream and 1790 bp downstream of the *F56A8.3* start and stop codons, respectively, which flank a P*rps-0*-controlled hygromycin-resistance gene (HygR) with an intergenic GFP expressed as part of an operon. Primer pairs F1+R1 and F2+R2 (bottom) flank the upstream and downstream genomic insertion sites, and their PCR products were detected in knockout mutant ERT425 *F56A8.3(jy8)* (right). (B) F56A8.3 protein in N2 and *F56A8.3* knockout mutation ERT425 *F56A8.3(jy8)* detected with anti-F56A8.3. Indicated molecular weight markers are in kilodaltons (kD), and actin loading controls are shown (bottom). (C) Larval arrest of *eri-1* and ERT430 *F56A8.3(jy8)* knockout (in an *eri* background) on control or *F56A8.3* RNAi after *N. parisii* infection, measured as the percent animals reaching the L4 stage at 2 dpi. Data are represented as mean values with SEM from two independent experiments (*p = 0.021 (left), ***p = 0.0006 (right), unpaired two-tailed t-test). (D) Pathogen load at 40 hpi of *eri-1* and ERT430 *F56A8.3(jy8)* knockout (in an *eri-1* background) on control or *F56A8.3* RNAi measured as the number of spores produced per animal. Data are represented as mean values with SEM from three biological replicates.

doi:10.1371/journal.pone.0124065.g005

involved. Acute microsporidian infection places a substantial burden on the resources of the host, as all of the pathogen replication occurs inside host cells. Thus, it is likely that *C. elegans* larvae can sense (e.g. through a nutritional cue) the extensive *N. parisii* replication occurring in their intestinal cells and then arrest development [1]. Other microsporidian infections have been described to arrest development of their hosts, such as *Nosema whitei* infection of the flour beetle [34, 35], and *Nosema bombycis* infection of the silkworm [36]. We used this

microsporidia-induced larval arrest to conduct an RNAi screen for host genes that mediate susceptibility to *N. parisii* infection. Indeed, one of the strongest hits in this screen (*F56A8.3* RNAi) resulted in lower pathogen load at multiple parasite stages. Thus, if larval arrest is a result of substantial pathogen burden on the host, then inhibition of pathogen growth via this RNAi clone would be expected to relieve some of this burden and allow larval development. However, it is possible that the *F56A8.3* RNAi clone is also able to disrupt the pathways that mediate arrest upon *N. parisii* infection.

C. elegans RNAi screen for host genes important for microsporidian infection identifies the *F56A8.3* RNAi clone

The *F56A8.3* RNAi clone was a hit from our screen and this RNAi clone was capable of knocking down the *F56A8.3* transcript and its protein products. However, the *N. parisii* infection phenotypes were not due to knockdown of this gene, based on our analysis of two *F56A8.3* mutants we made, including a complete deletion mutant. It is likely that the *F56A8.3* RNAi clone is knocking down another *C. elegans* gene, although candidate genes are not obvious based on homology to the *F56A8.3* RNAi clone sequence. In fact, only two other *C. elegans* genes were identified as weak putative targets of the RNAi clone using the program dsCheck, *fcd-2* and *F57E7.1*, and neither of these genes transcripts were reduced on *F56A8.3* RNAi, as measured by qRT-PCR (data not shown) [37]. It is likely that this off-target host gene is acting to facilitate *N. parisii* infection progression in the intestines of *C. elegans*, based on the reduced pathogenic outcome at numerous time points of infection, and the specificity of the larval arrest phenotype when RNAi was restricted to the intestine. It is also a possibility that the *F56A8.3* RNAi clone is knocking down a microsporidian transcript needed for pathogen replication. However, this would require pathogen transcripts to be secreted from an early, intracellular parasitic stage into the intestinal cytoplasm, or require the pathogen to take up small RNAs derived from the *F56A8.3* RNAi clone to have a biological impact in the parasite. Although some microsporidian genomes encode for RNAi machinery, *N. parisii* is not one of those genomes, suggesting it does not undergo RNAi [1]. Furthermore, BLAST analysis of the *N. parisii* ERTm1 genome did not identify any regions of the genome that would be targeted by this RNAi clone (data not shown). Thus, the mechanism by which the *F56A8.3* RNAi clone blocks infection-induced larval arrest remains unresolved.

The *F56A8.3* gene encodes a predicted transmembrane domain protein with LRR repeats that localizes to intestinal lysosome-related organelles

Because the *F56A8.3* gene initially appeared to be responsible for the infection-induced phenotype, we characterized the function and expression of this gene, and developed useful reagents for its future study. *F56A8.3* encodes a predicted single-pass transmembrane protein with an N-terminal LRR and coiled-coil domain, and a large C-terminal domain of unknown function (Fig 4A). The N-terminal domain, which includes the entire region upstream of the transmembrane domain, is conserved across numerous animal species including humans. In *C. elegans*, we found that the 5' region directly upstream of the *F56A8.3* start codon acts to drive transgene expression in the intestine, pharynx, and some neurons. Furthermore, we found that the endogenous F56A8.3 protein localized in the intestine to LROs, acidic organelles containing some lysosomal proteins that are thought to perform cell type-specific storage and secretion functions [38]. Some examples of LROs in other animals are melanosomes, platelet-dense granules, and acrosomes found in melanocytes, platelets, and sperm cells, respectively [39, 40]. Currently, only a handful of proteins have been found to localize to LROs in the *C. elegans* intestine, including CDF-2 and GLO-1. Despite comprising a significant portion of the intestine,

the function of these organelles is still relatively unknown, aside from their role in zinc storage to limit zinc toxicity [17, 41, 42].

In *C. elegans*, the *F56A8.3* gene was predicted to encode for two protein products, the full-length F56A8.3a and a truncated F56A8.3b that lacks approximately 75% of the N-terminal domain, including the entire LRR domain (Fig 4A). We show with Westerns blots that both of these proteins are indeed expressed in *C. elegans*, and that the *F56A8.3* RNAi clone can knockdown both proteins. We generated two mutants in these proteins using the CRISPR-Cas9 system: *F56A8.3a(jy4)* mutants completely lack the *F56A8.3a* isoform and *F56A8.3(jy8)* mutants completely lack both the *F56A8.3a* and *F56A8.3b* isoforms. Our analysis showed that in *F56A8.3a(jy4)* mutants, the amount of F56A8.3b protein is increased dramatically, which likely represents a compensatory mechanism and suggests that F56A8.3b might be involved in similar functions as F56A8.3a. However, both of these mutants appeared phenotypically normal with no obvious defects. In particular, we observed no defect in the number or appearance of LROs in *F56A8.3a(jy4)* mutants compared to wild-type animals (data not shown), so the functions of the F56A8.3 proteins are yet to be determined. The putative human ortholog of *F56A8.3* encodes LRRC59. This protein is localized to the ER membrane, with the N-terminal, LRR-containing domain projecting into the cytoplasm where it acts as a receptor for cytoplasmic fibroblast growth factor 1 (FGF1) [43, 44]. In light of the data here, it would be interesting to determine if the F56A8.3a and/or F56A8.3b proteins are acting to regulate the biogenesis or function of LROs in the *C. elegans* intestine.

Future Directions

The promising infection phenotypes seen using the *F56A8.3* RNAi clone were ultimately not due to knockdown of *F56A8.3*, but likely due to an off-target effect on another *C. elegans* gene. In future directions, this off-target gene could be identified by conducting RNA-seq to identify genes with reduced expression in *F56A8.3(jy8)* mutants treated with *F56A8.3* RNAi, compared to mutants treated with control RNAi. Genes with lowered expression could then be verified for their effects on larval arrest and *N. parisii* pathogen load with RNAi **and** mutant analysis. In addition to *F56A8.3*, there were several other hits from our screen that could be further explored, with the goal of providing more insight into the host/pathogen interactions that underlie infections by microsporidia.

Supporting Information

S1 Text. DNA sequence for *F56A8.3* RNAi clone.
(DOCX)

S1 Fig. *F56A8.3* RNAi clone reduces the level of *N. parisii* β-tubulin transcript in animals infected at L2/L3 stage. Pathogen load at 30 hpi on control or *F56A8.3* RNAi measured as the fold change in *N. parisii* β-tubulin transcript by qRT-PCR relative to L4440 infected at the lowest dose. Animals were infected at L2/L3 stage. Data are represented as mean values with SEM from three independent experiments ($^{**}p = 0.0022$, two-way analysis of variation, testing RNAi treatment effecting pathogen load at all doses).
(TIF)

S2 Fig. *F56A8.3* RNAi clone reduces the number of *N. parisii* spores produced in *C. elegans* infected as L1s. Pathogen load at 40 hpi with *C. elegans* infected at the L1 stage on control or *F56A8.3* RNAi measured as the average number of spores produced per animal. Data are represented as mean values with SEM from two independent experiments.
(TIF)

S3 Fig. *N. parisii* pathogen load is inversely correlated with *C. elegans* animal size. Animals were plated on L4440 bacteria for 18 hours and then infected for 24 hours using a low (3.63 x 10^5 spores), medium (1.45 x 10^6 spores), or high dose (5.80 x 10^6 spores) of *N. parisii* spores on a 10 cm RNAi plate. Pathogen load was measured by FISH to *N. parisii* 18s rRNA and the percent area of the animal infected was calculated using ImageJ. Animal size was calculated by ImageJ and presented as the percent of the mean size of uninfected animals conducted in parallel. Data are represented as mean values with SEM of 20 individual animals in a single experiment.
(TIF)

S4 Fig. F56A8.3 protein colocalizes with GLO-3::GFP. Representative image of endogenous F56A8.3 colocalization relative to GLO-3::GFP in the GH351 transgenic strain Scale bar = 10 μm.
(TIF)

S5 Fig. *F56A8.3* RNAi clone reduces the amount of *F56A8.3* transcript. qRT-PCR analysis of the amount of *F56A8.3* transcript in *C. elegans* grown on control or *F56A8.3* RNAi measured as the fold change relative to L4440. Transcript levels were normalized to *snb-1*. Data are represented as mean values with SEM from two independent experiments.
(TIF)

Acknowledgments

We thank Linda Tong and Tal Dror for their lab assistance and technical support. We thank the *Caenorhabditis* Genetics Center (CGC), Kerry Kornfeld, Greg Herman, Gary Ruvkun, Justine Melo, Sean Curran, Antony Jose, and Alex Soukas for *C. elegans* strains. We also thank John Calarco, Supriya Srinivasan, and Jason Chin for plasmids, and Jens Lykke-Andersen for the *E. coli* strain. We thank Rebecca Laplante, Kirthi Reddy, Suzy Szumowski, Michael Botts, and Aaron Reinke for their helpful comments on the manuscript.

Author Contributions

Conceived and designed the experiments: RJL MAB ERT. Performed the experiments: RJL MAB. Analyzed the data: RJL MAB ERT. Contributed reagents/materials/analysis tools: RJL MAB ERT. Wrote the paper: RJL ERT.

References

1. Cuomo CA, Desjardins CA, Bakowski MA, Goldberg J, Ma AT, Becnel JJ, et al. Microsporidian genome analysis reveals evolutionary strategies for obligate intracellular growth. Genome Res. 2012; 22(12):2478–88. doi: 10.1101/gr.142802.112 PMID: 22813931; PubMed Central PMCID: PMC3514677.
2. Keeling PJ, Fast NM. Microsporidia: biology and evolution of highly reduced intracellular parasites. Annu Rev Microbiol. 2002; 56:93–116. doi: 10.1146/annurev.micro.56.012302.160854 PMID: 12142484.
3. Texier C, Vidau C, Vigues B, El Alaoui H, Delbac F. Microsporidia: a model for minimal parasite-host interactions. Curr Opin Microbiol. 2010; 13(4):443–9. doi: 10.1016/j.mib.2010.05.005 PMID: 20542726.
4. Williams BA. Unique physiology of host-parasite interactions in microsporidia infections. Cell Microbiol. 2009; 11(11):1551–60. doi: 10.1111/j.1462-5822.2009.01362.x PMID: 19673893.
5. Didier ES, Weiss LM. Microsporidiosis: current status. Current opinion in infectious diseases. 2006; 19(5):485–92. doi: 10.1097/01.qco.0000244055.46382.23 PMID: 16940873; PubMed Central PMCID: PMC3109650.
6. Didier ES, Weiss LM. Microsporidiosis: not just in AIDS patients. Current opinion in infectious diseases. 2011; 24(5):490–5. doi: 10.1097/QCO.0b013e32834aa152 PMID: 21844802; PubMed Central PMCID: PMC3416021.

7. Didier ES, Maddry JA, Brindley PJ, Stovall ME, Didier PJ. Therapeutic strategies for human microsporidia infections. Expert review of anti-infective therapy. 2005; 3(3):419–34. doi: 10.1586/14787210.3.3.419 PMID: 15954858.
8. Félix M- A, Duveau F. Population dynamics and habitat sharing of natural populations of *Caenorhabditis elegans* and *C. briggsae*. BMC Biology. 2012; 10(1):59. doi: 10.1186/1741-7007-10-59
9. Troemel ER, Félix M- A, Whiteman NK, Barrière A, Ausubel FM. Microsporidia are natural intracellular parasites of the nematode *Caenorhabditis elegans*. PLoS biology. 2008; 6(12):2736–52. doi: 10.1371/journal.pbio.0060309 PMID: 19071962.
10. Bakowski MA, Luallen RL, Troemel ER. Microsporidia Infections in *Caenorhabditis elegans* and Other Nematodes. In: Weiss LM, Becnel JJ, editors. Microsporidia: Pathogens of Opportunity. Ames, IA: Wiley-Blackwell; 2014. p. 341–56.
11. Brenner S. The genetics of *Caenorhabditis elegans*. Genetics. 1974; 77(1):71–94. PMID: 4366476; PubMed Central PMCID: PMC1213120.
12. Estes KA, Szumowski SC, Troemel ER. Non-lytic, actin-based exit of intracellular parasites from *C. elegans* intestinal cells. PLoS Pathogens. 2011; 7(9):e1002227. doi: 10.1371/journal.ppat.1002227 PMID: 21949650.
13. Kennedy S, Wang D, Ruvkun G. A conserved siRNA-degrading RNase negatively regulates RNA interference in *C. elegans*. Nature. 2004; 427(6975):645–9. doi: 10.1038/nature02302 PMID: 14961122.
14. Jose AM, Smith JJ, Hunter CP. Export of RNA silencing from *C. elegans* tissues does not require the RNA channel SID-1. Proc Natl Acad Sci U S A. 2009; 106(7):2283–8. doi: 10.1073/pnas.0809760106 PMID: 19168628; PubMed Central PMCID: PMC2650148.
15. Melo JA, Ruvkun G. Inactivation of conserved *C. elegans* genes engages pathogen- and xenobiotic-associated defenses. Cell. 2012; 149(2):452–66. doi: 10.1016/j.cell.2012.02.050 PMID: 22500807.
16. Rabbitts BM, Ciotti MK, Miller NE, Kramer M, Lawrenson AL, Levitte S, et al. glo-3, a novel *Caenorhabditis elegans* gene, is required for lysosome-related organelle biogenesis. Genetics. 2008; 180(2):857–71. doi: 10.1534/genetics.108.093534 PMID: 18780725.
17. Roh HC, Collier S, Guthrie J, Robertson JD, Kornfeld K. Lysosome-related organelles in intestinal cells are a zinc storage site in *C. elegans*. Cell Metabolism. 2012; 15(1):88–99. doi: 10.1016/j.cmet.2011.12.003 PMID: 22225878.
18. Estes KA, Dunbar TL, Powell JR, Ausubel FM, Troemel ER. bZIP transcription factor zip-2 mediates an early response to Pseudomonas aeruginosa infection in Caenorhabditis elegans. Proceedings of the National Academy of Sciences. 2010; 107(5):2153–8. doi: 10.1073/pnas.0914643107 PMID: 20133860.
19. Parry DH, Xu J, Ruvkun G. A whole-genome RNAi Screen for *C. elegans* miRNA pathway genes. Curr Biol. 2007; 17(23):2013–22. doi: 10.1016/j.cub.2007.10.058 PMID: 18023351; PubMed Central PMCID: PMC2211719.
20. Pfaffl MW. A new mathematical model for relative quantification in real-time RT-PCR. Nucleic acids research. 2001; 29(9):e45. PMID: 11328886; PubMed Central PMCID: PMC55695.
21. Bakowski MA, Desjardins CA, Smelkinson MG, Dunbar TA, Lopez-Moyado IF, Rifkin SA, et al. Ubiquitin-mediated response to microsporidia and virus infection in *C. elegans*. PLoS Pathog. 2014; 10(6):e1004200. doi: 10.1371/journal.ppat.1004200 PMID: 24945527; PubMed Central PMCID: PMC4063957.
22. Szumowski SC, Botts MR, Popovich JJ, Smelkinson MG, Troemel ER. The small GTPase RAB-11 directs polarized exocytosis of the intracellular pathogen *N. parisii* for fecal-oral transmission from *C. elegans*. Proceedings of the National Academy of Sciences. 2014; 111(22):8215–20. doi: 10.1073/pnas.1400696111 PMID: 24843160; PubMed Central PMCID: PMC4050618.
23. Nielsen J, Christiansen J, Lykke-Andersen J, Johnsen AH, Wewer UM, Nielsen FC. A family of insulin-like growth factor II mRNA-binding proteins represses translation in late development. Mol Cell Biol. 1999; 19(2):1262–70. PMID: 9891060; PubMed Central PMCID: PMC116055.
24. Luallen RJ, Fu H, Agrawal-Gamse C, Mboudjeka I, Huang W, Lee FH, et al. A yeast glycoprotein shows high-affinity binding to the broadly neutralizing human immunodeficiency virus antibody 2G12 and inhibits gp120 interactions with 2G12 and DC-SIGN. Journal of virology. 2009; 83(10):4861–70. doi: 10.1128/JVI.02537-08 PMID: 19264785; PubMed Central PMCID: PMC2682088.
25. Friedland AE, Tzur YB, Esvelt KM, Colaiácovo MP, Church GM, Calarco JA. Heritable genome editing in *C. elegans* via a CRISPR-Cas9 system. Nature Methods. 2013. doi: 10.1038/nmeth.2532 PMID: 23817069.
26. OpenWetWare [Internet]. Round-the-horn site-directed mutagenesis. Accessed 15 September 2014. 2013. Available from: http://www.openwetware.org/index.php?title=%27Round-the-horn_site-directed_mutagenesis&oldid=686665.

27. Radman I, Greiss S, Chin JW. Efficient and rapid *C. elegans* transgenesis by bombardment and hygromycin B selection. PLoS One. 2013; 8(10):e76019. doi: 10.1371/journal.pone.0076019 PMID: 24130756; PubMed Central PMCID: PMC3794024.

28. Richardson CE, Kooistra T, Kim DH. An essential role for XBP-1 in host protection against immune activation in *C. elegans*. Nature. 2010; 463(7284):1092–5. doi: 10.1038/nature08762 PMID: 20182512.

29. Hope IA, Mounsey A, Bauer P, Aslam S. The forkhead gene family of *Caenorhabditis elegans*. Gene. 2003; 304:43–55. PMID: 12568714.

30. Zhou HM, Walthall WW. UNC-55, an orphan nuclear hormone receptor, orchestrates synaptic specificity among two classes of motor neurons in *Caenorhabditis elegans*. The Journal of Neuroscience. 1998; 18(24):10438–44. PMID: 9852581.

31. Chamaillard M, Girardin SE, Viala J, Philpott DJ. Nods, Nalps and Naip: intracellular regulators of bacterial-induced inflammation. Cellular Microbiology. 2003; 5(9):581–92. PMID: 12925128.

32. Takeda K, Kaisho T, Akira S. Toll-like receptors. Annual review of immunology. 2003; 21:335–76. doi: 10.1146/annurev.immunol.21.120601.141126 PMID: 12524386.

33. McGhee JD. The *C. elegans* intestine. WormBook: the online review of C elegans biology. 2007:1–36. doi: 10.1895/wormbook.1.133.1 PMID: 18050495.

34. Blaser M, Schmid-Hempel P. Determinants of virulence for the parasite *Nosema whitei* in its host *Tribolium castaneum*. Journal of invertebrate pathology. 2005; 89(3):251–7. doi: 10.1016/j.jip.2005.04.004 PMID: 15963529.

35. Becnel JJ, Andreadis TG. Microsporidia in Insects. In: Wittner M, Weiss LM, editors. The Microsporidia and Microsporidiosis. Washington DC: American Society for Microbiology; 1999. p. 447–501.

36. Ma Z, Li C, Pan G, Li Z, Han B, Xu J, et al. Genome-wide transcriptional response of silkworm (*Bombyx mori*) to infection by the microsporidian *Nosema bombycis*. PLoS One. 2013; 8(12):e84137. doi: 10.1371/journal.pone.0084137 PMID: 24386341; PubMed Central PMCID: PMC3875524.

37. Naito Y, Yamada T, Matsumiya T, Ui-Tei K, Saigo K, Morishita S. dsCheck: highly sensitive off-target search software for double-stranded RNA-mediated RNA interference. Nucleic acids research. 2005; 33:(Web Server issue)W589–91. doi: 10.1093/nar/gki419 PMID: 15980542; PubMed Central PMCID: PMC1160180.

38. Dell'Angelica EC, Mullins C, Caplan S, Bonifacino JS. Lysosome-related organelles. FASEB journal. 2000; 14(10):1265–78. PMID: 10877819.

39. King SM, Reed GL. Development of platelet secretory granules. Seminars in cell & developmental biology. 2002; 13(4):293–302. PMID: 12243729.

40. Raposo G, Marks MS. The dark side of lysosome-related organelles: specialization of the endocytic pathway for melanosome biogenesis. Traffic. 2002; 3(4):237–48. PMID: 11929605.

41. Delahaye JL, Foster OK, Vine A, Saxton DS, Curtin TP, Somhegyi H, et al. *Caenorhabditis elegans* HOPS and CCZ-1 mediate trafficking to lysosome-related organelles independently of RAB-7 and SAND-1. Mol Biol Cell. 2014; 25(7):1073–96. doi: 10.1091/mbc.E13-09-0521 PMID: 24501423; PubMed Central PMCID: PMC3967972.

42. Hermann GJ, Scavarda E, Weis AM, Saxton DS, Thomas LL, Salesky R, et al. *C. elegans* BLOC-1 functions in trafficking to lysosome-related gut granules. PLoS One. 2012; 7(8):e43043. doi: 10.1371/journal.pone.0043043 PMID: 22916203; PubMed Central PMCID: PMC3419718.

43. Skjerpen CS, Wesche J, Olsnes S. Identification of ribosome-binding protein p34 as an intracellular protein that binds acidic fibroblast growth factor. The Journal of Biological Chemistry. 2002; 277(26):23864–71. doi: 10.1074/jbc.M112193200 PMID: 11964394.

44. Zhen Y, Sørensen V, Skjerpen CS, Haugsten EM, Jin Y, Wälchli S, et al. Nuclear import of exogenous FGF1 requires the ER-protein LRRC59 and the importins Kpnα1 and Kpnβ1. Traffic. 2012; 13(5):650–64. doi: 10.1111/j.1600-0854.2012.01341.x PMID: 22321063.

2.1 Supplemental Figures

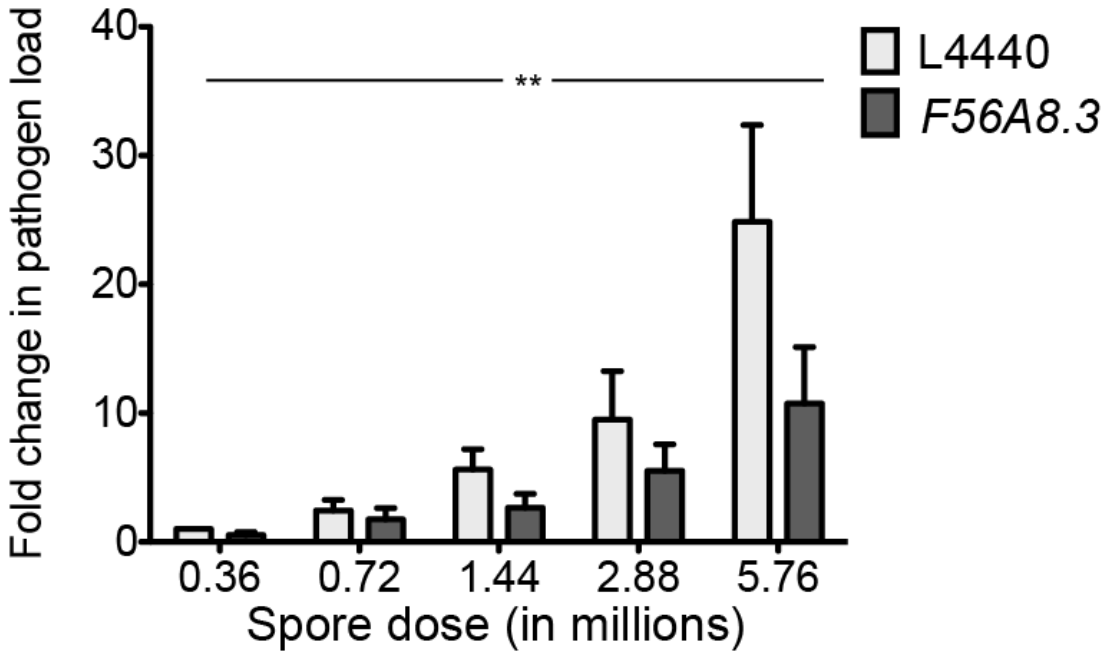

Figure 2-S1. *F56A8.3* RNAi clone reduces the level of *N. parisii* beta-tubulin transcript in animals at the L2/L3 stage

Pathogen load at 30 hpi on control or F56A8.3 RNAi measured as the fold change in *N. parisii* beta-tubulin transcript by qRT-PCR relative to L4440 infected at the lowest dose. Animals were infected at L2/L3 stage. Data are represented as mean values with SEM from three independent experiments (**p = 0.0022, two-way analysis of variation, testing RNAi treatment effecting pathogen load at all doses).

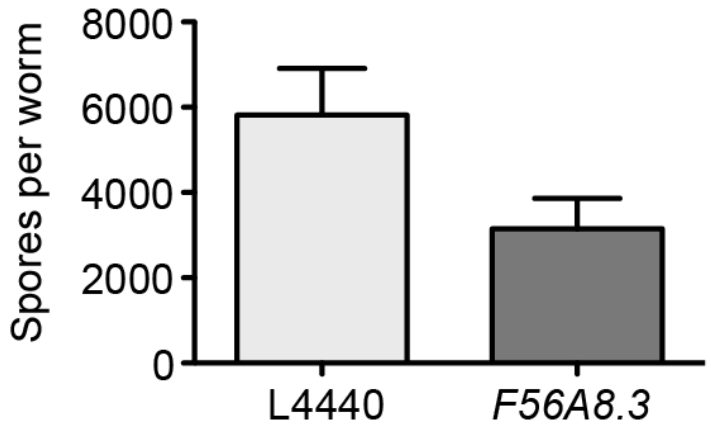

Figure 2-S2. *F56A8.3* RNAi reduces the number of *N. parisii* spores produced in *C. elegans* infected as L1s

Pathogen load at 40 hpi with *C. elegans* infected at the L1 stage on control or *F56A8.3* RNAi measured as the average number of spores produced per animal. Data are represented as mean values with SEM from two independent experiments.

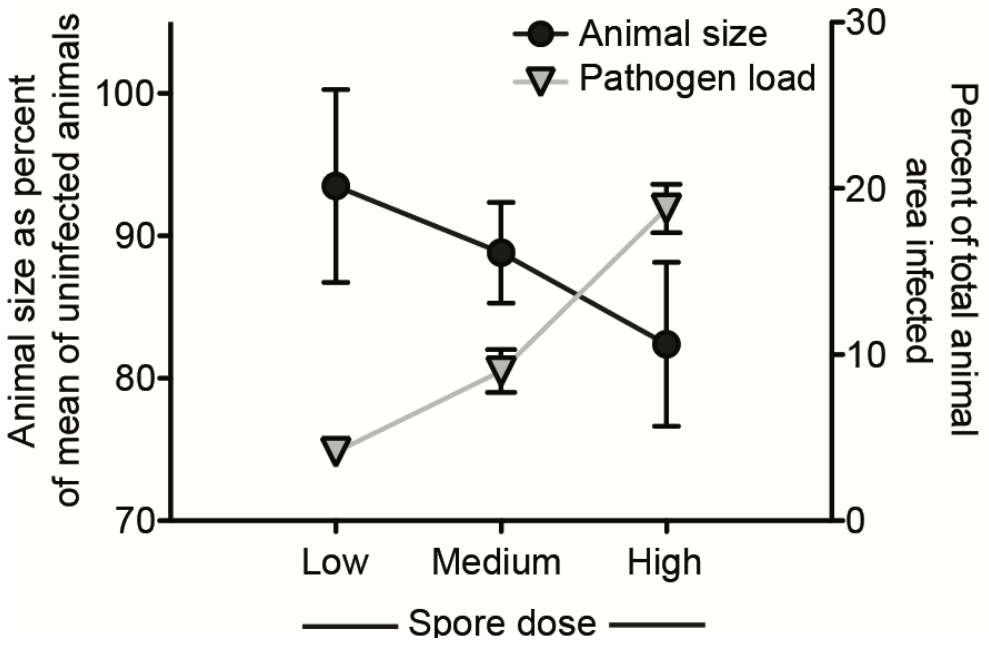

Figure 2-S3. *N. parisii* pathogen load is inversely correlated with *C. elegans* animal size

Animals were plated on L4440 bacteria for 18 hours and then infected for 24 hours using a low (3.63×10^5 spores), medium (1.45×10^6 spores), or high dose (5.80×10^6 spores) of *N. parisii* spores on a 10 cm RNAi plate. Pathogen load was measured by FISH to *N. parisii* 18s rRNA and the percent area of the animal infected was calculated using ImageJ. Animal size was calculated by ImageJ and presented as the percent of the mean size of uninfected animals conducted in parallel. Data are represented as mean values with SEM of 20 individual animals in a single experiment.

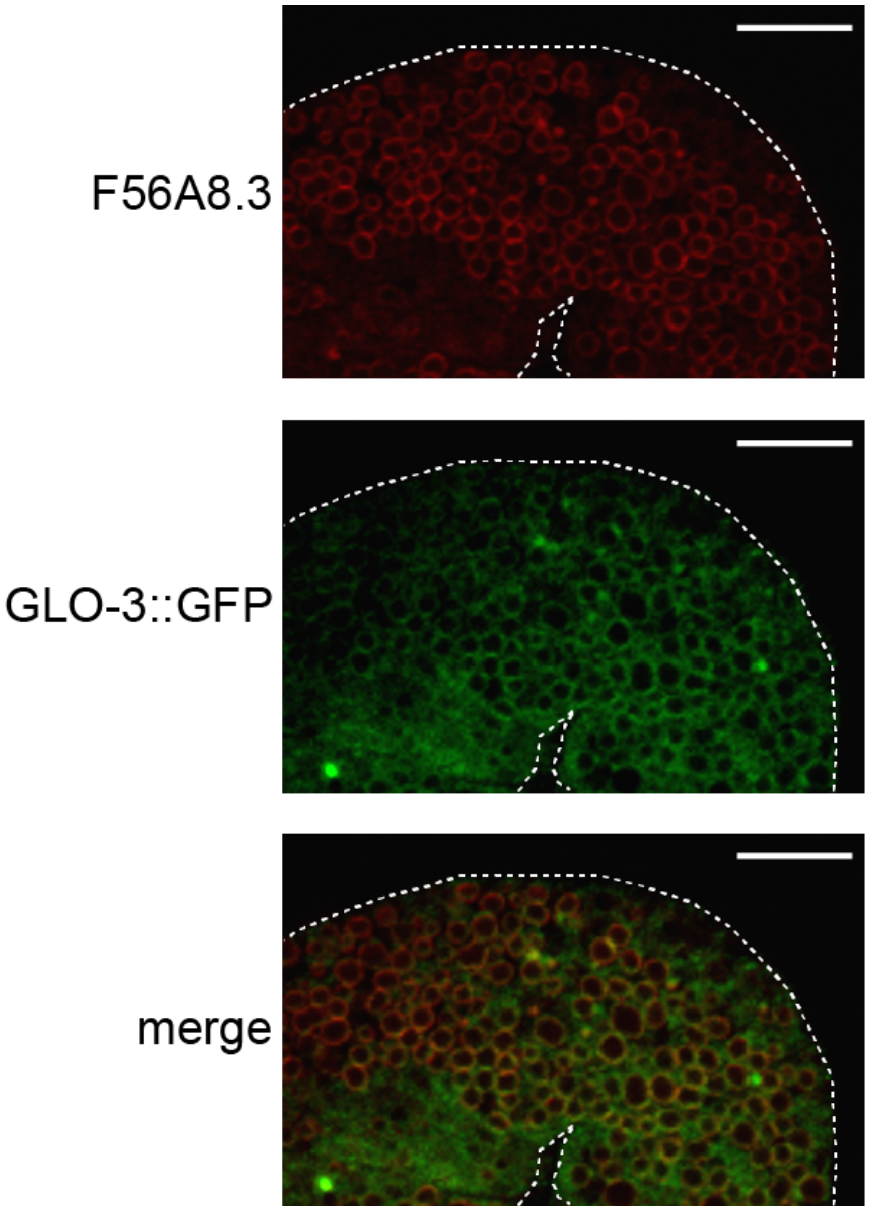

Figure 2-S4. F56A8.3 protein colocalizes with GLO-3::GFP
Representative image of endogenous F56A8.3 colocalization relative to GLO-3::GFP in the GH351 transgenic strain. Scale bar = 10 μm.

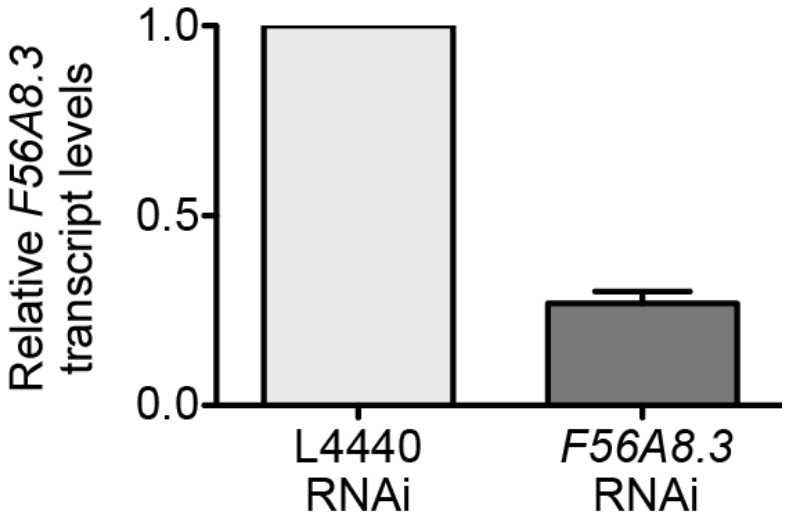

Figure 2-S5. *F56A8.3* RNAi clone reduces the amount of *F56A8.3* transcript
qRT-PCR analysis of the amount of *F56A8.3* transcript in *C. elegans* grown on control or *F56A8.3* RNAi measured as the fold change relative to L4440. Transcript levels were normalized to *snb-1.* Data are represented as mean values with SEM from two independent experiments.

GAGCTCAAAAACTTGCAAGAAGATGATGAGTTGGATTTATCGGCAAGCGGAA
TTCAAGAATTCCCCAATGCAATCGTCCAACTGCCACGGTTGACGAAATTGGA
TCTGAGCTCAAATGCAATCACTTTCTTGCCGGAATCTTTCTGCAAGATGACTA
AGCTTATTCGGTAAGAGTTTTAAGCTGAAAATTTTTGTATATTTTAATTTAATT
TTTCCCTTTTAAGGTTAGACTTCGGAAGTTGCCAGCTTCATCATCTCCCTGATG
GAATCGGGCTCTTGACAAGCTTGCAGCACTTGAACCTTTATAACAATCAAAT
AGAGGTATTTAAAAAATCGGCTAAGGCATGTAGAAATCAATCAATATTTTCC
AGGACTTGCCGCTCTCGTTCGCCAACTTAAAATCCTTGAAGTGGCTGGATTTG
AAGAAAAATCCGCTCAACTCGAAGCTCGCCGCCATCGCAGGAAACTGTGGGA
CTGATGCCGAGTGTAAGCAGGCTGCCAAGCAAGTCGTCGACGTTTATATGGG
CGAGCAGAAGAAGGCCATCGATAGCCTGAAAGCCCAGGAAGCTAAGCATAA
GGCCAAGGTGCAGAAGGCCCAGGAAGAGGAGAGAATGAAGAAGAATCAGG
AGAAAAAGGAGAAGGCGGCGGCTAAAAAGGGTACATTTGCAGGAAAAAAAA
CTATAGAAATATTCTGGAATTTGAGATATCAGAGCCCGTTTTCCATTAATAAC
GCATTTTCAGAATTTCCGGAAATTCTGCAGTTTCCTGGATGATTTTCTCAATTT
TACAGGAAAAAATGATCAAATTTTGACATTTTCTTTAAATATGGCGAGATAA
CTAGCCATAATATAATTGTTAAAAAATTAGTTAAATTTTGCAAAAATTACATA
ATCATCCGTTTTTTCTTTAACATGGTAAGAAATCTGGCTATTCTGGGAGAAAT
TCACTTTAAAAATACCAAAATTGGCTTAAAAATCGATAGTTCAACCGAAAAC
TGTCAGAAAAGTACTTTTAAAAGTGACACAAAAACTGAGAATTTTCAATTAA
TATATGTATTTGTATATTAATTGAAATTTCTCAGCTTTTGTGTCATTTTTCTGG
CAGTTTTCGGTGGAATTATCGATTTTTAAGCCAATTTTGATTTTTTTAAAGGCA
AATTTCCTCCAGACTGGCTAGTTT

Figure 2-S6. DNA sequence for *F56A8.3* RNAi clone

2.2 Additional Acknowledgements

Chapter 2, in full, is reprinted from Luallen RJ, Bakowski MA, Troemel ER (2015) Characterization of Microsporidia-Induced Developmental Arrest and a Transmembrane Leucine-Rich Repeat Protein in *Caenorhabditis elegans*, PLoS One 10(4): e0124065, doi:10.1371/journal.pone.0124065 with permission from Public Library of Science (PLoS). The dissertation author was the primary investigator and author of this material. Author contributions to manuscript are as follows: Luallen, R contributed all research for Figures 1-5 and all Supplemental Figures; Bakowski, M conducted the initially RNAi screen that originally identified the hits represented in Figure 1A prior to re-testing.

3. Discovery of a natural microsporidian pathogen with a broad tissue tropism in *Caenorhabditis elegans.*

PLOS | PATHOGENS

RESEARCH ARTICLE

Discovery of a Natural Microsporidian Pathogen with a Broad Tissue Tropism in *Caenorhabditis elegans*

Robert J. Luallen[1], Aaron W. Reinke[1], Linda Tong[1], Michael R. Botts[1], Marie-Anne Félix[2], Emily R. Troemel[1]*

1 Division of Biological Sciences, Section of Cell and Developmental Biology, University of California San Diego (UCSD), La Jolla, California, United States of America, **2** École Normale Supérieure, Institut de Biologie de l'ENS (IBENS), CNRS-INSERM, Paris, France

* etroemel@ucsd.edu

OPEN ACCESS

Citation: Luallen RJ, Reinke AW, Tong L, Botts MR, Félix M-A, Troemel ER (2016) Discovery of a Natural Microsporidian Pathogen with a Broad Tissue Tropism in *Caenorhabditis elegans*. PLoS Pathog 12 (6): e1005724. doi:10.1371/journal.ppat.1005724

Editor: James B. Lok, University of Pennsylvania, UNITED STATES

Received: April 7, 2016

Accepted: June 3, 2016

Published: June 30, 2016

Data Availability Statement: All relevant data are within the paper and its Supporting Information files, aside from the raw data for N. displodere genome sequencing. All data associated with the Whole Genome Shotgun project for N. displodere are currently available at DDBJ/ENA/GenBank under accession LTDL00000000 for N. displodere type strain JUm2807, and the version described in this paper is version LTDL01000000.

Funding: This work was supported by National Science Foundation Graduate Research (DGE-1144086) and Graduate Research Opportunities Worldwide fellowships to RJL, a Life Sciences

Abstract

Microbial pathogens often establish infection within particular niches of their host for replication. Determining how infection occurs preferentially in specific host tissues is a key aspect of understanding host-microbe interactions. Here, we describe the discovery of a natural microsporidian parasite of the nematode *Caenorhabditis elegans* that displays a unique tissue tropism compared to previously described parasites of this host. We characterize the life cycle of this new species, *Nematocida displodere*, including pathogen entry, intracellular replication, and exit. *N. displodere* can invade multiple host tissues, including the epidermis, muscle, neurons, and intestine of *C. elegans*. Despite robust invasion of the intestine very little replication occurs there, with the majority of replication occurring in the muscle and epidermis. This feature distinguishes *N. displodere* from two closely related microsporidian pathogens, *N. parisii* and *N.* sp. 1, which exclusively invade and replicate in the intestine. Comparison of the *N. displodere* genome with *N. parisii* and *N.* sp. 1 reveals that *N. displodere* is the earliest diverging species of the *Nematocida* genus. Over 10% of the proteins encoded by the *N. displodere* genome belong to a single species-specific family of RING-domain containing proteins of unknown function that may be mediating interactions with the host. Altogether, this system provides a powerful whole-animal model to investigate factors responsible for pathogen growth in different tissue niches.

Author Summary

Pathogens evolve under selective pressure from host organisms to successfully invade and proliferate in different cells and tissues of the host for their own benefit. Microsporidia represent one of the most successful phyla of pathogens, with severely reduced genomes and loss of core cellular and metabolic pathways making them dependent on host cells for their own proliferation. We sampled around Paris, France, for wild nematodes infected with natural pathogens, and discovered a wild *Caenorhabditis elegans* that was infected

Research Foundation Fellowship, Monsanto Fellow to AWR, and National Institute of Health grant R01GM114139, The Dave and Lucile Packard Foundation, and Burroughs Wellcome Fund fellowship to ERT. The funders had no role in study design, data collection and analysis, decision to publish, or preparation of the manuscript.

Competing Interests: I have read the journal's policy and the authors of this manuscript have the following competing interests: AWR was funded by a Life Sciences Research Foundation fellowship sponsored by Monsanto Company. Monsanto Company played no role in this study, including experimental design and data analysis. The other authors declare no competing interests.

with a new species of microsporidia. We characterize the life cycle of this new species, showing the pathogen enters via host feeding, replicates in multiple host tissues, and exits as new spores via a novel vulva bursting mechanism, leading us to name this species *Nematocida displodere*. Despite the capacity of *N. displodere* to invade multiple host tissues during infection, we found that the parasite showed very little replication in the intestine. This unique tissue specificity of *N. displodere* stands in stark contrast to its two closest-related species, *Nematocida parisii* and *Nematocida* sp. 1, which exclusively infect and proliferate in the intestine of *C. elegans*. We compared the genomes of these related species and found that *N. displodere* devotes over 10% of its genome to a single large gene family not found in any other species, and propose that their encoded proteins may be interacting with host factors during infection.

Introduction

Pathogens infect host organisms and then often establish themselves within a particular niche of the host environment in order to replicate [1–3]. This niche usually resides within a particular cell type or tissue, and is commonly referred to as cellular or tissue tropism. The mechanisms responsible for tissue tropism are broad and potentially multifactorial, and can involve features such as access, specific receptor/ligand interactions, pathogen competence for growth in particular tissue niches, and/or host defense [4–8]. Understanding the mechanistic and evolutionary bases for tissue tropism is key to understanding host/pathogen interactions and discovering therapeutics to prevent pathogens from causing disease.

Microsporidia represent a large phylum of obligate intracellular pathogens related to fungi, which can infect a diverse array of hosts from protists to humans [9–12]. They have features consistent with having adapted to proliferate exclusively within the host cellular environment, including greatly reduced genome sizes and the loss of true mitochondria [13]. Different species of microsporidia display a range of different tissue tropisms. For example, the microsporidian species *Encephalitozoon cuniculi* shows a broad tissue tropism in humans and is able to infect the liver, brain, kidneys, skin, and gastrointestinal tract, while *Enterocytozoon bieneusi* mainly infects the enterocytes of the small intestine [14]. Studying tissue tropism in higher animals can be confounded by the complexity of the host body plan, making it difficult to comprehensively describe the tissues that are subject to infection in vivo. In some cases, tropism is implied from in vitro studies based on cell types that are infected but may not reflect the true tropism within the live animal [15, 16].

The nematode *Caenorhabditis elegans* is a tractable, whole-animal system to study host/pathogen interactions because of its simple body plan and transparency, which facilitates assessment of tissue tropism in vivo. Sampling of proliferating populations of *Caenorhabditis* nematodes from rotting plant substrates in wild habitats has demonstrated that they are regularly infected by microsporidia [17–19]. Isolates of two closely related species, *Nematocida parisii* and *Nematocida* sp. 1, are thus far the only described microsporidian species found in wild *Caenorhabditis* nematodes, and both of these species are fecal/oral pathogens that infect and replicate exclusively in *C. elegans* intestinal cells [9, 18]. The intestinal-trophic nature of *N. parisii* has been well-studied, with all stages of the pathogen being solely observed in the intestine by light, fluorescence, and transmission electron microscopy (TEM) [18]. Additionally, multiple infection-induced changes have been observed in the intestine, including restructuring of the apical cytoskeleton [20] and hijacking of the intestinal recycling endosome pathway for the exit of newly made spores [21].

Here, we report the discovery of a new species of microsporidia found infecting non-intestinal tissues of a wild-caught *C. elegans* animal. Whole genome sequencing and phylogenomic analysis places this new species in the *Nematocida* genus, and we have named it *Nematocida displodere*, based on a vulva bursting mechanism for spore exit. *N. displodere* displays a distinct tropism from the other described *Nematocida* species and has the capacity to initially invade a wide array of tissues and cell types, including the intestine, epidermis, muscle, neurons, and specialized phagocytic cells called coelomocytes, with feeding being required for infection. Strikingly, the majority of intestinal infection fails to replicate. Comparison of the *N. displodere* genome with the other *Nematocida* species shows that despite *N. displodere* having a smaller genome, it contains an enormously expanded species-specific gene family encoding for RING-domain containing proteins of unknown function, which may explain its distinct infection life cycle. Altogether, we characterize a new species of microsporidia, *Nematocida displodere*, with a broader tissue tropism compared to other *Nematocida* species identified to date, and this system provides a convenient model to study the mechanistic and evolutionary bases of tissue tropism using closely related but distinct pathogens infecting a single tractable host.

Results

Discovery of a new species of microsporidia that infects a broad range of tissues in *C. elegans*

While sampling for nematodes near the Viosne stream in Santeuil, France, we isolated a wild-caught *C. elegans* infected by a microbe displaying microsporidian-like features in the head of the animal (S1A Fig). For reference, microsporidian species display certain stereotypical hallmarks in their life cycle [22]. Specifically, infection begins when an extracellular, transmissible spore fires an infection apparatus called a polar tube to deliver a single mononucleated parasite cell called a sporoplasm into the host cell. The sporoplasm then develops into a multinucleate, proliferative stage called a meront, and eventually differentiates into new spores that exit the host cell. The wild-caught *C. elegans* we found had structures that appeared like meronts and spores in an area that is likely the epidermis (S1A Fig). In the lab, we found that this P_0 adult was able to transmit infection to its progeny, as observed by the appearance of large, meront-like structures and spores in recipient animals (Fig 1A and 1B). These later stages of infection were seen along the anterior/posterior axis of the animal, including the head (Fig 1A and 1B), the mid-body (S1C Fig, Fig 1C), and the tail (Fig 1C). The majority of animals showed these later stages of infection in the body wall of *C. elegans*, which is the outer tube of the animal distal to the pseudocoelomic space that includes the epidermis, muscle, and neurons [23]. By contrast, tissues in the intestine (Fig 1A) and gonad remained for the most part symptom-free as observed by light microscopy. Consistent with a lack of infection in the gonad, we did not find that infection was vertically transmitted because the eggs from a bleached population of heavily infected animals developed into a population that remained uninfected for multiple generations (n = 100 animals analyzed by Nomarski and n = 100 animals analyzed by fluorescent in situ hybridization, FISH, over 4 months at 15°C).

We confirmed this pathogen as a new species of microsporidia in the *Nematocida* genus based on whole genome sequencing and phylogenomic comparison (see below), and we named this new species *Nematocida displodere*. To characterize the infection life cycle of *N. displodere* we labeled the pathogen with a FISH probe to label the small ribosomal subunit RNA (rRNA) or with a chitin binding dye, Direct Yellow 96 (DY96), to label spore walls. We synchronized wild-type N2 *C. elegans* animals, infected them with *N. displodere* spores and then observed them for the main hallmarks of microsporidia infection. These hallmarks include mononucleated sporoplasms observed at 1 day post-infection (dpi), multinucleate meronts from 2–4 dpi,

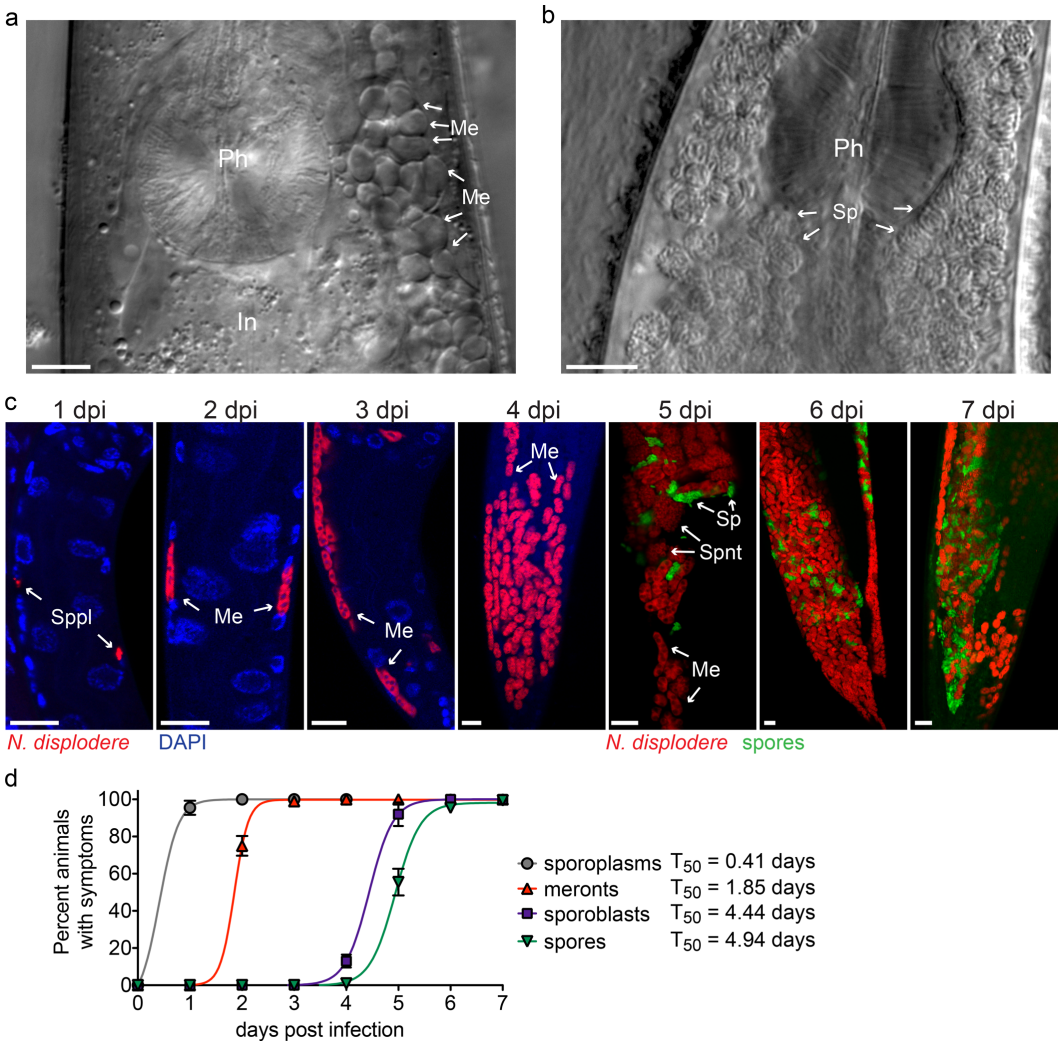

Fig 1. A new microsporidian species that infects *C. elegans*. (a) Infected head region of a live *C. elegans* animal from strain JU2807 (derived from the wild-isolated P_0 animal, see S1 Fig) showing a large group of structures that appear to be meronts (*Me*) adjacent to the pharynx (*Ph*) and intestine (*In*). (b) Infected head region with the area adjacent to the pharynx filled with spores (*Sp*). (c) The mid-posterior to tail region of N2 *C. elegans* infected with *N. displodere* from 1 dpi to 7 dpi at 15°C visualized by FISH to stain parasite rRNA (red), DAPI to stain nuclei (blue), and DY96 to stain the chitin of parasite spore walls (green). Animals were at the L2 larval stage at 1 dpi, L3 stage at 2 dpi, L4 stage at 3 dpi, and adult stage at 4–7 dpi. Sporoplasms (*Sppl*), meronts (*Me*), sporonts (*Spnt*), and spores (*Sp*) are indicated. Scale bars are 10 μm. (d) Quantification of symptoms of *N. displodere* infection over time at 15°C with N2 animals infected as starved L1 larvae at T_0. Sporoplasms are mononucleated structures, meronts are multinucleated structures, and sporoblasts are rounded, mononucleated structures stained by FISH (see c above). Spores are oblong DY96-stained structures in infected animals. Fifty animals were quantified for each replicate at each time point, and data points indicate the mean and standard deviation (SD) from four replicates across two experiments. Each symptom was fit to a Boltzmann sigmoidal curve (R square > 0.99 for each curve), and the time to 50% of the animals exhibiting symptoms (T_{50}) is shown.

doi:10.1371/journal.ppat.1005724.g001

and sporoblasts (pre-spores) and spores at 5 dpi, which eventually fill up a large proportion of the animal by 7 dpi (Fig 1C). We quantified the percent of animals exhibiting the symptoms of each stage of infection using FISH and DY96 staining from 1 to 7 dpi (Fig 1D), and found that 100% of animals in a population exhibited replicative forms of infection by 2 dpi, and 100% exhibited spores by 7 dpi. Thus, similar to the intestinal-trophic *N. parisii*, *N. displodere* appears to efficiently infect an entire *C. elegans* population on a plate in a laboratory setting [18].

To more closely examine the *N. displodere* life cycle in *C. elegans*, we conducted transmission electron microscopy (TEM) analysis on infected animals. When compared to uninfected animals (Fig 2A), we observed numerous structures by TEM that looked like distinct stages of microsporidia infection. These structures include large, multinucleate cells that are likely the proliferative meront stage (Fig 2B) and groups of mononucleate cells that likely correspond to the sporont stage of microsporidia, which are thought to be capable of further divisions (Fig 2C) [24]. Additionally, groups of cells were seen with nascent microsporidian spore structures that likely represent sporoblasts, which do not undergo further divisions before becoming spores (Fig 2D and 2E). Finally, darker, more fully differentiated spores were seen (Fig 2F and 2G). From the sporont to the spore stage of *N. displodere* we observed cross-sections of polar tube coils (the specialized infection apparatus of microsporidia). In spores that appeared fully developed, a maximum of five polar coils were observed per cell (seen in 19 of 70 TEM cross-sections of spores), with two coils on one side and three coils on the other (Fig 2C and 2G). Thus, *N. displodere* appears to undergo stereotypical developmental features of microsporidia, as assessed by TEM.

N. displodere can invade multiple *C. elegans* tissues, but preferentially proliferates and differentiates in the epidermis and muscle

Our observations of *N. displodere* infection by light and electron microscopy indicated that meronts and spores were predominantly in non-intestinal tissues, suggesting a different tropism than *N. parisii*, which exclusively infects the intestine. To simultaneously compare the tissue tropism of these two species, we co-infected N2 animals with *N. displodere* and *N. parisii* and found that indeed these two closely related microsporidian species infect distinct areas of the animal (Fig 3A). Next, to determine the range of tissues in which *N. displodere* can proliferate, we infected a panel of *C. elegans* strains that express GFP in distinct tissue types, and then looked for multinucleate meronts at 3 dpi by rRNA FISH, and newly differentiated spores at 5 dpi by DY96. Using this approach, we found the epidermis, body-wall muscle, and neurons had *N. displodere* meronts (Fig 3B) and newly-formed spores (Fig 3C). Additionally, we occasionally saw meronts of *N. displodere* in epidermal seam cells and coelomocytes (S2 Fig), but we did not observe new spores in these cells at later time points. In some cases, *N. displodere*-infected cells appear to become larger than corresponding uninfected cells, as can be seen in the neurons (Fig 3B, *bottom*) and seam cells (S2A Fig). Additionally, we found that multiple tissues can be infected in the same animal. For example, meronts were found both inside and outside of the GFP-positive muscle in one animal (Fig 3C, *middle*).

We observed far fewer animals infected in the intestine compared to the muscle and epidermis at 3 and 5 dpi, although a small fraction of animals did show meronts and newly made spores in the intestine (S3 Fig). Interestingly, the intestine was frequently invaded with *N. displodere* sporoplasms at 1 dpi, but was rarely infected with multinucleate meronts at 3 dpi (Fig 3D). This observation suggests that *N. displodere* can invade this tissue, but often fails to proliferate there. We quantified this observation by counting the total number of meront clusters in an animal at 3 dpi and then calculating the percentage of those clusters that are in a particular

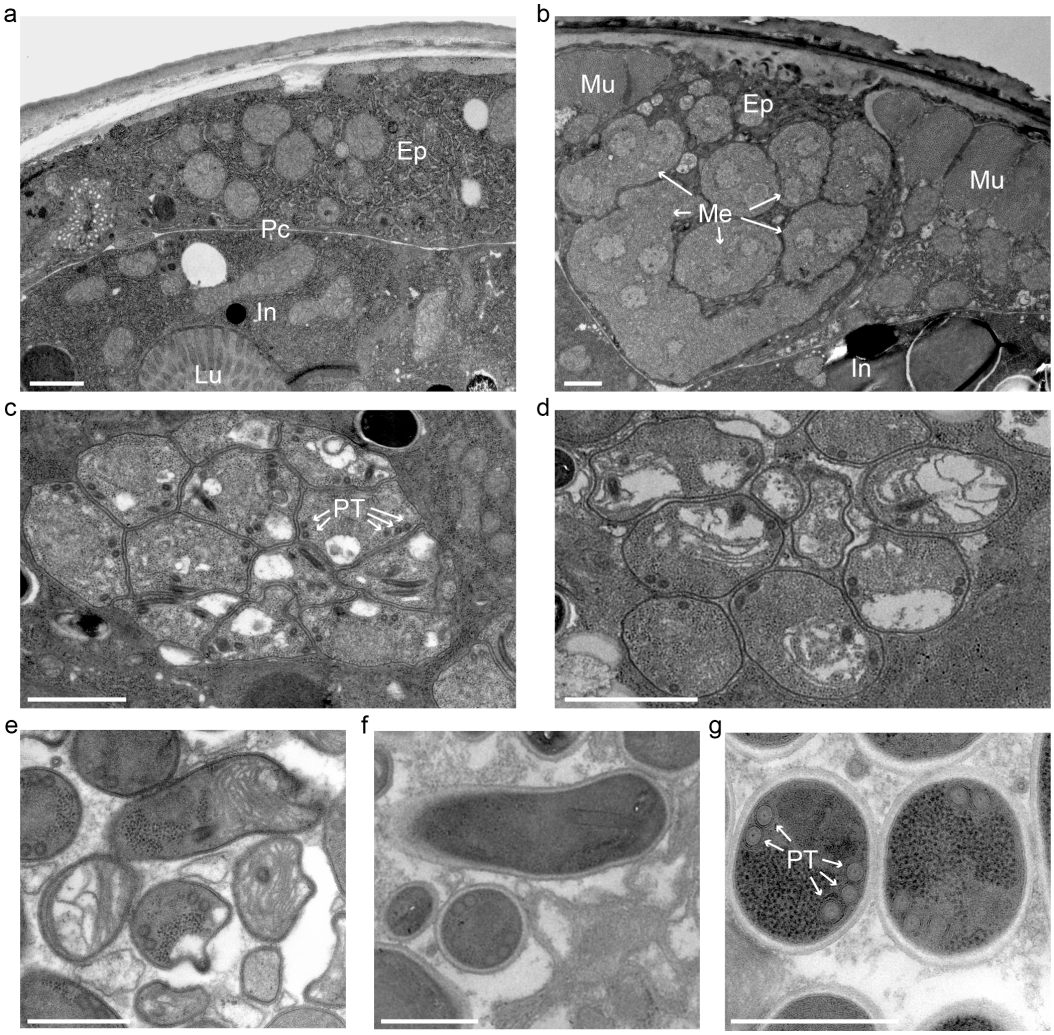

Fig 2. Transmission electron micrographs of *N. displodere*-infected *C. elegans*. (a) Cross-section of an uninfected adult with the epidermis (*Ep*) and intestine (*In*) shown, separated by the pseudocoelom (*Pc*). The intestinal lumen (*Lu*) is indicated. (b) Cross-section of an *N. displodere*-infected adult at 6 dpi with large multinucleate meronts (*Me*) presumably in the epidermis, adjacent to two flanks of the body wall muscle (*Mu*). (c) Large associated cluster of *N. displodere* sporonts with nascent polar tube coils (*PT*) in an infected animal at 8 dpi. (d-e) Groups of nascent spores, presumably sporoblasts, in an 8 dpi animal. (f-g) Longitudinal and cross-sectional views of spores in an 8 dpi animal, with five polar tube coils. Scale bars are 1 μm (a-d) and 0.5 μm (e-g).

doi:10.1371/journal.ppat.1005724.g002

GFP-labeled tissue. This analysis was performed separately for each tissue in its respective tissue-specific GFP expression strain, with each cluster of meronts assumed to have formed from a single invasion event. In this manner, we found that only about 5% of multinucleate meronts were found in the intestine, whereas 42% were in the epidermis, 53% in the muscle, 7% in the

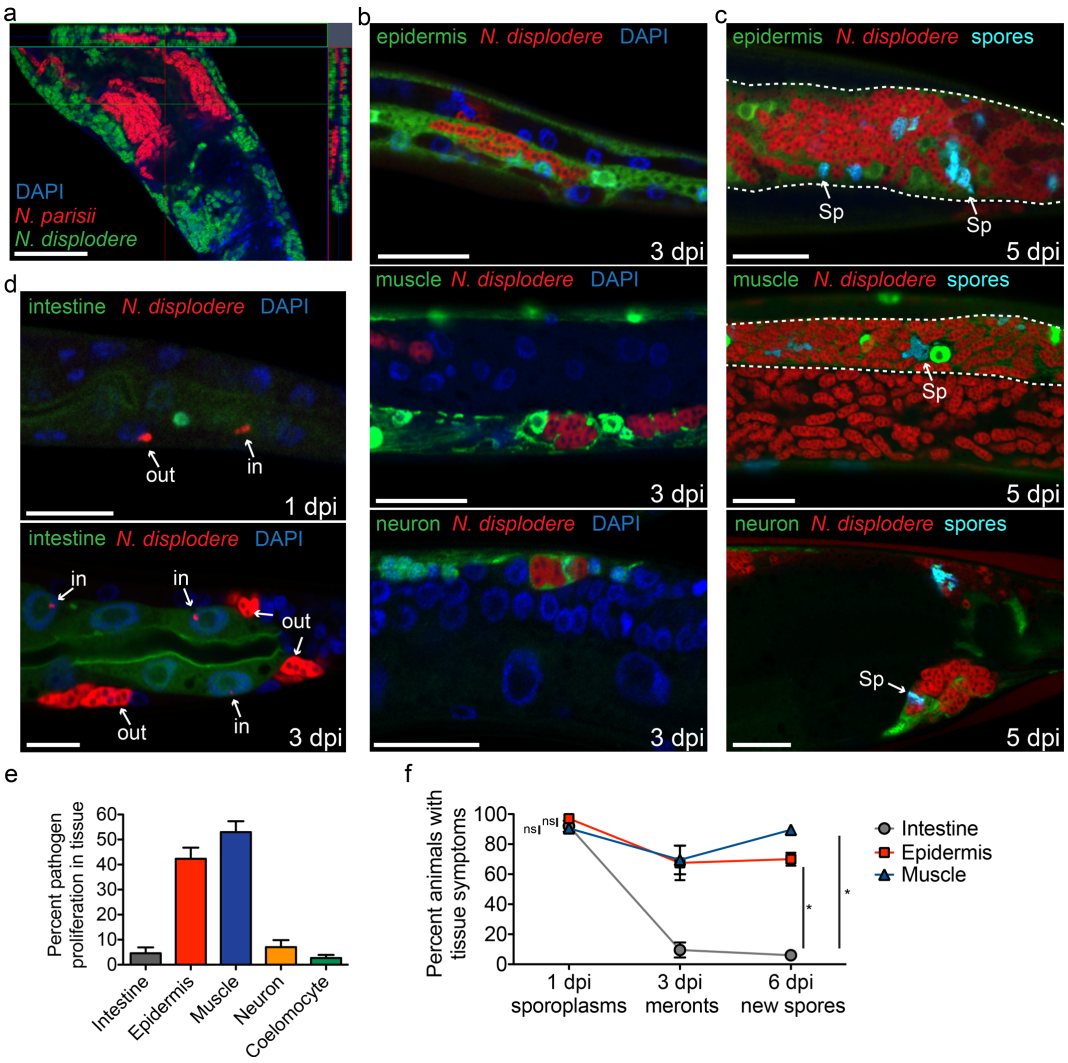

Fig 3. *N. displodere* infects multiple tissues but shows preferential proliferation in non-intestinal tissues. (a) The anterior region of a *C. elegans* animal co-infected with *N. displodere* (green) and *N. parisii* (red), visualized by FISH using species-specific rRNA probes and DAPI (blue). This image was captured by confocal microscopy with a single z-plane represented in the main inset, and orthogonal views of the x- and y-planes on the top and right insets, respectively, which show a cross-sectional view of the captured z-stacks within those planes. Scale bar is 50 μm. (b) *C. elegans* tissue-specific GFP-expression strains in the epidermis (*top*), body wall muscle (*middle*), and neurons (*bottom*), were infected with *N. displodere* and imaged at 3 dpi by FISH and DAPI. The neuron infected was in the ventral nerve cord (*bottom*). (c) Tissue-specific GFP strains were infected and imaged at 5 dpi with FISH and DY96 to stain clusters of spores (*Sp*). GFP-positive tissues that are difficult to see due to heavy infection are outlined with dashed white lines. The neuron infected was in the pre-anal ganglia (*bottom*). Scale bars are 20 μm. (d) The mid-body of the *C. elegans* intestinal GFP-expression strain infected with *N. displodere* at 1 dpi (*top*) and 3 dpi (*bottom*). Infection events are labeled as either inside (*in*) or outside (*out*) of the GFP-labeled intestine. Scale bar is 10 μm. (e) The tissue distribution of proliferating *N. displodere* infection was analyzed at 3 dpi, and was calculated individually in each *C. elegans* tissue-expression strain as the percent of FISH-stained meront clusters occurring in the GFP-positive tissues compared to the total number of events throughout the animals. Data are represented as the mean with SD of four replicates across two experiments, with a total of 50 animals counted for each replicate. (f) A comparison of the percent of animals infected in the specified

GFP-positive tissue at three time points at which the three main stages of *N. displodere* infection occur, with sporoplasms analyzed at 1 dpi, meronts at 3 dpi, and new spores at 6 dpi. Each time point was calculated individually in each *C. elegans* tissue-expression strain as the percent of 50 animals that show a given symptom in the GFP-positive tissues. Data are represented as the mean with SD of four replicates across two experiments (ns = not significant, comparing intestine to muscle (p = 0.55) or intestine to epidermis (p = 0.11) at 1 dpi; *p = 0.03 comparing intestine to muscle and comparing intestine to epidermis at 6 dpi, two-tailed Mann-Whitney test).

doi:10.1371/journal.ppat.1005724.g003

neurons, and 3% in the coelomocytes (Fig 3E). Although the infections in each tissue were quantified separately using individually marked *C. elegans* strains, this approach appears to provide a good estimate of the overall tissue distribution of meronts at 3 dpi, because the total percent of pathogen in these five tissues adds up to about 100%.

We next looked at other time points to quantify the tissues in which *N. displodere* could invade to deliver sporoplasms, proliferate into multinucleate meronts, and differentiate into spores. We infected the intestinal, muscle, and epidermal GFP expression strains for 1, 3, or 6 days and counted the fraction of animals displaying a given *N. displodere* stage at that time point in the GFP-labeled tissue. While greater than 90% of animals were initially infected with sporoplasms in either the intestine, epidermis, or muscle at 1 dpi, very few of these invasion events appeared to proliferate and differentiate in the intestine, with less than 10% of animals exhibiting meronts in the intestine at 3 dpi and 6% exhibiting new spores in the intestine at 6 dpi (Fig 3F). By contrast, greater than two-thirds of animals showed meronts and new spores in both the muscle and the epidermis at these later time points. Together, these results suggest that *N. displodere* can initially invade multiple tissues in *C. elegans*, including the intestine, but shows preferential proliferation and differentiation in the epidermis and muscle.

C. elegans infection with *N. displodere* is dependent on feeding

We next investigated how *N. displodere* is able to access the host environment to invade host tissues. Invasion via the epidermis or the intestine after feeding are the only two routes described for pathogens infecting *C. elegans* [25, 26], and these two tissues represent the largest surface areas with exposure to the environment. To investigate whether *N. displodere* infection of *C. elegans* might occur through feeding or external penetration through the cuticle, we investigated transcriptional responses characteristic of intestinal infection and cuticle damage. First, we analyzed the *C. elegans* intestinal GFP reporter strains for the genes *F26F2.1* and *C17H1.6*, which are highly induced upon infection with both *N. parisii* and another natural *C. elegans* intestinal pathogen, the Orsay virus [27]. Here, we found that *N. displodere* infection caused induction of both the *F26F2.1p*::*GFP* (Fig 4A, *left*) and the *C17H1.6p*::*GFP* reporter strains (S4 Fig). In fact, *N. displodere* caused a greater degree of induction of these reporter strains than *N. parisii*. By contrast, an epidermal infection/damage reporter strain for *nlp-29*, a gene highly induced upon infection by the fungus *D. coniospora* and epidermal wounding through the cuticle [26, 28], did not show induction after infection by *N. displodere* (Fig 4A, *right*). *N. parisii* infection also failed to induce *nlp-29*, as has been previously described [18]. The lack of *nlp-29* induction suggests that despite its capacity to infect the epidermis, *N. displodere* is unlikely to cause damage through external cuticle disruption, which is known to induce *nlp-29* [26]. These results, together with the fact that *N. displodere* spores were seen in the intestinal lumen soon after infection (S5 Fig), suggest that feeding could be a major route for infection.

To further examine if *N. displodere* infects through *C. elegans* feeding, we assessed infection in *C. elegans* strains that have a reduced or no ability to feed. First, we used the temperature sensitive (ts) strain *daf-2(e1368)* [29], which constitutively enters the non-feeding dauer stage at the restrictive temperature of 25°C. Dauers of *daf-2(ts)* animals grown at 25°C were inoculated with *N. displodere* and showed no infection in any tissues, while 100% of L3 animals of

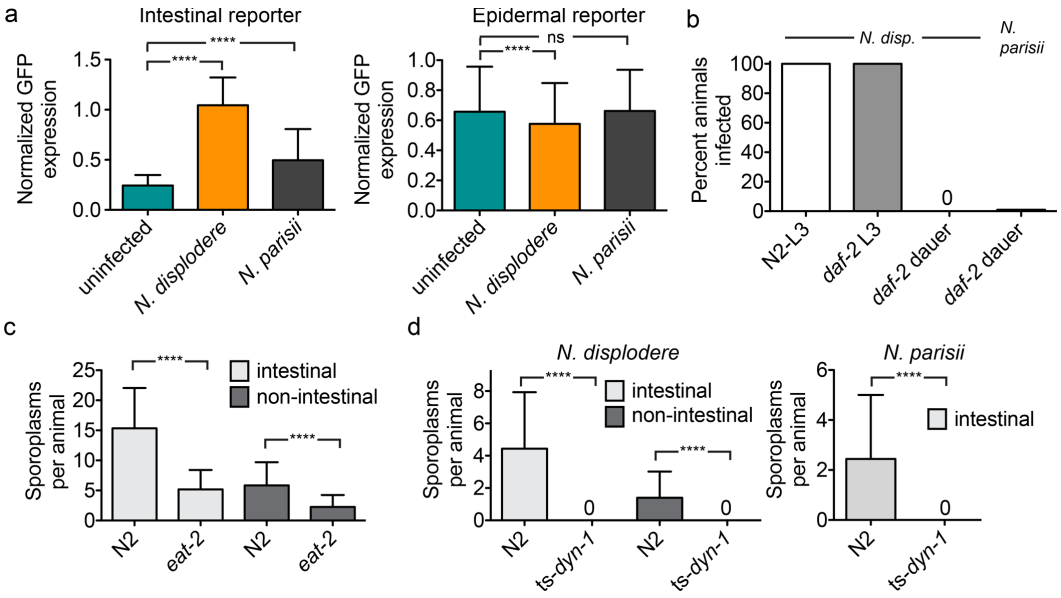

Fig 4. *N. displodere* induces an intestinal response, and host feeding is required for infection. (a) Normalized GFP induction after *N. displodere* or *N. parisii* infection of an intestinal infection reporter strain (ERT54 *F26F2.1p*::*GFP*, *left*), and an epidermal infection/cuticle damage reporter (AU189 *nlp-29p*::*GFP*, *col-12p*::*dsRed*, *right*), as measured by a COPAS Biosort. Experimental replicates were normalized by animal body size for ERT54 or by red fluorescence (*col12p*::*dsred*) for AU189. For ERT54, data are represented as mean values with SD from n = 882 animals from six replicates across two independent experiments (****p<0.0001, two-tailed Mann-Whitney test). For AU189, due to a batch effect, only data are shown from three replicates in one experiment, with mean values shown with SD from n = 900 animals (****p<0.0001, ns = not significant, two-tailed Mann-Whitney test). Data from the other AU189 replicates are shown in the supplement (S4 Fig). (b) Comparison of *N. displodere* infection of *daf-2(ts)* animals at the L3 stage (maintained at 15°C) or *daf-2(ts)* animals induced to form dauer larvae (maintained at 25°C). As controls, N2 animals were maintained at 15°C and infected with *N. displodere* as L3 animals at 25°C, and *N. parisii* spores were used to infect *daf-2(ts)* dauer larvae. (c) Comparison of the number of invasion events (counted as sporoplasms) occurring in N2 and *eat-2* animals at 1 dpi. Events were counted as either intestinal (co-localizing with intestinal gut) or non-intestinal. Data are represented as mean values with SD from n = 75 animals from three independent experiments (****p<0.0001, two-tailed Mann-Whitney test). (d) Comparison of the number of invasion events (counted as sporoplasms) occurring in *dyn-1(ts)* and N2 animals at 30°C for 30 minutes for *N. displodere* (*left*) and *N. parisii* infection (*right*). Infection events were distinguished as either intestinal or non-intestinal as above. *dyn-1(ts)* animals are paralyzed and cease to feed at the non-permissive temperature (30°C). Data are represented as mean values with SD from n = 80 *dyn-1(ts)* animals and n = 50 N2 animals across two independent experiments (****p<0.0001, two-tailed Mann-Whitney test).

doi:10.1371/journal.ppat.1005724.g004

daf-2(ts) maintained at a permissive temperature did show infection (Fig 4B). Similar results were seen with *N. parisii* infection. A caveat to these results being evidence for a feeding-based mechanism of infection is that the dauer stage not only ceases feeding, but also develops a tougher cuticle surface.

Next, we used a *C. elegans eat-2* mutant to investigate whether feeding was important for *N. displodere* infection. The *eat-2* mutant shows an approximately 70% reduction in feeding rate compared to wild-type animals, either in the absence or presence of *N. displodere* spores (S6 Fig). Consistent with this feeding defect, we saw a 66% reduction in sporoplasms in the intestine (Fig 4C). We also saw a 61% reduction in sporoplasms in non-intestinal tissues in *eat-2* mutants compared to wild-type animals (Fig 4C). These results, like the dauer results described above, show that feeding is likely a route of entry for both intestinal and non-intestinal tissue infection by *N. displodere*.

Finally, we tested the *C. elegans* temperature-sensitive endocytosis strain, *dyn-1(ts)* which stops feeding and moving at 30°C. We shifted adult N2 and *dyn-1(ts)* animals to 30°C for 2.5 hours and then infected with *N. displodere* for 30 minutes. Even with this short infection time, wild-type animals showed a substantial level of infection, with an average of 4.4 sporoplasms inside of the intestine and 1.4 sporoplasms outside of the intestine (Fig 4D, left). By contrast, the *dyn-1(ts)* mutants showed a complete lack of infection in any tissue of the animals. We saw similar results for *N. parisii* infection (Fig 4D, right), with substantial intestinal infection in wild-type animals, and no infection in *dyn-1(ts)* mutants. As a control, we verified that *dyn-1 (ts)* animals were infected by *N. displodere* at the permissive temperature (S7 Fig). Altogether, these data strongly suggest that *C. elegans* feeding is required for the majority, if not all, *N. displodere* infection in susceptible tissues of *C. elegans*.

***N. displodere* likely accesses non-intestinal tissues from the intestinal lumen through the use of its polar tube.** The dependence of non-intestinal infection on feeding raises the question of how these tissues are accessed from the pharyngeal-intestinal lumen. Notably, the muscle, epidermis, and neurons are in the body wall of *C. elegans* and are separated from the intestine by multiple cell membranes and the pseudocoelom [23]. Ingested *N. displodere* spores can be seen in the pharyngeal and intestinal lumen soon after infection, but they are never observed in any other locations in the animals at the early time points of 1 hpi and 24 hpi, including in any other tissue, the pseudocoelom, or even inside intestinal cells (see S5 Fig). These observations suggest that the majority of *N. displodere* infection in non-intestinal tissues originates from the lumen of either the pharynx or intestine. However, the pharynx of *C. elegans* is coated by its own secreted cuticle [30], and we have never observed invasion events (sporoplasms) anterior to the posterior bulb of the pharynx (0 of 100 infected animals at 1 hpi) (Fig 5A, S8 Fig). In fact, on the occasions in which *N. displodere* sporoplasms are observed anterior to the intestine, they are seen very near the intestinal lumen, which forms a wide lumenal pocket where the pharyngeal valve cells meet the four most anterior intestinal cells (S8 Fig). Together, these observations suggest infection originates not from the pharyngeal lumen, but from the intestinal lumen.

Microsporidia invade host cells using a specialized infection apparatus called a polar tube, which is fired upon external stimulus in order to breach the host cell and inject the sporoplasm [31]. We have been unable to observe this invasion process via light microscopy or TEM with either *N. displodere* or *N. parisii* in *C. elegans*. However, we investigated whether it was theoretically possible for the polar tube of *N. displodere* to reach non-intestinal tissues from the intestinal lumen. First, we measured the in vitro length of the *N. displodere* polar tube at 12.55 μm (+/- 3.20 μm), and found that these polar tubes were three-fold longer than those of *N. parisii* small spores (measured at 4.03 μm +/- 1.61 μm) (Fig 5B). *N. parisii* develops two different sized spores, large and small, with small spores being sufficient for transmitting infection in *C. elegans* [18]. We found that *N. displodere* produced only one observable spore size, measured as 2.38 μm (+/- 0.26 μm) long and 1.03 μm (+/- 0.18 μm) wide (S9 Fig), which are similar to previous measurements of *N. parisii* small spores (2.18 μm long, 0.8 μm wide) [18].

Next, to estimate if the polar tube of *N. displodere* is long enough to reach non-intestinal tissues from the lumen, we measured the average distance from the lumen to the basolateral side of the intestine in L3 larvae and young adult *C. elegans* using an intestinal GFP expression strain. At the posterior end of the intestine, this distance was measured at 8.8 μm in L3 animals and 15.0 μm in young adults, while at the anterior end it was 14.3 μm in L3 animals and 27.2 μm in young adults (Fig 5C). These measurements are rough estimates, as the lumen of the intestine is dynamic and can have a convoluted path instead of just being a straight line (see Fig 5A, S8 Fig), which results in variable distances from the lumen to the basolateral side of the intestine. Altogether, however, these data show that the *N. displodere* polar tube is long

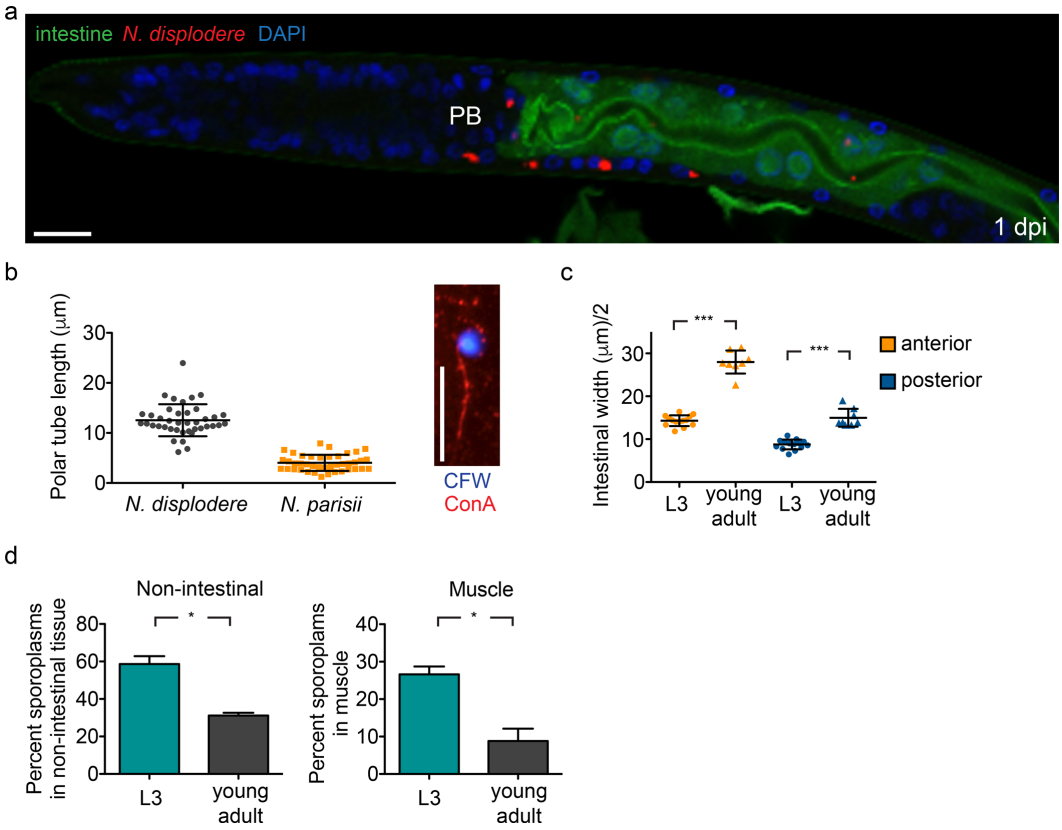

Fig 5. *N. displodere* likely accesses non-intestinal tissues from the intestinal lumen. (a) *C. elegans* intestinal GFP expression strain ERT413 at 1 dpi stained with *N. displodere* rRNA FISH. Sporoplasms are seen inside and outside of the GFP-labeled intestine, in close proximity to the intestine, but never anterior to the posterior bulb (*PB*). Scale bar is 10 μm. (b) Exterior polar tubes associated with a spore were measured for *N. displodere* and *N. parisii* small spores. Each data point represents a measured polar tube, with the line and error bars showing the mean and SD of n = 40 for *N. displodere* and n = 41 for *N. parisii*. Note polar tubes of *N. displodere* and *N. parisii* were measured with separate techniques on separate occasions. The image (*right*) shows an *N. displodere* spore stained by Calcofluor white (CFW) with the associated polar tube stained by Concanavalin A-rhodamine (ConA). Scale bar is 10 μm. (c) The widths of GFP-labeled intestine from L3 larvae and young adults were measured in the anterior and posterior regions of the animal and halved to estimate the distance from the lumen to the basal lateral side of the intestine. The mean and SD from n = 14 L3 animals and n = 8 young adults are indicated (***p = 0.0002, two-tailed Mann-Whitney test). (d) The tissue distribution of invasion events of *N. displodere* infection (sporoplasms) was analyzed after 30 minutes of infection in L3 larvae versus young adults, and was calculated in the tissue-specific strains expressing GFP in the intestine (*left*) and muscle (*right*). Invasion events were calculated as the percent of FISH-stained sporoplasms occurring outside of the GFP-expressing intestine (*left)* or inside the GFP-expressing muscle (*right*) compared to the total number of events throughout the animals. Data are represented as mean with SD of four replicates across two experiments, with a total of 25 animals counted for each replicate (*p = 0.0286, two-tailed Mann-Whitney test).

doi:10.1371/journal.ppat.1005724.g005

enough to traverse through an intestinal cell from at least some locations of the lumen, and that these distances are on average shorter in younger compared to older animals.

If infection of non-intestinal tissue were dependent on the polar tube, then we would expect younger animals would have a higher percentage of non-intestinal infection compared to older animals, because the distances from the lumen to the basolateral side of the intestine are shorter in L3 larvae compared to young adults. To test this model, we compared the percent of

intestinal versus non-intestinal invasion events in L3 larvae and young adults. We found that L3 animals showed more invasion events in non-intestinal tissues compared to young adults. Around 59% of all sporoplasms were found in non-intestinal tissues when animals were at the L3 stage, while 31% of all sporoplasms were found in non-intestinal tissues when animals were young adults (Fig 5D). Similarly when we looked specifically at the muscle, on average 27% of sporoplasms in a given animal at the L3 stage were in the muscle, but this percentage decreases to 9% in young adults.

Together, these data support a model whereby sporoplasms may be directly delivered to both intestinal and non-intestinal tissue, for example by firing a polar tube from the lumen that can span the distance of the intestinal cell to access tissues on the other side. Another possible model is that *N. displodere* sporoplasms initially invade intestinal cells, but then move independently of the polar tube to traverse the intestinal cell and reach other tissues as infection progresses. However, we were unable to find any evidence that sporoplasms move from one tissue to another. In fact, we found that sporoplasms were found in non-intestinal tissues as early as 2 minutes post-infection (S10 Fig), suggesting an incredibly rapid transit of the pathogen from intestinal lumen into non-intestinal tissue. In addition, we were unable to observe a significant increase in non-intestinal infection over time when L3 animals were pulsed with spores for exactly 1 hour and sampled immediately (1 hpi) versus 23 hours later (24 hpi) (S11 Fig), suggesting that if sporoplasm movement occurred from the intestine to non-intestinal tissues it would happen exclusively within the first hour of infection.

***N. displodere* spores are not released continuously, but can exit when *C. elegans* burst.** We next examined how newly differentiated *N. displodere* spores are released from infected animals. First, we quantified the production of *N. displodere* spores over the course of infection, measuring both the number of internal spores as well as the number of spores shed by infected animals. When we counted the number of spores inside intact (non-burst) *N. displodere*-infected animals from 4–10 dpi, we found a continuous increase in spore numbers over time such that by the last time point there was an average of 269,000 spores inside each animal (Fig 6A, *left*). By contrast, *N. parisii*-infected animals contained many fewer internal spores, with a maximum of 34,000 internal spores per animal (Fig 6A, *right*). At these same timepoints, there were virtually no *N. displodere* spores shed into the media by these intact (non-burst) infected animals (Fig 6A, *left*), while *N. parisii* had a large number of spores being shed into the media at all timepoints in which internal spores were seen, with a peak observed at 6 dpi (Fig 6A, *right*). These results for *N. parisii* are consistent with our previous data showing that once new spores have differentiated they have a continuous exit route from the *C. elegans* intestine by hijacking the host endocytic recycling pathway [21]. In contrast, *N. displodere* spores appear to have no continuous route of exit and steadily accumulate inside the animal over time.

To understand how *N. displodere* spores escape the host, we investigated a burst vulva phenotype seen in infected animals at late stages of infection. In this phenotype, the cuticle around the vulva breaks and internal tissues can be seen spilling from the opening, with the animal still alive and moving (S1 Video). By 11 dpi, 36% of *N. displodere*-infected wild-type animals displayed a burst vulva phenotype (Fig 6B). For reference, several infected animals with a burst vulva on a plate are shown (Fig 6C). By contrast, only 10% of uninfected and less than 1% of *N. parisii*-infected animals at this time point display this phenotype. Analysis of burst *N. displodere*-infected animals by microscopy shows that spores exit through this break in the vulva (see S1 Video, S12 Fig). In fact, when we tested for spore shedding in intact versus burst animals, we found that only burst animals shed *N. displodere* spores at 8 and 9 dpi (Fig 6D). By 10 dpi, the difference between these populations disappears, mostly due to a decrease in spores shed by burst animals. Additionally, these burst animals are infectious to new animals, while non-

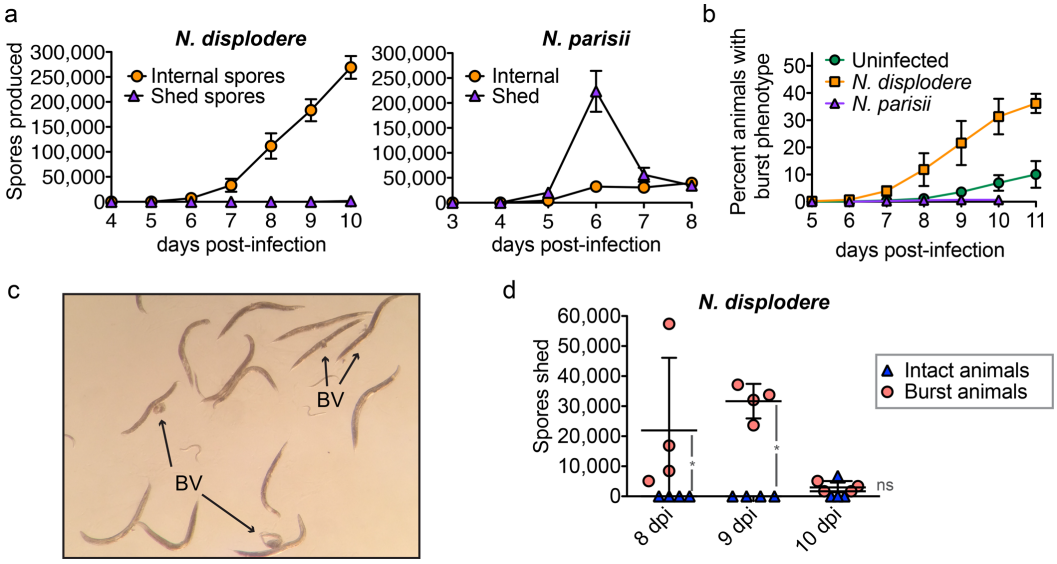

Fig 6. *N. displodere* spores exit through a bursting route. (a) Time course comparing the total number of internal spores compared to shed spores in *N. displodere*-infected (*left*) and *N. parisii*-infected (*right*) animals at 15°C. Note that only intact (non-burst) animals were picked for this assay. Internal spores indicate the average number of internal spores per animal, while external spores indicate the average number of spores shed by twenty animals into the media in four hours. Data points indicate the mean with SD of n = 6 replicates of 20 animals across 3 experiments for internal *N. displodere* spores and n = 4 replicates of 20 animals across 2 experiments for *N. displodere* shed spores and all *N. parisii* data. (b) Time course depicting the percent of animals with a burst vulva phenotype of uninfected, *N. displodere*-infected, and *N. parisii*-infected animals at 15°C. Data points depict the mean and SD from n = 4 independent experiments for uninfected and *N. displodere* and n = 3 experiments for *N. parisii* where each experiment consisted of triplicate samples containing at least 150 animals per replicate. (c) Image from a plate of wild-type *C. elegans* infected with *N. displodere* at 10 dpi. Indicated are adult animals with a burst vulva (*BV*) and internal organs spilling out. Image taken from a Nikon SMZ800 dissecting scope with an iPhone 5S. (d) Analysis of spores shed by late stage *N. displodere*-infected animals split into two groups, intact animals versus animals with a burst phenotype. Each data point indicates the number of spores shed by twenty animals for four hours of a single replicate, with the line and error bars showing the mean and SD of n = 4 replicates across two independent experiments (*p = 0.0211, two-tailed Mann-Whitney test; ns = not significant, p = 0.298).

doi:10.1371/journal.ppat.1005724.g006

burst animals are not (S13 Fig). Based on this bursting phenotype, we have named this new microsporidian species *Nematocida displodere*, or 'nematode-killer by causing to explode'.

Analysis of the *N. displodere* genome. To investigate the genetic basis for traits displayed by *N. displodere* that distinguish this species from other *Nematocida* species, we sequenced, assembled, and annotated its genome. Assembly of the data resulted in a 3.066 Mb genome that is of comparable quality to other sequenced microsporidian genomes, both in terms of assembly statistics and the identification of proteins conserved throughout microsporidia (S1 Table). Phylogenomic analysis based on 87 single-copy orthologs present in 18 other sequenced microsporidia genomes and the outgroup *Rozella allomycis* revealed *N. displodere* to be a sister group to *N. parisii* and *N.* sp. 1 (Fig 7A). *N. displodere* proteins showed an average amino acid identity of 48.6% and 48.3% compared to *N. parisii* and *N.* sp. 1 proteins, respectively. For reference, there is 66% average amino acid identity between the proteins of *N. parisii* and *N.* sp. 1. The *N. displodere* genome is also smaller than the 4.148 Mb *N. parisii* (strain ERTm3) genome and the 4.700 Mb *N.* sp. 1 (strain ERTm2) genome [9]. This reduction is partly due to smaller intergenic regions in *N. displodere*, with 85.8% of this genome being protein coding, compared to 69.2% for *N. parisii* and 63.7% for *N.* sp. 1 (Fig 7B). Additionally, at

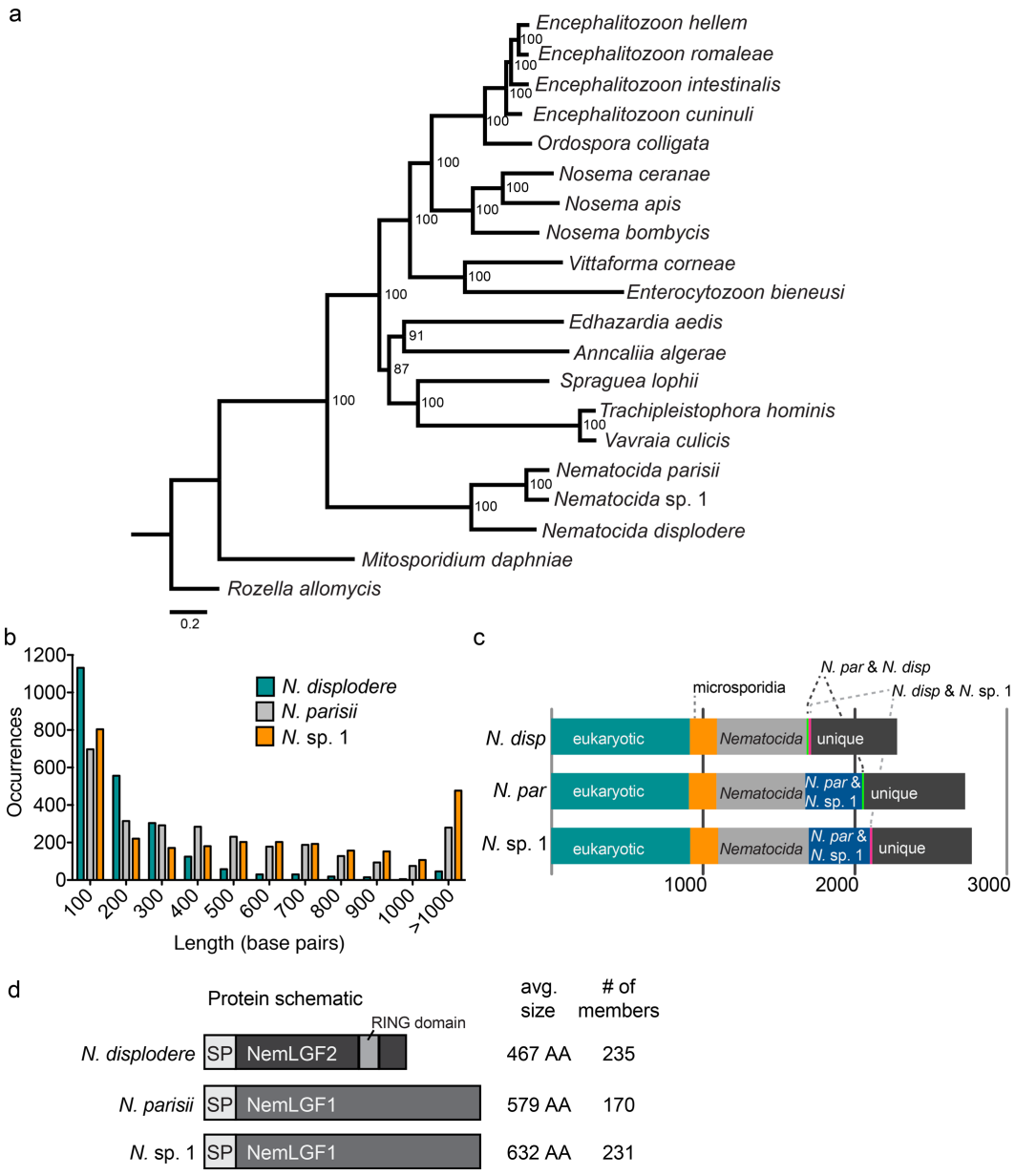

Fig 7. Analysis and comparison of *N. displodere*, *N. parisii*, *and N.* sp. 1 genomes. (a) Phylogenomic tree of *N. displodere* and 18 other microsporidia genomes, with *Rozella allomycis* as an outgroup. Bootstrap support is indicated next to each node. Scale bar indicates changes per site. The tree was created with FigTree 1.4.2 (http://tree.bio.ed.ac.uk/software/figtree/). (b) Histogram of intergenic region lengths of the three *Nematocida* species. (c) Comparison of protein content among the three *Nematocida* species. Proteins were classified into 7 categories: proteins

shared with all *Nematocida* and at least 1 other non-microsporidian eukaryotic species (*eukaryotic*), proteins shared between all *Nematocida* and at least 1 other microsporidian species (*microsporidia*), proteins shared only between all the three *Nematocida* species (Nematocida), proteins shared by *N. displodere* and *N. parisii*, proteins shared by *N. displodere* and *N.* sp. 1, proteins shared by *N. parisii* and *N.* sp. 1, and proteins not in any other species (*unique*). (d) Protein schematic of a generalized member of each of the large gene families in the *Nematocida* species, which contain signal peptides (*SP*). The average size of the gene family and the number of proteins in each species are indicated at the right.

doi:10.1371/journal.ppat.1005724.g007

2278 predicted proteins, *N. displodere* has fewer proteins than either *N. parisii* or *N.* sp. 1, but shares 73.8% percent of its proteins with both species (Fig 7C, S1 Table, S2 Table). For comparison, there are 776 proteins that *N. parisii* and *N.* sp. 1 share that are not found in *N. displodere*, but only 29 proteins that *N. displodere* shares with one *Nematocida* species that are not found in the other.

One of the most striking features of the *N. displodere* genome is the presence of a large, expanded gene family containing 235 members, of which only two members were found in the *N. parisii* (NEPG_01491, NEPG_01930) and *N.* sp. 1 genomes (NERG_01194, NERG_02097) (Fig 7D), but no members were found in any other sequenced microsporidia species. This large gene family, named *Nematocida* large gene family 2 (NemLGF2) comprises over 10% of the predicted protein coding genes in *N. displodere*. The characteristics of NemLGF2 include an average length of 467 amino acids, the presence of a predicted signal peptide or N-terminal transmembrane domain in 152 members, and the presence of a RING domain in 113 members. The *N. parisii* and *N.* sp. 1 genomes contain another large expanded family (named NemLGF1) [9] with 170 and 231 members, respectively (Fig 7D, S3 Table), but no members of this family were detected in *N. displodere*. We also identified several potential cases of horizontal gene transfer (HGT) in *N. displodere* including a bacterial formamidopyrimidine-DNA glycosylase (NEDG_02224), which is a base excision enzyme involved in DNA repair, and an FAD binding oxidase (NEDG_00514). Phylogenetic trees of homologous proteins support the idea that both of these enzymes are of bacterial origin (S14 Fig). These genes are unlikely to be derived from bacterial contamination in the DNA isolation because the assembled scaffolds containing these putative HGT genes are flanked by genes of non-bacterial origin. Additionally, we identified homologs of an N-acyl phosphatidylethanolamine-specific phospholipase-D in the *N. parisii* (NEPG_01645) and *N.* sp. 1 (NERG_00761) genomes, which was absent from *N. displodere*. A phylogenetic tree of these homologs supports this enzyme being of metazoan origin, most likely being acquired from a nematode (S14 Fig). These genes are unlikely to be derived from *C. elegans* contamination in the DNA isolation because they are present in four different *N. parisii* and *N.* sp. 1 assembled genomes and have non-identical sequences with each other. Thus, several features, including large species-specific gene families and distinct HGT events, appear to distinguish the *N. displodere* genome from the *N. parisii* and *N.* sp. 1 genomes.

For a **taxonomic summary** of this new species, *Nematocida displodere*, see S1 File.

Discussion

Our study describes a new *Nematocida* species of microsporidia that infects *C. elegans*, and has characteristics distinct from the other species in the genus described to date. We found that *N. displodere* has a broad tissue tropism, with the capacity to infect and replicate in the muscle, neurons, epidermis, intestine, coelomocytes, and seam cells. Compared to *N. parisii*, which only infects and replicates in the intestine, *N. displodere* showed preferential tropism for the epidermis and muscle over the intestine. Likely due to this difference in tropism, we also found that *N. displodere* has an unusual mechanism for newly differentiated spore exit via bursting, while new spores of *N. parisii* continuously exit through defecation. When we analyzed the genomes of these related *Nematocida* species for differences, we found that *N. displodere* has a

greatly expanded family of proteins with a RING domain of which only a couple members were found in the intestinal-trophic *Nematocida* species. Conversely, a separate expanded family was found in *N. parisii* and *N.* sp. 1 that was completely absent in *N. displodere*.

To our knowledge, *N. displodere* has the broadest tissue tropism yet seen for a pathogen infecting *C. elegans*, and is the first pathogen with the capacity to infect the neurons, muscle, or coelomocytes of *C. elegans*. *N. displodere* infection is dependent on *C. elegans* feeding, which is consistent with other invertebrate-infecting microsporidia which display two major pathways for infection, either through ingestion of spores or transovum/transovarial passage [32]. Once in the intestinal lumen, the polar tube of *N. displodere* can infect intestinal cells, but is also long enough to theoretically reach other tissues, more so in younger animals than older animals. Because our data shows that *N. displodere* invasion of non-intestinal tissues can occur very rapidly, and microsporidia are not known to have standard movement apparatuses, like cilia or flagella [22, 33], it is likely that the polar tube is used to access other tissues. One model of infection is that *N. displodere* spores fire their polar tubes in the lumen to invade any tissue, intestinal or non-intestinal, to which the polar tube gains access. This 'general access' model could explain why larger tissues like the muscle and epidermis showed a higher percent of pathogen than the neurons or less frequent cells, like seam cell and coelomocytes (see Fig 3D), assuming relatively similar proliferation rates in non-intestinal tissues. By contrast, we found that the polar tube lengths of similarly sized *N. parisii* spores were three-fold shorter than *N. displodere*. These measurements are consistent with the number of polar tube coils seen in TEM cross-sections, as *N. displodere* spores had up to five coils (see Fig 3G) while prior TEM images showed that small *N. parisii* spores had only one coil [18]. A shorter polar tube likely limits *N. parisii* infection to shorter distances from the intestinal lumen compared to *N. displodere* infection. However, given that the distance from the lumen to the basolateral side of the intestine is variable within an animal, with some distances being as short as 2 μm (see Figs 2A and 5A), polar tube lengths are not the only limiting factor for infecting non-intestinal tissues from the intestinal lumen. It is possible that spores must convey enough force on the polar tube upon germination in order to pierce through multiple membranes to reach non-intestinal tissues [31], or that specific proteins are required on the polar tube for interaction with tissue-specific host factors on a cell for polar tube entry and invasion [34, 35].

Strikingly, although *N. displodere* can successfully invade the intestine, we found that the majority of intestinal infection fails to thrive in comparison to robust infection of the epidermis and the muscle. One possible reason for this tropism is that competition among other microbes in the intestine has put evolutionary pressure on *N. displodere* to efficiently proliferate in non-intestinal tissue. Multiple examples of potential competition among microsporidian species have been described. For example, ecological observations have shown that the honey bee-infecting microsporidian *Nosema ceranae* can almost completely displace other naturally occurring microsporidia species when introduced into a new area [36]. Additionally, laboratory experiments have shown that different microsporidia species of the gypsy moth can exclude or suppress the growth of each other in a particular tissue [37]. For *C. elegans* in the wild, there may be an increased competition for resources in the intestine compared to other tissues, as several distinct pathogens can naturally infect and proliferate in the intestine [17, 18, 25].

A potential mechanistic reason for the tropism of *N. displodere* is that there is distinct induction of or sensitivity to tissue-specific host defense responses. For *C. elegans*, different tissue-specific transcriptional responses to intracellular pathogens have been identified for the epidermis upon *D. coniospora* infection and epidermal wounding, and for the intestine upon *N. parisii* and Orsay virus infection [27, 38]. Components of these transcriptional responses have been shown to play a role in tissue-specific host defense against their respective pathogens, including anti-microbial genes induced in the epidermis and Skp1-Cullin-F-box (SCF)

ubiquitin ligase components induced in the intestine [26, 27]. For the epidermis we found that *N. displodere* failed to induce a reporter gene representative of the epidermal response, but induced reporter genes representative of the intestinal response to a higher degree than *N. parisii*. These observations could be representative of differential induction of tissue-specific defense responses upon infection by *N. displodere*, resulting in better proliferation in the epidermis compared to the intestine. Another possibility is that *N. displodere* has greater sensitivity to ubiquitin-mediated clearance in the intestine, resulting in the failure of the majority of infection in this tissue [27]. Future studies will investigate the mechanistic basis on the host side for the distinct tissue tropism of *N. displodere*.

To investigate the genetic basis for the distinct features of *N. displodere*, we sequenced its genome and compared it with the other, intestinal-trophic *Nematocida* species. *N. displodere* is the earliest known diverging member of the *Nematocida* genus, but shares over 70% of its proteins with both *N. parisii* and *N.* sp. 1. The most striking difference between the genomes is the presence of species-specific expanded gene families, NemLGF2 and NemLGF1, found in *N. displodere* and the intestinal-trophic *Nematocida*, respectively, which are completely absent in any other sequenced genomes. An impressive 10% of the coding sequences in the *N. displodere* genome, or up to 33% of the proteins not shared with *N. parisii* and *N.* sp. 1, belongs to NemLGF2. These gene families likely evolved after the divergence from the last common ancestor and expanded as they adapted to their respective host environments. Considering the fact that microsporidia are obligate intracellular pathogens, it is likely that evolutionary pressure from the host played a role in the expansion, as has been shown for expanded gene families in other microsporidia species [39, 40]. In fact, the proteins in these expanded gene families are likely secreted into *C. elegans* cells at some point during infection, as both NemLGF1 and NemLGF2 have a high percentage of predicted signal peptides among their members. Additionally, almost half of the NemLGF2 proteins from *N. displodere* contain a C-terminal RING domain, typically found in ubiquitin E3 proteins that function to bind to E2 ligases [41]. The RING domains in NemLGF2 may serve as protein-protein interaction modules in the host cells, allowing these proteins to bind to host proteins and perform some yet unknown function. It is intriguing to speculate that the NemLGF2 proteins may play a role in interacting with the host ubiquitin system, as it has been shown to play a role in response to *N. parisii* infection [27], and RING domains are found in E3 ubiquitin ligases. Despite having a broader tissue tropism than *N. parisii* and *N.* sp. 1, *N. displodere* has a smaller genome and fewer predicted proteins, which runs contrary to expectations that a broader range might require more genes to adapt to growth in varying niches and avoid different defense responses. However, a related observation was recently made in a study of two microsporidian species that infect mosquitos, as the microsporidia with a broad host range, *Vavraia culici*, had a smaller genome than the specialist microsporida, *Edhazardia aedis*, known to infect only one mosquito species [42]. Altogether, the discovery and characterization of *N. displodere* presents a unique model system in *C. elegans* to study the mechanistic and evolutionary bases of pathogen tissue tropism.

Materials and Methods

Nematode sampling and isolation

Wild nematodes were sampled from the woods near the Viosne stream in Santeuil, France on September 30, 2014 using methods previously described [17]. Wild *Caenorhabditis* animals that looked 'sick' were individually picked to nematode growth media (NGM) plates seeded with *E. coli* strain OP50-1, as described [43], and incubated at 20°C. P_0 adults were allowed to self-fertilize to produce F_1 progeny and these P_0 adults were analyzed by light microscopy for infection. *N. displodere* (designated isolate JUm2807, ZooBank ID, urn:lsid:zoobank.org:

act:35CF055F-C311-4D9B-BFF0-B7B09FC441E4) was found in the head of the P_0 of wild *C. elegans* strain (designated JU2807), isolated from the rotting stem of an *Asteraceae* plant (GPS coordinates: 49.12165, 1.95101) containing a proliferating population of approximately 500 *C. elegans* of various stages.

N. displodere spore preparations

C. elegans strain JU2807 containing *N. displodere* isolate JUm2807 was cleared of all bacterial and fungal contamination by thoroughly washing a starved population of infected animals with sterile H_2O and incubating 1 h in 15 ml H_2O. Animals were incubated 2 h in S-basal (50 mM potassium phosphate, pH 6.0, 100 mM NaCl, 5 μg/ml cholesterol) containing 100 μg/ml gentamycin, 50 μg/ml carbenicillin, 50 μg/ml kanamycin, 20 μg/ml tetracyclin, and 50 μg/ml streptomycin. Sodium dodecyl sulfate (SDS) was added to a final concentration of 1% and incubated for 15 m. Finally, animals were washed with H_2O and plated on NGM plates containing 50 μg/ml carbenicillin, 25 μg/ml kanamycin, 12.5 μg/ml tetracyclin, and 37.5 μg/ml chloramphenicol seeded with concentrated OP50-1 bacteria, and incubated at 15°C for 5 d.

N. displodere spores were prepared as previously described for *N. parisii* [20]. Briefly, *N. displodere* JUm2807 was cultured by expanding large-scale cultures of antibiotic-treated *C. elegans* JU2807, followed by mechanical disruption of the nematodes, and then filtering to isolate spores away from animal debris. Similar methods were used to make *N. parisii* spore preparations using the isolate ERTm1 infected in *C. elegans* N2.

C. elegans strains and maintenance

All *C. elegans* strains were maintained as previously described [43]. The intestinal GFP strain ERT413 *jySi21[spp-5p::GFP; cb-unc-119(+)] II* was made in this study using Mos1-mediated single-copy insertion (MosSCI) [44]. Additional strains used in this study include:

- ERT54 *jyIs8[C17H1.6p::GFP; myo-2::mCherry] X*
- ERT71 *jyIs14[F26F2.1p::GFP; myo-2::mCherry]* [27]
- OH441 *otIs45[unc-119p::GFP] V*
- HC46 *ccIs4251[myo-3::GFP-NLS, myo-3::GFP-MITO] I; mIs11[myo-2::GFP] IV* [45]
- OH910 *otIs77[ttx-3p::kal-1, unc-122p::GFP] II*
- AU189 *frIs7[nlp-29p::GFP, col-12p::dsRed] IV* [26]
- DA465 *eat-2(ad465)*
- ERT125 *dyn-1(ky51)* [46]
- CB1368 *daf-2(e1368)*.

Fluorescent in situ hybridization (FISH)

FISH was performed as described using FISH probes to the small subunit rRNA conjugated to CAL Fluor Red 610 (CF610) or 5-Carboxyfluorescein (FAM), with slight modification [27]. For single-species infections, a mixture of *Nematocida*-specific probes MicroA-CF610 (CTCTG TCCATCCTCGGCAA), MicroC-CF610 (CAGAATCAACCTGGTGCCTT), MicroD-CF610 (CGAAGGTTTCCTCGGATGTC), and MicroE-CF610 (GTACTGGAAATTCCGTGTTC) were used at 2.5 μg/ml each, with hybridization at 46°C and washes at 48°C. As indicated, the chitin-staining dye direct yellow 96 (DY96) was added at 10 μg/ml to the hybridization buffer to

stain microsporidia spores in the animals [21]. For co-infection, a *N. displodere*-binding probe Microsp1A-FAM (CAGGTCACCCCACGTGCT) and a *N. parisii*-specific probe MicroF-CF610 (AGACAAATCAGTCCACGAATT) were used at 5 μg/ml each, with hybridization at 52°C and washes at 54°C.

C. elegans infections with microsporidia

C. elegans strains were infected on NGM plates with purified *N. displodere* spores (isolate JUm2807) or *N. parisii* spores (isolate ERTm1) as described previously [9]. All infections in this study were conducted using a standardized dose of *N. displodere* or *N. parisii*, defined here as 3.5 x 10^4 spores per cm^2 (calculated from infecting a 6 cm NGM plate with 1.0 x 10^6 spores). *N. displodere* was capable of being continually transmitted within *C. elegans* for multiple generations at 15°C, so all experiments were conducted at this temperature unless otherwise indicated.

For kinetics of infection, synchronized N2 L1 larvae were infected with a standard dose and sampled at 1–7 dpi for small subunit rRNA FISH in 24 h increments. Fifty animals per replicate were analyzed for sporoplasms, meronts, sporoblasts, and spores at each time point. For microscopy with the tissue-specific GFP expression lines, strains ERT413, AU189, HC46, and OH441 were infected with the standard dose of *N. displodere* as synchronized L1 larvae. Animals were fixed at 3 dpi and stained by small subunit rRNA FISH, or at 5 dpi and stained by rRNA FISH plus DY96.

For analysis of the tissue distribution of *N. displodere* infection, synchronized L1 larvae of strains ERT413, AU189, HC46, and OH441 were infected at 15°C with half a standard dose of *N. displodere* spores in duplicate and fixed at 3 dpi for small subunit rRNA FISH. A total of 50 infected animals for each replicate were analyzed by confocal microscopy for meronts or meront clusters in GFP-positive tissues or GFP-negative tissues. Meront clusters were counted once if they were in distinct areas of the animal and/or separated from another cluster by at least 10 μm. The percent of meront clusters in the GFP-positive tissue was calculated based on the total number of meront clusters calculated for each replicate.

For analyzing the percent of animals with tissue-localized symptoms at different time points, synchronized L1 larvae of strains ERT413, AU189, and HC46 were infected in duplicate at 15°C with half a standard dose of *N. displodere* spores in duplicate. Note that for 1 dpi animals, the L1 larvae were infected at the end of the L1 stage, by first growing for 22 h at 15°C before infecting with *N. displodere* so that the animals were in the L3 stage by the end of the experiment and express enough GFP for analysis. Animals were fixed at 24 hpi and 144 hpi for 1 dpi and 6 dpi, respectively, and stained by small subunit rRNA FISH for 1 dpi and FISH plus DY96 (10 μg/ml) for 6 dpi. The 3 dpi animals were calculated from the tissue distribution experiment (see above). Animals were analyzed for sporoplasms at 1 dpi, meronts at 3 dpi, and DY96-stained spores at 6 dpi and then the percent of animals with the symptom in the GFP-positive tissue were calculated for fifty animals per replicate.

Transmission Electron Microscopy (TEM)

TEM was performed at the Electron Microscopy Facility, Department of Cellular and Molecular Medicine, UCSD. Synchronized N2 L1 larvae were infected with a standard dose of *N. displodere* at 15°C and harvested at 6 dpi and 8 dpi, and an uninfected sample was collected at 6 dpi. Animals were fixed with 2% of paraformaldehyde, 2.5% of glutaraldehyde in 150 mM sodium cacodylate buffer (SC), and washed with 150 mM SC buffer. Samples were post-fixed 3 h in 2% osmium tetroxide in 150 mM SC on ice, washed in 150 mM SC followed by ddH_2O, pelleted in 2% agarose, and incubated in 2% uranyl acetate overnight at 4°C. Samples were dehydrated on ice with a graded series of ethanol from 50% to 100%, followed with 50%

ethanol/50% acetone for 20 m, and twice in 100% acetone for 10 m. Samples were incubated in a graded series of Durcupan from 25% to 100% at RT. Finally, samples were incubated in 100% Durcupan ON at 60°C. Blocks were cut on Leica microtome with a diamond knife to 60 nm sections and collected on 300 mesh grids. Digital images were collected on a Tecnai TEM (Field Emission Inc.) at 80 kv by using an Eagle 4K digital camera.

Tissue-specific reporter infections

Synchronized ERT54, ERT71, and AU189 L1 larvae were grown on OP50-1 for 20°C for 24 h and 15°C for 24 h to the L3 larval stage. Animals were split and infected in triplicate with a standard dose of either *N. displodere* or *N. parisii* for 20 h at 15°C with approximately 800 animals per replicate. Animals were harvested and washed with M9 buffer and loaded onto a COPAS Biosort (Union Biometrica) to measure GFP, dsRed fluorescence, and time-of-flight (TOF) of each animal. Data was analyzed using the R package COPASutils [47], with GFP expression of ERT54 and ERT71 normalized to TOF and AU189 normalized to *pcol-12*::*dsRed* expression.

Infection of feeding mutants

For the *eat-2* mutant, synchronized N2 and *eat-2* L1 larvae were grown at 15°C to the gravid adult stage for 3 and 4 d, respectively, and then infected for 24 h with *N. displodere* at 1/10 the standard dose (3.5 x 10^3 spores per cm^2) to reduce the number of infection events per animal. For the temperature-sensitive feeding mutant *dyn-1(ts)*, synchronized N2 and ERT125 L1 larvae were grown to the adult stage at 20°C for 3 d. Animals were then shifted for 2.5 h to either 30°C to stop ERT125 pharyngeal pumping (as monitored on a dissecting scope) or 20°C as a control, and infected with five times the standard dose (1.75 x 10^5 spores per cm^2) for 30 m at the respective temperatures. FISH was conducted as above and sporoplasms were counted and localized using a Zeiss LSM700 confocal microscope with a 40x objective.

To test dauer infection, synchronized *daf-2(e1368)* L1 larvae were grown for 2 d at 25°C to initiate dauer formation. As a control, *daf-2(e1368)* and N2 L1 larvae were grown for 2 d at 15°C to the L3 stage. All animals were infected with the standard dose of *N. displodere* at 25°C for 18 h. FISH was conducted as described above, except all animals were fixed in 100% acetone for 10 m to permeate the dauer cuticle.

Stage-specific infection with *N. displodere*. Synchronized L1 larvae of strains ERT413 and HC46 were grown in duplicate for 50 h at 15°C to reach the L3 stage or 90 h at 15°C to reach the young adult stage. Synchronized L3 larvae or young adults were infected with a standard dose of *N. displodere* for 30 m at 15°C, then fixed for rRNA FISH. Twenty-five infected animals were analyzed by confocal microscopy and the number of sporoplasms in the GFP-positive tissue was compared to the total number of sporoplasms in the animal. To measure intestinal widths, a single z-plane image of an animal was taken with the lumen visible, and the distance was measured from the basal-lateral side of one cell, through the intestinal lumen to the basolateral side of the opposing intestinal cell. These values were halved to give an estimate of the distance from the intestinal lumen to the basal lateral side of the intestine.

C. elegans bursting assay

Synchronized N2 L1 larvae were infected or mock-infected in triplicate with the standard dose of *N. displodere* and *N. parisii* at 100–200 animals per 6 cm plate, and grown at 15°C for 11 d. Infected adults were transferred to new plates at 5–8 dpi to remove the F_1 generation. At 5–11 dpi all animals from each condition were analyzed by a dissecting microscope for a bursting phenotype and removed.

Spore shedding and production assays

Synchronized N2 L1 larvae were infected in duplicate with the standard dose of *N. displodere* and *N. parisii* and grown at 15°C for 10 d. For quantifying spores produced in the animals, 20 animals were picked into 1 ml PBS + 0.1% Tween-20 (PBS-T) at 4–10 dpi for *N. displodere* and 3–8 dpi for *N. parisii*, and washed three times with 1 ml PBS-T. Animals were lysed and the number of spores produced per animal was counted as described [48]. For quantifying spores shed by the animals, 20 animals were picked into 500 μl of a 1:10 OP50-1 and M9 mixture at 5–10 dpi for *N. displodere* and 4–8 dpi for *N. parisii*. Animals were incubated for 4 h at RT with rotation, and secreted spores were separated from the animals and counted as previously described [21].

Measurement of spore characteristics. For measuring spore dimensions, *N. displodere* spores were stained by 1:100 dilution of CFW (Sigma) and imaged with a 100x objective on a Zeiss AxioImager M1 upright microscope. Spores stained by CFW were measured using the light microscopy image with ImageJ (NIH) by length and width. One spore was removed as an outlier in the analyses because its length was greater than 1.5 times the interquartile range above the third quartile.

N. displodere polar tubes were stained by suspending spores in 0.5 ml PBS containing 0.5 mM H_20_2, incubating on silane coated slide at room temperature in a humid chamber for 4 h, and adding 5 μl of 5 mg/ml NHS-succinyl-Rhodamine (Roche) for 1 h in the dark. *N. parisii* polar tube lengths were stained by subjecting *N. parisii* spores to two cycles of freeze-thaw, incubating on slides at room temperature for 4 h in PBS, and adding 20 ng/ml Concanavalin A conjugated to fluorescein isothiocyanate (FITC) and 10 ng/ml Calcofluor white for 30 m at room temperature [49]. Spores were visualized by washing twice with PBS and imaging at 100x objective on a Zeiss AxioImager M1. We measured the lengths of polar tubes that were still attached to spores with ImageJ (NIH) if the entire polar tube was in frame.

Genome sequencing, assembly, and analysis. Spores were isolated as described above and further purified using a 50% Percoll (Sigma) gradient. DNA was extracted using a MasterPure Yeast DNA purification kit (Epicentre Biotechnologies). DNA was further purified using a DNeasy column (Qiagen). Genomic DNA sequencing data was generated using the MiSeq sequencing platform (Illumina), which resulted in 26,240,016 paired-end reads of 301 base pairs, resulting in ~2500X coverage. Sequencing reads were assembled into contigs and scaffolds using Abyss 1.5.2 with a Kmer value of 96 [50]. Only scaffolds and contigs of at least 500 bp were retained. Assembly statistics are presented in S1 Table. Gene prediction and orthology determination were done following procedures previously applied to other microsporidia genomes [9, 42]. This Whole Genome Shotgun project is available at DDBJ/ENA/GenBank under accession LTDL00000000 for *N. displodere* JUm2807, and the version described in this paper is version LTDL01000000.

Genes were predicted from assembled scaffolds using Prodigal 2.60 [51]. Predicted proteins less than 100 amino acids were removed unless they had a PFAM match [52] of at least 10^{-3} or BLAST match against UniRef90 database [53] with an E-value of at least 10^{-3}. A total of 2278 proteins were predicted. Each protein was assigned a standard name with the prefix NEDG. Proteins are listed in S2 Table.

Orthologous gene families were identified using OrthoMCL 2.0.9 [54] using an inflation index of 1.5 and a BLAST E-value cutoff of 10^{-5}. Conservation of proteins for each microsporidian species was determined by counting the number of orthogroups conserved between all 19 species divided by the number of orthogroups conserved between the other 18 species. Phylogeny was constructed from 87 single copy orthologs present in *R. allomycis* and 19 microsporidian species (S1 Table). Proteins from each orthogroup were aligned using MUSCLE 3.8.31

[55]. These alignments were trimmed using trimAl 1.2 with the option-gappyout [56]. Each orthogroup alignment was then concatenated into a single alignment using FASconCAT 1.0 resulting in a total of 30,556 aligned amino acid sites [57]. ProtTest 3.4 was then used to determine that PROTGAMMALG was the best fitting model for the data [58]. Phylogeny was then inferred using the RAxML 8.2.4 with the PROTGAMMALG model and 1000 bootstrap replicates [59].

Categorization of protein conservation for the *Nematocida* species was done by identifying orthologous gene families with OrthoMCL. Six eukaryotes (*Saccharomyces cerevisiae*, *Monosiga brevicollis*, *Rozella allomycis*, *Neurospora crassa*, *Ustilago maydis*, and *Allomyces macrogynus*) and 19 microsporidia genomes were used (S1 Table).

Large gene families were identified from OrthoMCL analysis. The proteins in these groups were used to build models of the families by aligning proteins with MUSCLE and building profile hidden Markov models using HMMER 3.0 with an 10^{-5} E-value cutoff [60]. The RING domain model for NemLGF2 was made by taking RING domains from NemLGF2 proteins and then searching for additional RING domains in NemLGF2 proteins. This process was iteratively repeated until no more domains with an E-value of at least 10^{-3} could be found.

Protein function was predicted with BlastKOALA [61]. PFAM domains in proteins were predicted with an E-value of 10^{-3}. Signal peptides predicted with SignalP 4.1 [62], using the best model with a cutoff of 0.34 for both the noTM model and for the TM model. Transmembrane domains were predicted with TMHMM 2.0 [63].

Intergenic regions were calculated by subtracting the start of each coding gene from the closest preceding coding gene's stop. Additionally the region before the start of the first predicted gene of a scaffold and the region after the stop of the last gene of the scaffold were included. Coding genes that were predicted to overlap were included and their intergenic value set to 0. Pairwise protein identities between species were calculated by aligning single copy orthologs with MUSCLE.

Putative cases of horizontal gene transfer were identified by BLAST hits against the NCBI non-redundant protein database, but not having a BLAST match with an E-value less then of 10^{-5} to any proteins encoded by the non-*Nematocida* microsporidia species listed in S1 Table. Both putative cases in *N. displodere* are in contigs that are bordered by genes that either have homology to a microsporidian protein or do not have detectable homology to any protein. The one putative case identified in *N. parisii* and *N.* sp. 1 is conserved between the two species and thus not likely to be contamination.

Supporting Information

S1 Fig. Identification of microsporidia infection in the body wall of a wild *C. elegans*. (a) The head region of a wild-caught *C. elegans* animal with structures resembling microsporidia at different stages of infection, including meronts (*Me*) and groups of spores (*Sp*). The pharynx (*Ph*) is indicated for orientation. (b) The head region of a live, uninfected N2 *C. elegans* for comparison, with storage granules (*SG*) indicated. (c) Infected mid-body region of a live animal from strain JU2807 (progeny of the animal shown in Panel a) showing both meront-like structures and groups of spores. Scale bars are 10 μm.
(TIF)

S2 Fig. *N. displodere* proliferation in seam cells and coelomocytes. (a) *C. elegans* strain AU189 expressing GFP in the epidermis was infected with *N. displodere* and fixed at 3 dpi for *N. displodere* rRNA FISH and counterstained with DAPI. Seam cells (SC) were identified as nuclei-containing, GFP-negative cells within the GFP-positive epidermis, in the top or bottom plane of the animal laying on its left or right side. Images without (*left*) or with (*right*) the red

channel (*N. displodere* FISH) are shown. (b) *C. elegans* strain OH910 expressing GFP in coelomocytes was infected with *N. displodere* and fixed at 5 dpi for *N. displodere* rRNA FISH and counterstained with DAPI. Two images of two separate animals are shown with meronts inside coelomocytes. Scale bars are 10 μm.
(TIF)

S3 Fig. *N. displodere* proliferation and differentiation is occasionally observed in the intestine. (a) *C. elegans* intestinal-specific GFP-expression strain ERT413 was infected with *N. displodere* and fixed at 3 dpi for *N. displodere* rRNA FISH and DAPI. Meronts are seen in the GFP-labeled intestine. (b) Strain ERT413 was infected with *N. displodere* and treated as above at 6 dpi, except DY96 was used to stain spores. Meronts and spores are observed both inside and outside of the GFP-labeled intestine. Scale bars are 10 μm.
(TIF)

S4 Fig. *N. displodere* infection of *C. elegans* intestinal and epidermal reporter strains. (a) Normalized GFP induction of an intestinal infection reporter strain (ERT54 *C17H1.6p*::*GFP*) after *N. displodere* or *N. parisii* infection. Signal was normalized by body size using time of flight on the COPAS Biosort. Data are represented as mean values with SD from n = 1800 animals from six replicates across two independent experiments (****$p<0.0001$, two-tailed Mann-Whitney test). (b) Another independent experiment showing GFP induction of the epidermal damage/infection reporter strain AU189 after *N. displodere* or *N. parisii* infection (for the other independent replicates see Fig 5A). Animals were normalized by red fluorescence (*pcol12*::*dsred*). Data show mean values with SD from n = 900 animals across three replicates (***$p<0.0001$, *$p = 0.038$, two-tailed Mann-Whitney test).
(TIF)

S5 Fig. *N. displodere* spores are observed in the intestinal lumen. (a) *C. elegans* strain ERT413 expressing GFP in the intestine was infected at the L4 stage with *N. displodere* for 10 m and fixed for staining by DAPI (blue) and DY96 (turquoise). Spores (*Sp*) are seen as DY96-positive oval structures in the intestinal lumen, delineated by dashed lines. (b) *C. elegans* strain ERT413 expressing GFP in the intestine was infected at the L3 stage with *N. displodere* for 1 hour and stained for *N. displodere* rRNA FISH and DY96. Spores are seen only in the intestinal lumen and sporoplasms (Sppl) are indicated. Scale bars are 10 μm.
(TIF)

S6 Fig. Pharyngeal pumping of *eat-2* mutants. Tukey boxplots of N2 and *eat-2* pharyngeal pumping rates with or without *N. displodere* (*N.d.*) infection at 15°C from n = 50 animals examined across two independent replicates. The lines indicate the median, the box extends from the 25th to 75th percentiles, and the whiskers extend to the minimum and maximum data point, excluding an outlier (indicated with a black dot).
(TIF)

S7 Fig. Infection comparison between N2 and *dyn-1(ts)* at the permissive temperature for *dyn-1(ts)*. Comparison of the number of invasion events (counted as sporoplasms) occurring in *dyn-1(ts)* and N2 animals after *N. displodere* infection at 20°C for 30 min. Events were counted as either intestinal or non-intestinal. Data are represented as mean values with SD from n = 25 animals from one experiment (*$p = 0.038$, ns = not significant ($p = 0.432$), two-tailed Mann-Whitney test).
(TIF)

S8 Fig. *N. displodere* invasion events are seen in close proximity to the intestine. (a) *C. elegans* strain ERT413 expressing GFP in the intestine was infected as L1 larvae with *N. displodere*

and fixed at 1 dpi for *N. displodere* rRNA FISH. Sporoplasms are seen inside and outside of the GFP-labeled intestine, in close proximity to the intestine, but never anterior to the posterior bulb (*PB*). (b) Strain ERT413 was infected as adults for 30 min with *N. displodere* and treated as above. Sporoplasms (*Sppl*) in the anterior region are observed in close proximity to the wide intestinal lumen at the anterior part of the intestine. The anterior bulb (*AB*) and posterior bulb (*PB)* of the pharynx are indicated. Scale bars are 10 μm.
(TIF)

S9 Fig. Measurement *N. displodere* spore size. (a) The graph depicts mean length and width of *N. displodere* spores with SD from n = 202 CFW-stained spores. (b) The histogram depicts the frequency distribution of *N. displodere* spore lengths (*left*) and widths (*right*).
(TIF)

S10 Fig. *N. displodere* invasion events are seen in non-intestinal tissues as early as 2 minutes post-infection. *C. elegans* strain ERT413 expressing GFP in the intestine was infected as L4 larvae with *N. displodere* and fixed at 2 minutes post-infection for *N. displodere* rRNA FISH. Sporoplasms (*Sppl*) are seen outside of the GFP-labeled intestine. Scale bar = 10 μm
(TIF)

S11 Fig. Non-intestinal *N. displodere* infection remains unchanged over time after a pulse infection. Comparison of the number of invasion events (counted as sporoplasms) occurring when L3 animals of ERT413 were infected with *N. displodere* spores for 1 hour and immediately fixed (T_0) or washed to remove spores and allowed to grow at 15°C for an additional 23 hours (1 dpi). Events were counted as either intestinal or non-intestinal based on localization with intestinal GFP. Data are represented as mean values with SD from n = 30 animals from one experiment (ns = not significant, two-tailed Mann-Whitney test).
(TIF)

S12 Fig. *N. displodere*-infected *C. elegans* with a burst vulva. A micrograph of a live animal infected for 9 days with *N. displodere* and observed to have a burst vulva on the plate. This animal was picked to an agarose pad on a slide, calcofluor white (CFW) at 1:100 dilution was added to stain external spores, and imaged with a 63x objective on a Zeiss AxioImager M1 upright microscope. The vulva (Vu) is seen with *C. elegans* tissue seen inside the animal (outline with dashed lines) and outside the animal. *N. displodere* spores (Sp) are seen stained with CFW outside of the animal.
(TIF)

S13 Fig. *N. displodere*-infected animals with a burst vulva can transmit the infection to uninfected animals. Wild-type N2 animals infected with *N. displodere* for 8 days were split into two groups, intact animals and animals with a burst vulva. Twenty animals of each group were transferred to a fresh plate with starved ERT413 animals for 4 hours and then removed. ERT413 animals were grown at 15°C for 4 days and fixed for *N. displodere* rRNA FISH. Fifty GFP-positive animals were inspected for *N. displodere* infection per replicate. Data are represented as mean values with SD from two replicates from one experiment.
(TIF)

S14 Fig. Phylogenetic trees of putative cases of horizontal gene transfer. Phylogenetic trees of possible horizontal gene transfer involving (a) formamidopyrimidine-DNA glycosylase (NEDG_02224, *N. displodere*), (b) FAD binding oxidase (NEDG_00514, *N. displodere*), and (c) NAPE-2 (NEPG_01645, *N. parisii*; NERG_00761, *N.* sp. 1). Representative homologs of each *Nematocida* enzyme were used to infer trees with RAxML 8.2.4 using the PROTGAMMALG model and 1000 bootstrap replicates. Proteins belonging to the following groups were colored:

fungi (red), metazoans (blue), microsporidia (orange), bacteria (magenta), and nematodes (green). Bootstrap supports are indicated next to each node. Scale bars indicate changes per site. The tree was created with FigTree 1.4.2 (http://tree.bio.ed.ac.uk/software/figtree/).
(TIF)

S1 Video. Video of *N. displodere*-infected *C. elegans* with a burst vulva discharging spores. Video of a live animal infected with *N. displodere* for 9 days that was noticed to have a burst vulva on the plate. This animal was picked to an agarose pad on a slide and imaged with an 63x objective on a Zeiss AxioImager M1 upright microscope. Material is seen being discharged from the animal interior, through the burst vulva (Vu) and expelled to the exterior, including spore-shaped structure. The animal is still alive and the body can be seen subtly moving in the video.
(MOV)

S1 File. Taxonomic summary of *N. displodere*.
(DOCX)

S1 Table. Summary of genome assembly statistics.
(XLSX)

S2 Table. Summary of *N. displodere* genes.
(XLSX)

S3 Table. NemLGF1 proteins.
(XLSX)

Acknowledgments

A special thanks to Gaotian Zhang for helping in the early identification of the genus of *N. displodere*. We thank the *Caenorhabditis* Genetics Center, Jonathan Ewbank, Yishi Jin, Amy Pasquinelli, Sylvia Lee, and Andy Samuelson for *C. elegans* strains. Thanks to Lise Frézal for assistance with sampling and identifying wild nematodes. Thanks to Jimmy Becnel for his helpful comments on our TEM images. We thank Timothy Merloo and Ying Jones for preparing the TEM samples. Thanks to Robert Shoemaker for help with statistics and Reggie Harris for help with Latin and naming *N. displodere* (Mo). We thank Kirthi Reddy and Keir Balla for their helpful comments on the manuscript.

Author Contributions

Conceived and designed the experiments: RJL AWR MRB MAF. Performed the experiments: RJL LT MRB. Analyzed the data: RJL AWR LT. Wrote the paper: RJL AWR ERT. Discovered N. displodere: RJL MAF.

References

1. Frydman HM, Li JM, Robson DN, Wieschaus E. Somatic stem cell niche tropism in *Wolbachia*. Nature. 2006; 441(7092):509–12. doi: 10.1038/nature04756 PMID: 16724067.
2. Ryan CM, de Miguel N, Johnson PJ. *Trichomonas vaginalis*: current understanding of host-parasite interactions. Essays Biochem. 2011; 51:161–75. doi: 10.1042/bse0510161 PMID: 22023448.
3. Sin J, Mangale V, Thienphrapa W, Gottlieb RA, Feuer R. Recent progress in understanding coxsackievirus replication, dissemination, and pathogenesis. Virology. 2015; 484:288–304. doi: 10.1016/j.virol.2015.06.006 PMID: 26142496; PubMed Central PMCID: PMC4567421.
4. Abdelsamed H, Peters J, Byrne GI. Genetic variation in *Chlamydia trachomatis* and their hosts: impact on disease severity and tissue tropism. Future Microbiol. 2013; 8(9):1129–46. doi: 10.2217/fmb.13.80 PMID: 24020741; PubMed Central PMCID: PMC4009991.

5. Schilling JD, Mulvey MA, Hultgren SJ. Structure and function of *Escherichia coli* type 1 pili: new insight into the pathogenesis of urinary tract infections. J Infect Dis. 2001; 183 Suppl 1:S36–40. doi: 10.1086/318855 PMID: 11171011.

6. Takeuchi H, Matano T. Host factors involved in resistance to retroviral infection. Microbiol Immunol. 2008; 52(6):318–25. doi: 10.1111/j.1348-0421.2008.00040.x PMID: 18577167.

7. Toomey ME, Panaram K, Fast EM, Beatty C, Frydman HM. Evolutionarily conserved *Wolbachia*-encoded factors control pattern of stem-cell niche tropism in *Drosophila* ovaries and favor infection. Proc Natl Acad Sci U S A. 2013; 110(26):10788–93. doi: 10.1073/pnas.1301524110 PMID: 23744038; PubMed Central PMCID: PMC3696799.

8. Tsai YH, Disson O, Bierne H, Lecuit M. Murinization of internalin extends its receptor repertoire, altering *Listeria monocytogenes* cell tropism and host responses. PLoS Pathog. 2013; 9(5):e1003381. doi: 10.1371/journal.ppat.1003381 PMID: 23737746; PubMed Central PMCID: PMC3667765.

9. Cuomo CA, Desjardins CA, Bakowski MA, Goldberg J, Ma AT, Becnel JJ, et al. Microsporidian genome analysis reveals evolutionary strategies for obligate intracellular growth. Genome Res. 2012; 22 (12):2478–88. doi: 10.1101/gr.142802.112 PMID: 22813931; PubMed Central PMCID: PMC3514677.

10. Keeling PJ, Fast NM. Microsporidia: biology and evolution of highly reduced intracellular parasites. Annual review of microbiology. 2002; 56:93–116. doi: 10.1146/annurev.micro.56.012302.160854 PMID: 12142484.

11. Texier C, Vidau C, Vigues B, El Alaoui H, Delbac F. Microsporidia: a model for minimal parasite-host interactions. Curr Opin Microbiol. 2010; 13(4):443–9. doi: 10.1016/j.mib.2010.05.005 PMID: 20542726.

12. Williams BA. Unique physiology of host-parasite interactions in microsporidia infections. Cell Microbiol. 2009; 11(11):1551–60. doi: 10.1111/j.1462-5822.2009.01362.x PMID: 19673893.

13. Corradi N. Microsporidia: Eukaryotic Intracellular Parasites Shaped by Gene Loss and Horizontal Gene Transfers. Annual review of microbiology. 2015; 69:167–83. doi: 10.1146/annurev-micro-091014-104136 PMID: 26195306.

14. Didier ES, Khan IA. The Immunology of Microsporidiosis in Mammals. In: Weiss LM, Becnel JJ, editors. Microsporidia: Pathogens of Opportunity. Ames, IA: Wiley-Blackwell; 2014. p. 307–25.

15. Brothers KM, Newman ZR, Wheeler RT. Live imaging of disseminated candidiasis in zebrafish reveals role of phagocyte oxidase in limiting filamentous growth. Eukaryot Cell. 2011; 10(7):932–44. doi: 10.1128/EC.05005-11 PMID: 21551247; PubMed Central PMCID: PMC3147414.

16. de Vries RD, Lemon K, Ludlow M, McQuaid S, Yuksel S, van Amerongen G, et al. In vivo tropism of attenuated and pathogenic measles virus expressing green fluorescent protein in macaques. Journal of virology. 2010; 84(9):4714–24. doi: 10.1128/JVI.02633-09 PMID: 20181691; PubMed Central PMCID: PMCPMC2863733.

17. Félix M-A, Duveau F. Population dynamics and habitat sharing of natural populations of *Caenorhabditis elegans* and *C. briggsae*. BMC Biology. 2012; 10(1):59. doi: 10.1186/1741-7007-10-59

18. Troemel ER, Félix M-A, Whiteman NK, Barrière A, Ausubel FM. Microsporidia are natural intracellular parasites of the nematode *Caenorhabditis elegans*. PLoS biology. 2008; 6(12):2736–52. doi: 10.1371/journal.pbio.0060309 PMID: 19071962.

19. Bakowski MA, Priest M, Young S, Cuomo CA, Troemel ER. Genome Sequence of the Microsporidian Species *Nematocida* sp1 Strain ERTm6 (ATCC PRA-372). Genome Announc. 2014; 2(5). doi: 10.1128/genomeA.00905-14 PMID: 25237020; PubMed Central PMCID: PMC4172269.

20. Estes KA, Szumowski SC, Troemel ER. Non-lytic, actin-based exit of intracellular parasites from *C. elegans* intestinal cells. PLoS Pathogens. 2011; 7(9):e1002227. doi: 10.1371/journal.ppat.1002227 PMID: 21949650.

21. Szumowski SC, Botts MR, Popovich JJ, Smelkinson MG, Troemel ER. The small GTPase RAB-11 directs polarized exocytosis of the intracellular pathogen *N. parisii* for fecal-oral transmission from *C. elegans*. Proc Natl Acad Sci U S A. 2014; 111(22):8215–20. doi: 10.1073/pnas.1400696111 PMID: 24843160; PubMed Central PMCID: PMC4050618.

22. Vavra J, Lukes J. Microsporidia and 'the art of living together'. Adv Parasitol. 2013; 82:253–319. doi: 10.1016/B978-0-12-407706-5.00004–6 PMID: 23548087.

23. Hall DH, Altun ZF. *C. elegans* Atlas. Cold Spring Harbor, New York: Cold Spring Harbor Press; 2008.

24. Becnel JJ, Jeyaprakash A, Hoy MA, Shapiro A. Morphological and molecular characterization of a new microsporidian species from the predatory mite *Metaseiulus occidentalis* (Nesbitt) (Acari, Phytoseiidae). Journal of invertebrate pathology. 2002; 79(3):163–72. PMID: 12133705.

25. Félix M-A, Ashe A, Piffaretti J, Wu G, Nuez I, Bélicard T, et al. Natural and experimental infection of *Caenorhabditis* nematodes by novel viruses related to nodaviruses. PLoS Biology. 2011; 9(1): e1000586. doi: 10.1371/journal.pbio.1000586 PMID: 21283608.

26. Pujol N, Cypowyj S, Ziegler K, Millet A, Astrain A, Goncharov A, et al. Distinct innate immune responses to infection and wounding in the C. elegans epidermis. Current biology: CB. 2008; 18(7):481–9. doi: 10.1016/j.cub.2008.02.079 PMID: 18394898.

27. Bakowski MA, Desjardins CA, Smelkinson MG, Dunbar TA, Lopez-Moyado IF, Rifkin SA, et al. Ubiquitin-mediated response to microsporidia and virus infection in *C. elegans*. PLoS Pathog. 2014; 10(6): e1004200. doi: 10.1371/journal.ppat.1004200 PMID: 24945527; PubMed Central PMCID: PMC4063957.

28. Zugasti O, Bose N, Squiban B, Belougne J, Kurz CL, Schroeder FC, et al. Activation of a G protein-coupled receptor by its endogenous ligand triggers the innate immune response of *Caenorhabditis elegans*. Nat Immunol. 2014; 15(9):833–8. doi: 10.1038/ni.2957 PMID: 25086774; PubMed Central PMCID: PMC4139443.

29. Gems D, Sutton AJ, Sundermeyer ML, Albert PS, King KV, Edgley ML, et al. Two pleiotropic classes of *daf-2* mutation affect larval arrest, adult behavior, reproduction and longevity in *Caenorhabditis elegans*. Genetics. 1998; 150(1):129–55. PMID: 9725835; PubMed Central PMCID: PMC1460297.

30. George-Raizen JB, Shockley KR, Trojanowski NF, Lamb AL, Raizen DM. Dynamically-expressed prion-like proteins form a cuticle in the pharynx of *Caenorhabditis elegans*. Biol Open. 2014; 3 (11):1139–49. doi: 10.1242/bio.20147500 PMID: 25361578; PubMed Central PMCID: PMC4232772.

31. Xu Y, Weiss LM. The microsporidian polar tube: a highly specialised invasion organelle. Int J Parasitol. 2005; 35(9):941–53. doi: 10.1016/j.ijpara.2005.04.003 PMID: 16005007; PubMed Central PMCID: PMC3109658.

32. Solter LF. Epizootiology of Microsporidiosis in Invertebrate Hosts. In: Weiss LM, Becnel JJ, editors. Microsporidia: Pathogens of Opportunity. Ames, IA: Wiley-Blackwell; 2014. p. 165–94.

33. Cali A, Takvorian PM. Development Morphology and Life Cycles of the Microsporidia. In: Weiss LM, Becnel JJ, editors. Microsporidia: Pathogens of Opportunity. Ames, IA: Wiley-Blackwell; 2014. p. 71–133.

34. Foucault C, Drancourt M. Actin mediates *Encephalitozoon intestinalis* entry into the human enterocyte-like cell line, Caco-2. Microb Pathog. 2000; 28(2):51–8. doi: 10.1006/mpat.1999.0329 PMID: 10644491.

35. Weiss LM, Delbac F, Hayman JR, Pan G, Xiaoqun D, Zhou Z. The Microsporidian Polar Tube and Spore Wall. In: Weiss LM, Becnel JJ, editors. Microsporidia: Pathogens of Opportunity. Ames, IA: Wiley-Blackwell; 2014. p. 261–306.

36. Klee J, Besana AM, Genersch E, Gisder S, Nanetti A, Tam DQ, et al. Widespread dispersal of the microsporidian *Nosema ceranae*, an emergent pathogen of the western honey bee, *Apis mellifera*. Journal of invertebrate pathology. 2007; 96(1):1–10. doi: 10.1016/j.jip.2007.02.014 PMID: 17428493.

37. Solter LF, Siegel JP, Pilarska DK, Higgs MC. The impact of mixed infection of three species of microsporidia isolated from the gypsy moth, *Lymantria dispar* L. (Lepidoptera: Lymantriidae). Journal of invertebrate pathology. 2002; 81(2):103–13. PMID: 12445794.

38. Couillault C, Pujol N, Reboul J, Sabatier L, Guichou JF, Kohara Y, et al. TLR-independent control of innate immunity in *Caenorhabditis elegans* by the TIR domain adaptor protein TIR-1, an ortholog of human SARM. Nat Immunol. 2004; 5(5):488–94. doi: 10.1038/ni1060 PMID: 15048112.

39. Campbell SE, Williams TA, Yousuf A, Soanes DM, Paszkiewicz KH, Williams BA. The genome of *Spraguea lophii* and the basis of host-microsporidian interactions. PLoS Genet. 2013; 9(8):e1003676. doi: 10.1371/journal.pgen.1003676 PMID: 23990793; PubMed Central PMCID: PMC3749934.

40. Nakjang S, Williams TA, Heinz E, Watson AK, Foster PG, Sendra KM, et al. Reduction and expansion in microsporidian genome evolution: new insights from comparative genomics. Genome Biol Evol. 2013; 5(12):2285–303. doi: 10.1093/gbe/evt184 PMID: 24259309; PubMed Central PMCID: PMC3879972.

41. Deshaies RJ, Joazeiro CA. RING domain E3 ubiquitin ligases. Annu Rev Biochem. 2009; 78:399–434. doi: 10.1146/annurev.biochem.78.101807.093809 PMID: 19489725.

42. Desjardins CA, Sanscrainte ND, Goldberg JM, Heiman D, Young S, Zeng Q, et al. Contrasting host-pathogen interactions and genome evolution in two generalist and specialist microsporidian pathogens of mosquitoes. Nat Commun. 2015; 6:7121. doi: 10.1038/ncomms8121 PMID: 25968466; PubMed Central PMCID: PMC4435813.

43. Brenner S. The genetics of *Caenorhabditis elegans*. Genetics. 1974; 77(1):71–94. PMID: 4366476; PubMed Central PMCID: PMC1213120.

44. Frøkjaer-Jensen C, Davis MW, Hopkins CE, Newman BJ, Thummel JM, Olesen S-P, et al. Single-copy insertion of transgenes in *Caenorhabditis elegans*. Nature Genetics. 2008; 40(11):1375–83. doi: 10.1038/ng.248 PMID: 18953339.

45. Winston WM, Molodowitch C, Hunter CP. Systemic RNAi in *C. elegans* requires the putative transmembrane protein SID-1. Science. 2002; 295(5564):2456–9. doi: 10.1126/science.1068836 PMID: 11834782.

46. Dunbar TL, Yan Z, Balla KM, Smelkinson MG, Troemel ER. *C. elegans* detects pathogen-induced translational inhibition to activate immune signaling. Cell Host Microbe. 2012; 11(4):375–86. doi: 10.1016/j.chom.2012.02.008 PMID: 22520465; PubMed Central PMCID: PMC3334869.

47. Shimko TC, Andersen EC. COPASutils: an R package for reading, processing, and visualizing data from COPAS large-particle flow cytometers. PLoS One. 2014; 9(10):e111090. doi: 10.1371/journal.pone.0111090 PMID: 25329171; PubMed Central PMCID: PMC4203834.

48. Luallen RJ, Bakowski MA, Troemel ER. Characterization of microsporidia-induced developmental arrest and a transmembrane leucine-rich repeat protein in *Caenorhabditis elegans*. PLoS One. 2015; 10(4):e0124065. doi: 10.1371/journal.pone.0124065 PMID: 25874557; PubMed Central PMCID: PMC4395247.

49. Xu Y, Takvorian PM, Cali A, Orr G, Weiss LM. Glycosylation of the major polar tube protein of *Encephalitozoon hellem*, a microsporidian parasite that infects humans. Infect Immun. 2004; 72(11):6341–50. doi: 10.1128/IAI.72.11.6341–6350.2004 PMID: 15501763; PubMed Central PMCID: PMC523040.

50. Simpson JT, Wong K, Jackman SD, Schein JE, Jones SJ, Birol I. ABySS: a parallel assembler for short read sequence data. Genome Res. 2009; 19(6):1117–23. doi: 10.1101/gr.089532.108 PMID: 19251739; PubMed Central PMCID: PMC2694472.

51. Hyatt D, Chen GL, Locascio PF, Land ML, Larimer FW, Hauser LJ. Prodigal: prokaryotic gene recognition and translation initiation site identification. BMC Bioinformatics. 2010; 11:119. doi: 10.1186/1471-2105-11-119 PMID: 20211023; PubMed Central PMCID: PMC2848648.

52. Finn RD, Bateman A, Clements J, Coggill P, Eberhardt RY, Eddy SR, et al. Pfam: the protein families database. Nucleic acids research. 2014; 42(Database issue):D222–30. doi: 10.1093/nar/gkt1223 PMID: 24288371; PubMed Central PMCID: PMC3965110.

53. Suzek BE, Wang Y, Huang H, McGarvey PB, Wu CH, UniProt C. UniRef clusters: a comprehensive and scalable alternative for improving sequence similarity searches. Bioinformatics. 2015; 31(6):926–32. doi: 10.1093/bioinformatics/btu739 PMID: 25398609; PubMed Central PMCID: PMC4375400.

54. Li L, Stoeckert CJ Jr., Roos DS. OrthoMCL: identification of ortholog groups for eukaryotic genomes. Genome Res. 2003; 13(9):2178–89. doi: 10.1101/gr.1224503 PMID: 12952885; PubMed Central PMCID: PMC403725.

55. Edgar RC. MUSCLE: multiple sequence alignment with high accuracy and high throughput. Nucleic acids research. 2004; 32(5):1792–7. doi: 10.1093/nar/gkh340 PMID: 15034147; PubMed Central PMCID: PMC390337.

56. Capella-Gutierrez S, Silla-Martinez JM, Gabaldon T. trimAl: a tool for automated alignment trimming in large-scale phylogenetic analyses. Bioinformatics. 2009; 25(15):1972–3. doi: 10.1093/bioinformatics/btp348 PMID: 19505945; PubMed Central PMCID: PMC2712344.

57. Kuck P, Meusemann K. FASconCAT: Convenient handling of data matrices. Mol Phylogenet Evol. 2010; 56(3):1115–8. doi: 10.1016/j.ympev.2010.04.024 PMID: 20416383.

58. Darriba D, Taboada GL, Doallo R, Posada D. ProtTest 3: fast selection of best-fit models of protein evolution. Bioinformatics. 2011; 27(8):1164–5. doi: 10.1093/bioinformatics/btr088 PMID: 21335321.

59. Stamatakis A. RAxML version 8: a tool for phylogenetic analysis and post-analysis of large phylogenies. Bioinformatics. 2014; 30(9):1312–3. doi: 10.1093/bioinformatics/btu033 PMID: 24451623; PubMed Central PMCID: PMC3998144.

60. Eddy SR. Accelerated Profile HMM Searches. PLoS Comput Biol. 2011; 7(10):e1002195. doi: 10.1371/journal.pcbi.1002195 PMID: 22039361; PubMed Central PMCID: PMC3197634.

61. Kanehisa M, Sato Y, Morishima K. BlastKOALA and GhostKOALA: KEGG Tools for Functional Characterization of Genome and Metagenome Sequences. J Mol Biol. 2015. doi: 10.1016/j.jmb.2015.11.006 PMID: 26585406.

62. Petersen TN, Brunak S, von Heijne G, Nielsen H. SignalP 4.0: discriminating signal peptides from transmembrane regions. Nat Methods. 2011; 8(10):785–6. doi: 10.1038/nmeth.1701 PMID: 21959131.

63. Krogh A, Larsson B, von Heijne G, Sonnhammer EL. Predicting transmembrane protein topology with a hidden Markov model: application to complete genomes. J Mol Biol. 2001; 305(3):567–80. doi: 10.1006/jmbi.2000.4315 PMID: 11152613.

3.1 Taxonomic Summary of *N. displodere*

***Nematocida displodere* defines a new species**

(urn:lsid:zoobank.org:act:35CF055F-C311-4D9B-BFF0-B7B09FC441E4).

Its host is the nematode, *Caenorhabditis elegans*. It is orally transmitted, with no evidence of vertical transmission. There was no continuous route detected for new spore exit from infected nematodes. One means by which spores exit the host to be transmitted to new hosts is through infection-induced vulva bursting.

Life cycle and symptoms in the host.

Symptoms of infection are detected by Nomarski light microscopy as large roundish vesicle structures with multiple circular nuclei often in association with oblong spores. Symptoms are most often seen in tissues of the body wall of *C. elegans,* anywhere along the anterior/posterior axis, although the first occurrences of symptoms are seen along this axis between the *C. elegans* posterior bulb and anus. Occasionally these symptoms are seen in the intestine, but usually at late stages of infection. The replicative stages (meronts) are seen by Nomarski as early as 3 dpi at 15°C, and their association with spores are seen as early as 5 dpi at 15°C. Spores are usually seen in groups, and often appear to be in membrane-enclosed structures, as Brownian motion of groups of spores in live, infected animals is limited to small circular-like areas.

There were multiple sites of infection observed by rRNA FISH, including epidermis, muscle, neurons, intestine, coelomocytes, and seam cells. Newly formed spores were seen predominantly in the muscle and epidermis, but were occasionally seen in the neurons and intestine. All post-embryonic stages showed signs of infection, except the non-feeding dauer stage.

Only one spore size was observed, measuring 2.38 μm (+/- 0.26 μm) long and 1.03 μm (+/- 0.18 μm) wide. Externalized polar tubes were measured as 12.55 μm (+/- 3.20 μm), while internal polar tubes were observed by TEM with up to five polar tube coils per spores seen in radial cross-sections.

The type strain was isolated from a rotting *Asteraceae* stem near the Viosne stream in Santeuil, Val-d'Oise, Île-de-France, France (GPS coordinates: 49.12165, 1.95101) on September 30, 2014.

The etymology of the type species name *N. displodere* is based on the host infection phenotype whereby infected nematodes burst from the vulva and release spores.

3.2 Supplemental Figures and Tables

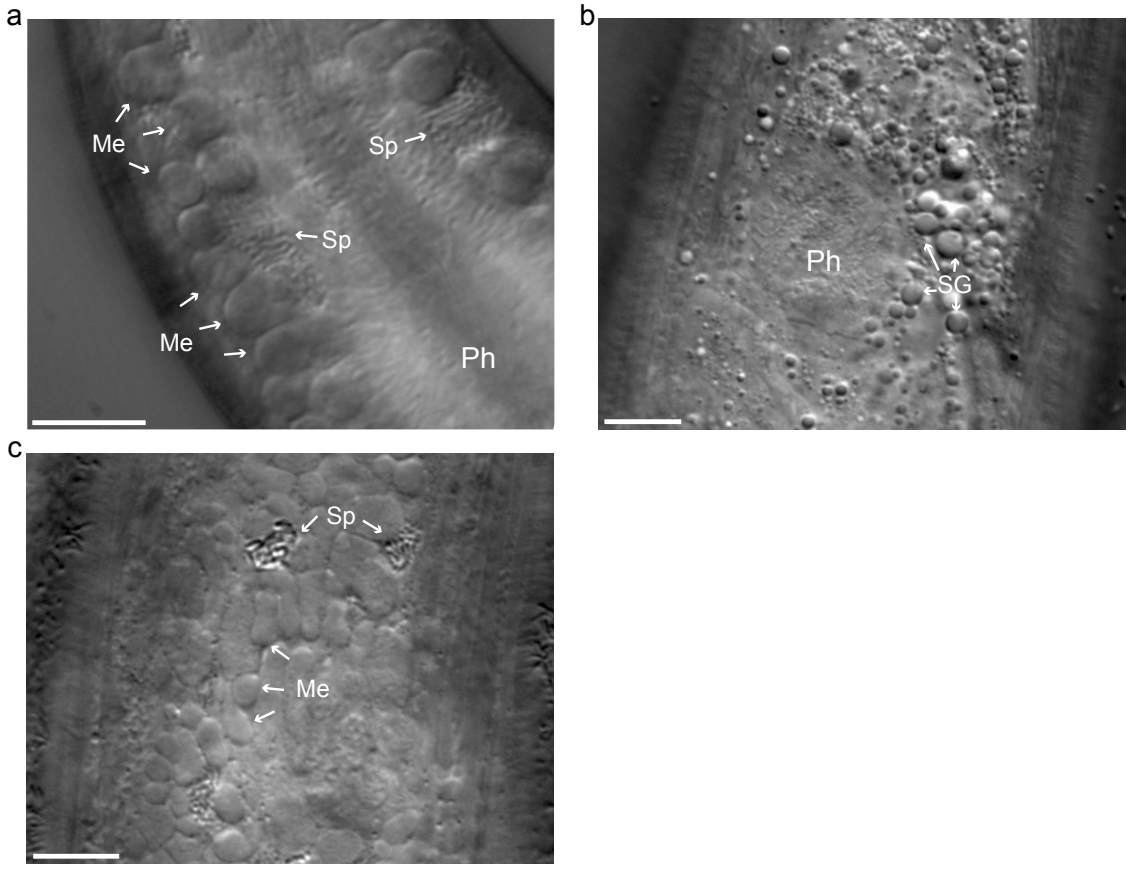

Figure 3-S1. Identification of microsporidia infection in the body wall of a wild *C. elegans*
(a) The head region of a wild-caught *C. elegans* animal with structures resembling microsporidia at different stages of infection, including meronts (*Me*) and groups of spores (*Sp*). The pharynx (*Ph*) is indicated for orientation. (b) The head region of a live, uninfected N2 *C. elegans* for comparison, with storage granules (*SG*) indicated. (c) Infected mid-body region of a live animal from strain JU2807 (progeny of the animal shown in Panel a) showing both meront-like structures and groups of spores. Scale bars are 10 μm.

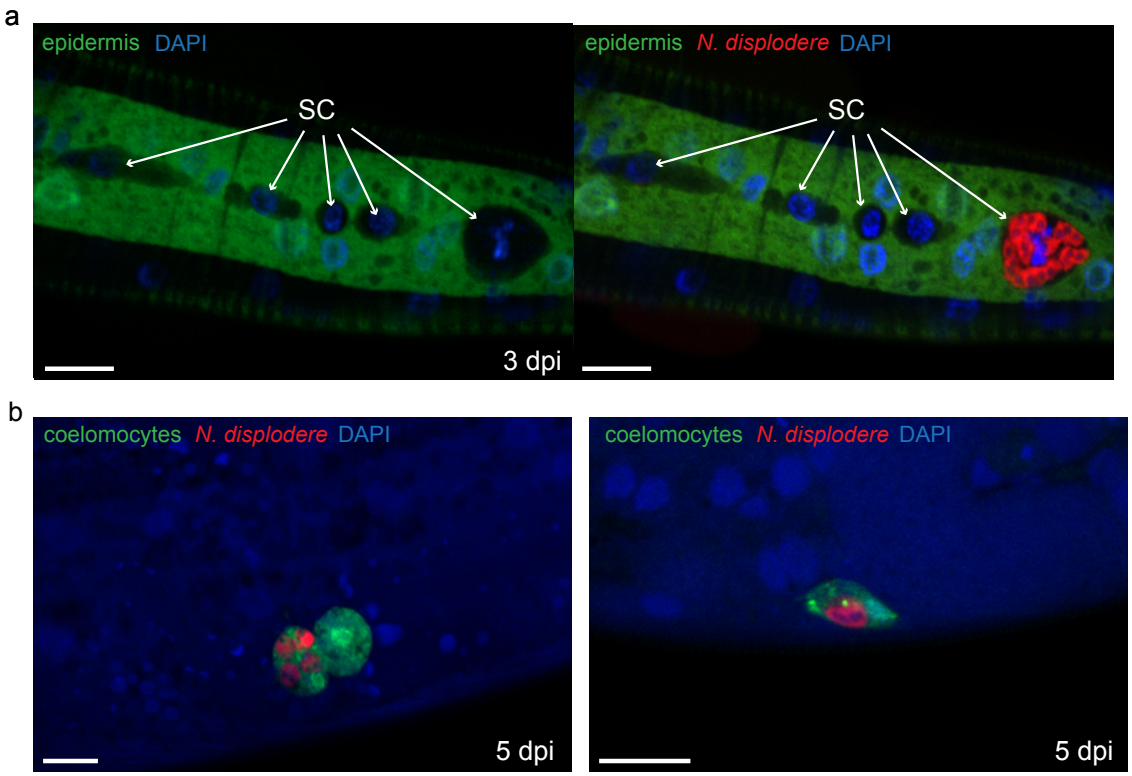

Figure 3-S2. *N. displodere* proliferation in seam cells and coelomocytes
(a) *C. elegans* strain AU189 expressing GFP in the epidermis was infected with *N. displodere* and fixed at 3 dpi for *N. displodere* rRNA FISH and counterstained with DAPI. Seam cells (SC) were identified as nuclei-containing, GFP-negative cells within the GFP-positive epidermis, in the top or bottom plane of the animal laying on its left or right side. Images without (*left*) or with (*right*) the red channel (*N. displodere* FISH) are shown. (b) *C. elegans* strain OH910 expressing GFP in coelomocytes was infected with *N. displodere* and fixed at 5 dpi for *N. displodere* rRNA FISH and counterstained with DAPI. Two images of two separate animals are shown with meronts inside coelomocytes. Scale bars are 10 μm.

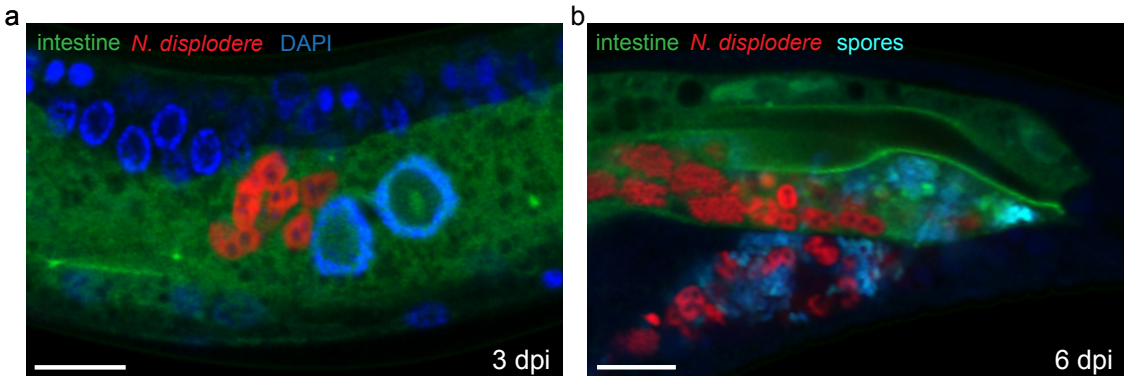

Figure 3-S3 *N. displodere* proliferation and differentiation is occasionally observed in the intestine

(a) *C. elegans* intestinal-specific GFP-expression strain ERT413 was infected with *N. displodere* and fixed at 3 dpi for *N. displodere* rRNA FISH and DAPI. Meronts are seen in the GFP-labeled intestine. (b) Strain ERT413 was infected with *N. displodere* and treated as above at 6 dpi, except DY96 was used to stain spores. Meronts and spores are observed both inside and outside of the GFP-labeled intestine. Scale bars are 10 μm.

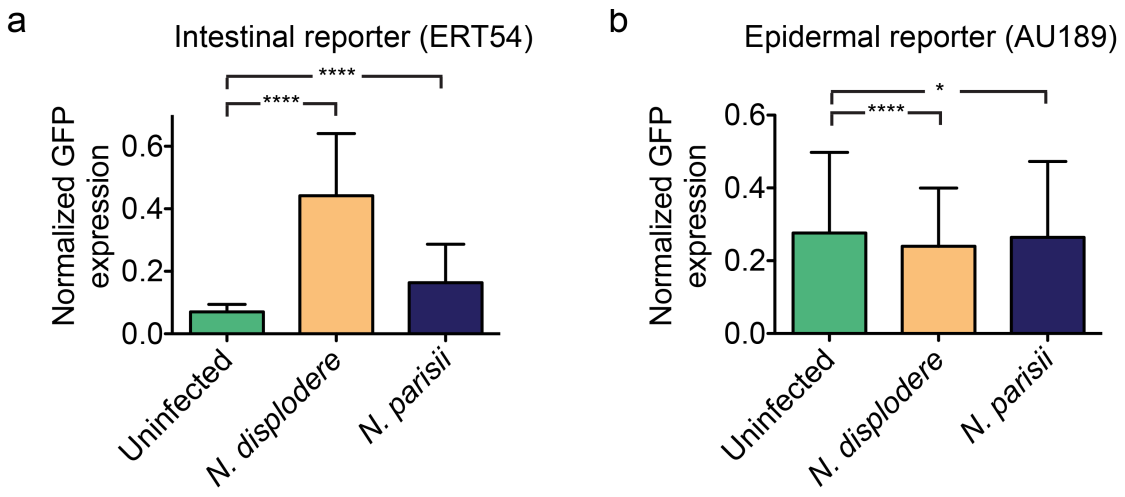

Figure 3-S4. *N. displodere* infection of *C. elegans* intestinal and epidermal reporter strains

(a) Normalized GFP induction of an intestinal infection reporter strain (ERT54 *C17H1.6p::GFP*) after *N. displodere* or *N. parisii* infection. Signal was normalized by body size using time of flight on the COPAS Biosort. Data are represented as mean values with SD from n=1800 animals from six replicates across two independent experiments (****p<0.0001, two-tailed Mann-Whitney test). (b) Another independent experiment showing GFP induction of the epidermal damage/infection reporter strain AU189 after *N. displodere* or *N.parisii* infection (for the other independent replicates see Fig 5a). Animals were normalized by red fluorescence (*pcol12::dsred*). Data show mean values with SD from n=900 animals across three replicates (***p<0.0001, *p=0.038, two-tailed Mann-Whitney test).

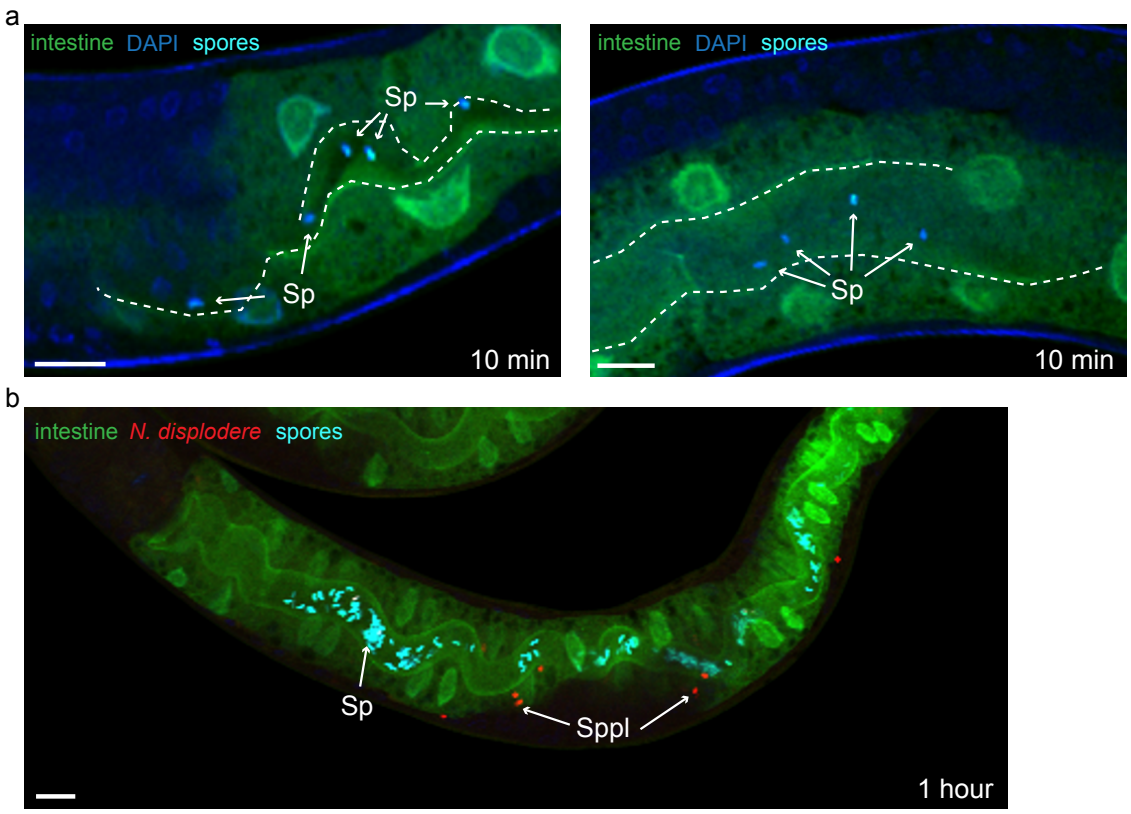

Figure 3-S5. *N. displodere* spores are observed in the intestinal lumen
(a) *C. elegans* strain ERT413 expressing GFP in the intestine was infected at the L4 stage with *N. displodere* for 10 m and fixed for staining by DAPI (blue) and DY96 (turquoise). Spores (*Sp*) are seen as DY96-positive oval structures in the intestinal lumen, delineated by dashed lines. (b) *C. elegans* strain ERT413 expressing GFP in the intestine was infected at the L3 stage with *N. displodere* for 1 hour and stained for *N. displodere* rRNA FISH and DY96. Scale bars are 10 μm.

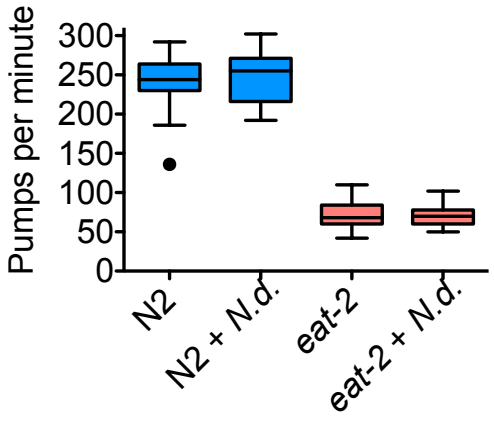

Figure 3-S6. Pharyngeal pumping of *eat-2* mutants
Tukey boxplots of N2 and *eat-2* pharyngeal pumping rates with or without *N. displodere* (*N.d.*) infection at 15°C from n=50 animals examined in two independent replicates. The lines indicate the median, the box extends from the 25th to 75th percentiles, and the whiskers extend to the minimum and maximum data point, excluding an outlier (indicated with a black dot).

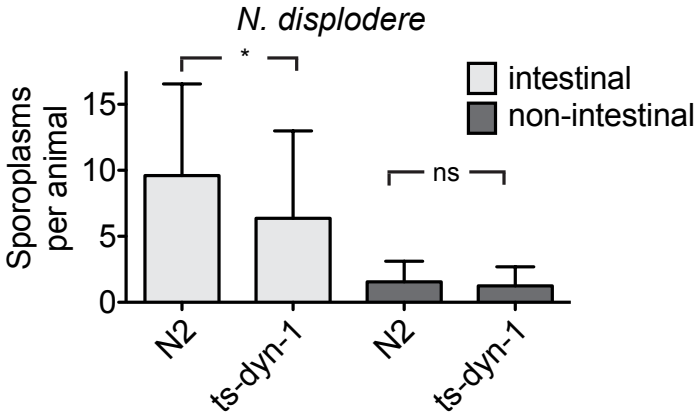

Figure 3-S7. Infection comparison between N2 and *dyn-1(ts)* at the permissive temperature

Comparison of the number of invasion events (counted as sporoplasms) occurring in *dyn-1(ts)* and N2 animals after *N. displodere* infection at 20°C for 30 min. Events were counted as either intestinal or non-intestinal. Data are represented as mean values with SD from n=25 animals from one experiment (*p=0.038, ns=not significant (p=0.432), two-tailed Mann-Whitney test).

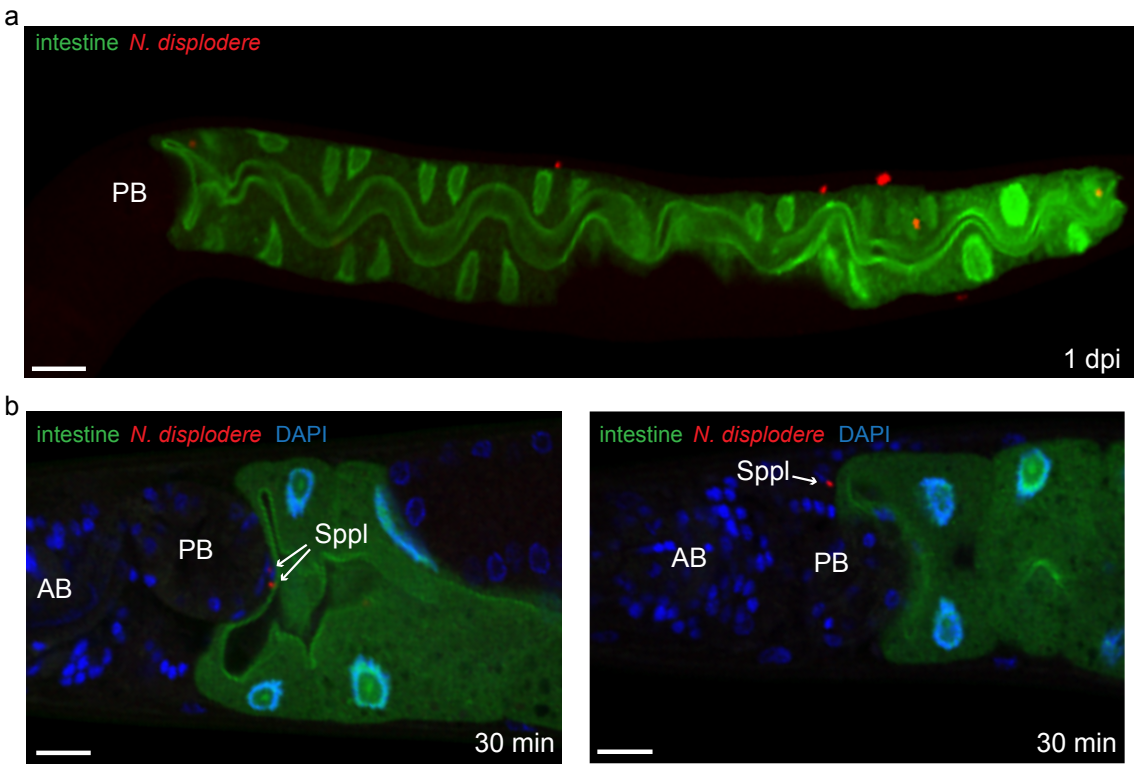

Figure 3-S8. *N. displodere* invasion events are seen in close proximity to the intestine

(a) *C. elegans* strain ERT413 expressing GFP in the intestine was infected as L1 larvae with *N. displodere* and fixed at 1 dpi for *N. displodere* rRNA FISH. Sporoplasms are seen inside and outside of the GFP-labeled intestine, in close proximity to the intestine, but never anterior to the posterior bulb (*PB*). (b) Strain ERT413 was infected as adults for 30 min with *N. displodere* and treated as above. Sporoplasms (*SppI*) in the anterior region are observed in close proximity to the wide intestinal lumen at the anterior part of the intestine. The anterior bulb (*AB*) and posterior bulb (*PB)* of the pharynx are indicated. Scale bars are 10 μm.

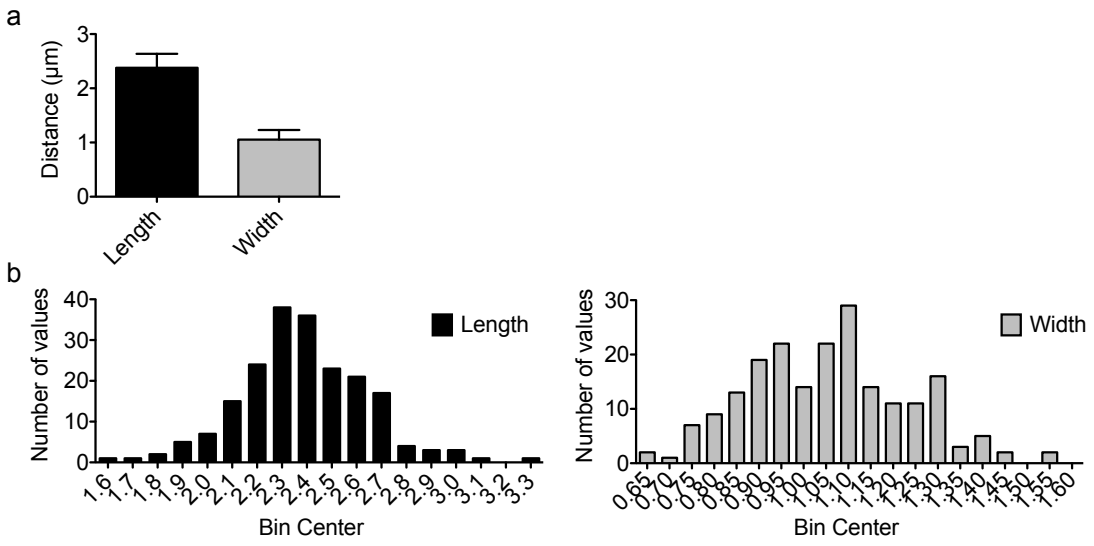

Figure 3-S9. Measurement *N. displodere* spore size
(a) The graph depicts mean length and width of *N. displodere* spores with SD from n=202 CFW-stained spores. (b) The histogram depicts the frequency distribution of *N. displodere* spore lengths (*left*) and widths (*right*).

a

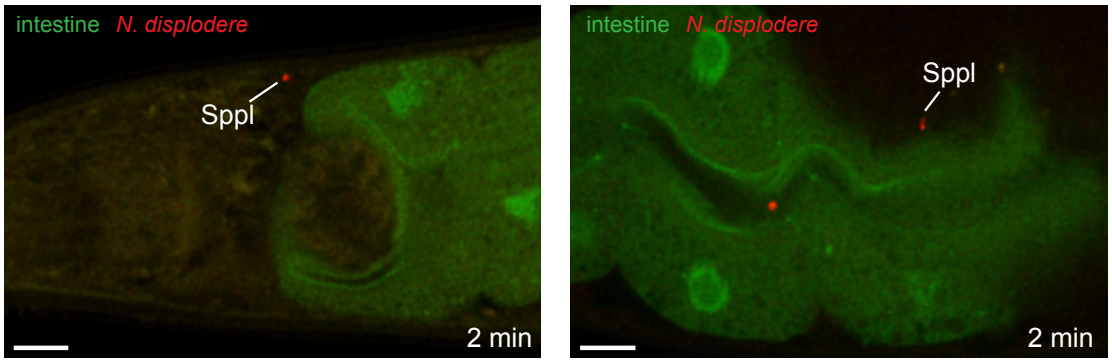

Figure 3-S10. *N. displodere* invasion events are seen in non-intestinal tissues as early as 2 minutes post-infection

(a) *C. elegans* strain ERT413 expressing GFP in the intestine was infected as L4 larvae with *N. displodere* and fixed at 2 minutes post-infection for *N. displodere* rRNA FISH. Sporoplasms (*Sppl*) are seen outside of the GFP-labeled intestine. Scale bar = 10 μm

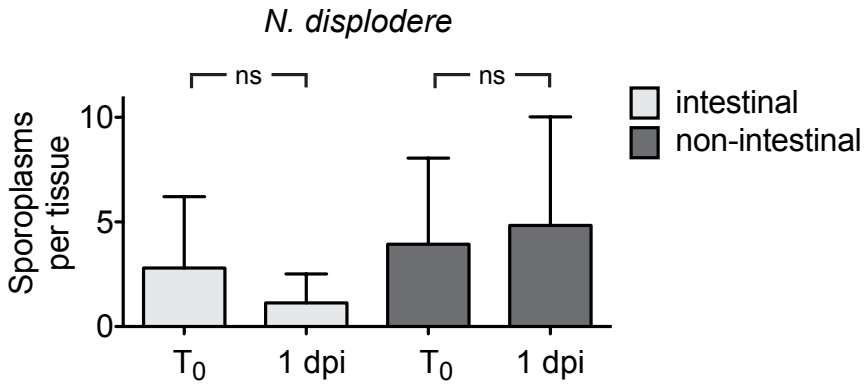

Figure 3-S11. Non-intestinal *N. displodere* infection remains unchanged over time after a pulse infection

Comparison of the number of invasion events (counted as sporoplasms) occurring when L3 animals of ERT413 were infected with *N. displodere* spores for 1 hour and immediately fixed (T_0) or washed to remove spores and allowed to grow at 15°C for an additional 24 hours (1 dpi). Events were counted as either intestinal or non-intestinal based on localization with intestinal GFP. Data are represented as mean values with SD from n=30 animals from one experiment (ns=not significant, two-tailed Mann-Whitney test).

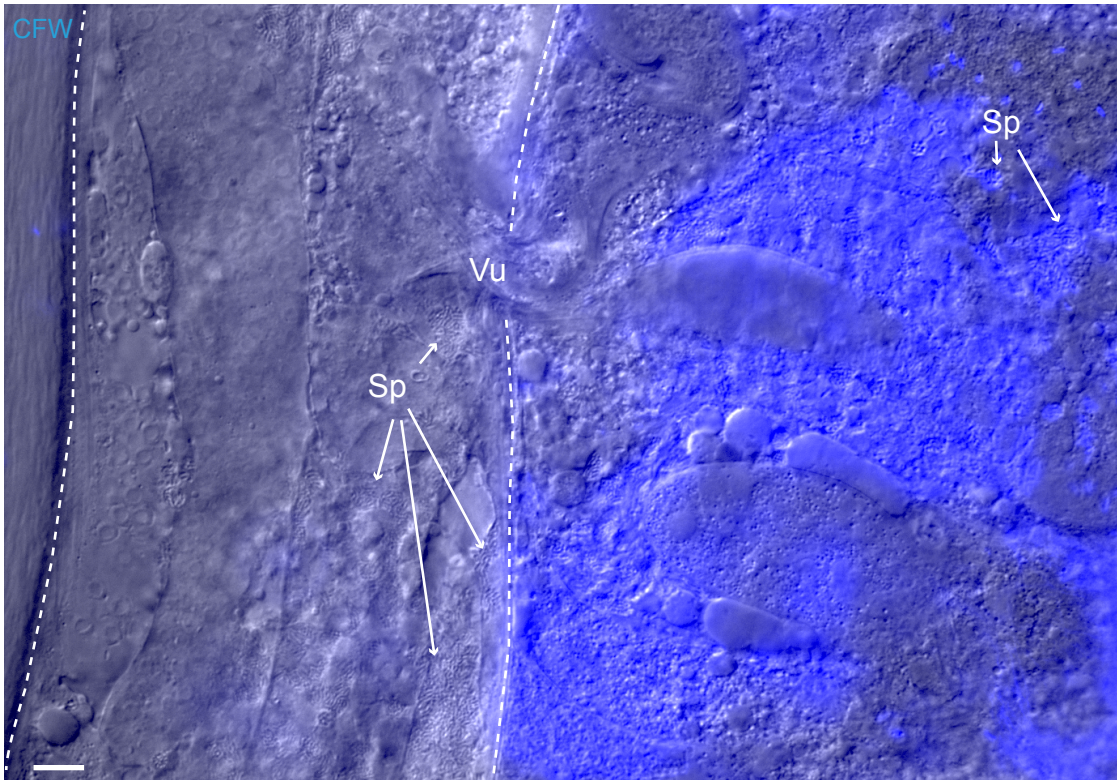

Figure 3-S12. *N. displodere*-infected *C. elegans* with a burst vulva
A micrograph of a live animal infected for 9 days with *N. displodere* and observed to have a burst vulva on the plate. This animal was picked to an agarose pad on a slide, calcofluor white (CFW) at 1:100 dilution was added to stain external spores, and imaged with a 63x objective on a Zeiss AxioImager M1 upright microscope. The vulva (Vu) is seen with *C. elegans* tissue seen inside the animal (outline with dashed lines) and outside the animal. *N. displodere* spores (Sp) are seen stained with CFW outside of the animal.

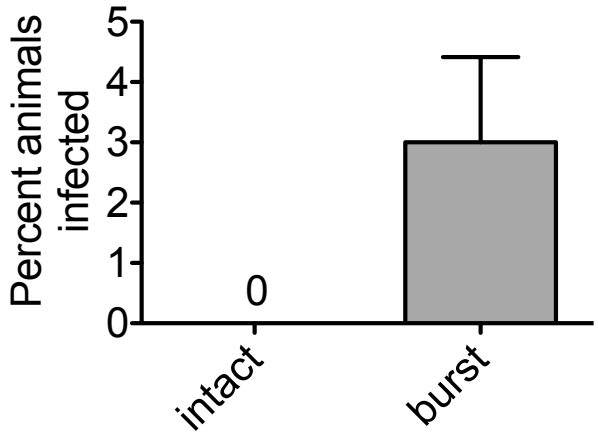

Figure 3-S13. *N. displodere*-infected animals with a burst vulva can transmit the infection to uninfected animals

Wild-type N2 animals infected with *N. displodere* for 8 days were split into two groups, intact animals and animals with a burst vulva. Twenty animals of each group were transferred to a fresh plate with starved ERT413 animals for 4 hours and then removed. ERT413 animals were grown at 15°C for 4 days and fixed for *N. displodere* rRNA FISH. Fifty GFP-positive animals were inspected for *N. displodere* infection per replicate. Data are represented as mean values with SD from two replicates from one experiment.

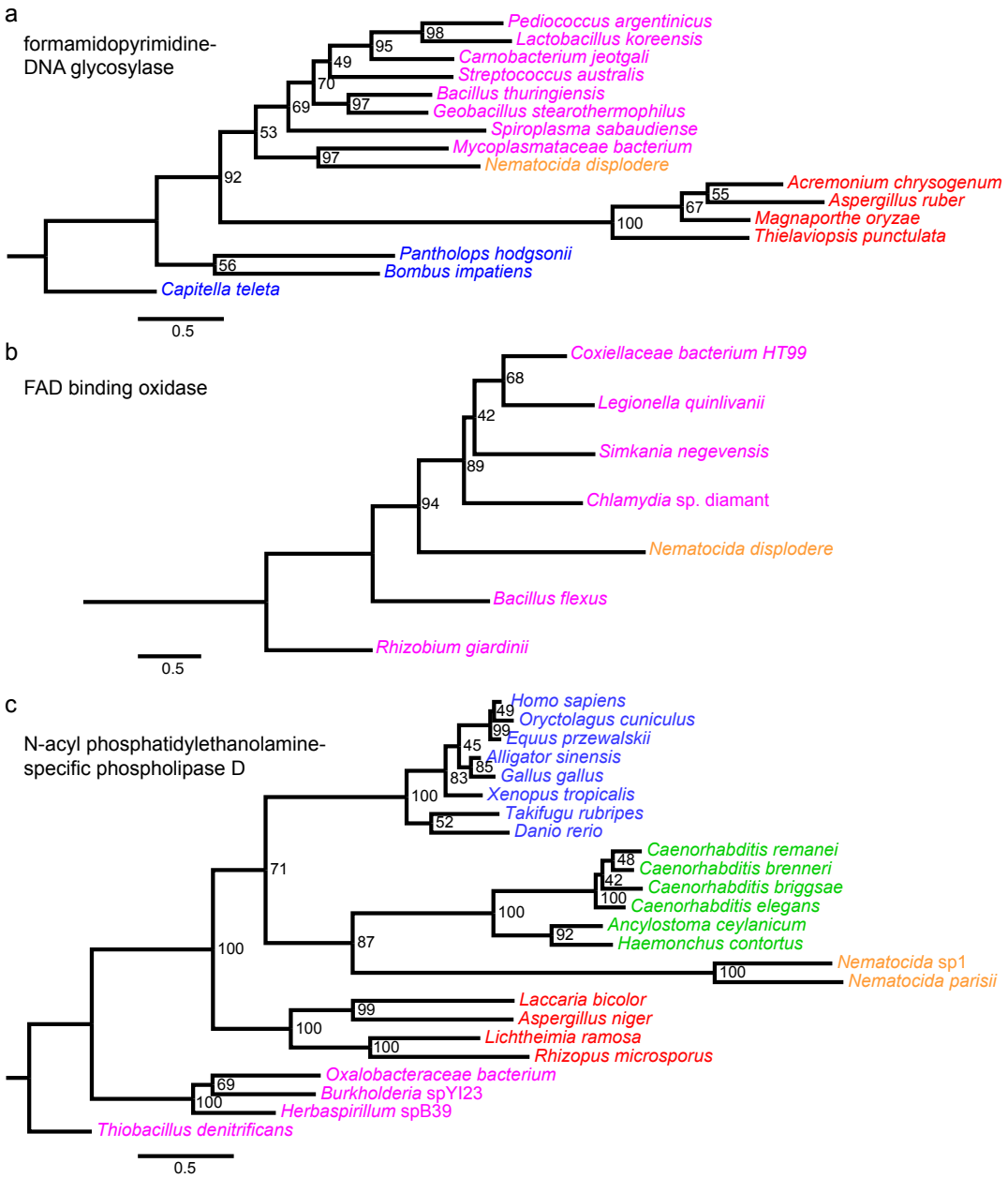

Figure 3-S14. Phylogenetic trees of putative cases of horizontal gene transfer
Phylogenetic trees of possible horizontal gene transfer involving (a) formamido-pyrimidine-DNA glycosylase (NEDG_02224, *N. displodere*), (b) FAD binding oxidase (NEDG_00514, *N. displodere*), and (c) NAPE-2 (NEPG_01645, *N. parisii*; NERG_00761, *N.* sp. 1). Representative homologs of each *Nematocida* enzyme were used to infer trees with RAxML 8.2.4 using the PROTGAMMALG model and 1000 bootstrap replicates. Proteins belonging to the following groups were colored: fungi (red), metazoans (blue), microsporidia (orange), bacteria (magenta), and nematodes (green). Bootstrap supports are indicated next to each node. Scale bars indicate changes per site. The tree was created with FigTree 1.4.2 (http://tree.bio.ed.ac.uk/software/figtree/).

Table 3-S1. Summary of genome assembly statistics

Species	Strain (assembly)	Total sequence length	Total assembly gap length	Number of contigs	Contig N50	Contig L50	Number of scaffolds	Scaffold N50	Scaffold L50	Proteins	% Orthogroups conserved
Spraguea lophii	42_110 (Sprlop1.0)	4980876	0	1392	5952	232	N/A	N/A	N/A	2499	95.9
Nosema bombycis	CQ1 (NosBomCQ1_v1.0)	15689776	1333150	3558	6053	696	1607	57394	47	4468	92.5
Mitosporidium daphniae	(UGP1.0)	5636959	0	612	32031	51	N/A	N/A	N/A	3330	78.4
Nematocida displodere	JUm2807 (Nema_displodere_ERTm0_V1)	3066405	9219	69	2E+05	4	42	440850	3	2278	100.0
Nematocida sp. 1	ERTm2 (Nema_parisii_ERTm2_V1)	4700711	51068	289	1E+05	10	202	733311	3	2770	100.0
Nematocida parisii	ERTm3 (Nema_parisii_ERTm3_V1)	4147597	26210	96	2E+05	9	53	567515	3	2726	99.7
Ordospora colligata	OC4 (ASM80326v1)	2290528	0	15	2E+05	5	N/A	N/A	N/A	1820	99.2
Enterocytozoon bieneusi	H348 (ASM20948v1)	3860738	1000	1743	1977	145	1733	1983	136	3632	87.7
Encephalitozoon hellem	ATCC 50504 (ASM27781v3)	2251784	0	12	2E+05	6	N/A	N/A	N/A	1846	100.0
Trachipleistophora hominis	(ASM31613v1)	8498182	791627	1632	9528	212	310	50307	46	3212	97.1
Encephalitozoon cuniculi	GB-M1 (ASM9122v1)	2497519	800	12	2E+05	6	N/A	N/A	N/A	1996	100.0
Encephalitozoon intestinalis	ATCC 50506 (ASM14646v1)	2216898	100	12	2E+05	6	N/A	N/A	N/A	1939	100.0
Encephalitozoon romaleae	SJ-2008 (ASM28003v2)	2187595	0	13	2E+05	6	N/A	N/A	N/A	1831	99.7
Vittaforma corneae	ATCC 50505 (Vitt_corn_V1)	3213516	64779	314	50887	22	220	114968	9	2239	99.7
Vavraia culicis	subsp. floridensis (Vavr_culi_floridensis_V1)	6118689	84852	501	54534	34	379	94471	21	2773	100.0
Edhazardia aedis	USNM 41457 (Edha_aedis_V4b)	51348006	599171	2379	1E+05	126	N/A	N/A	N/A	4190	98.4
Anncaliia algerae	PRA339 (Annc_alge_insect_USDA_JJB_V2)	12163397	2285449	3295	5402	520	431	71704	36	3659	98.7
Nosema apis	BRL 01 (NapisBRLv01)	8569501	55615	1133	14029	181	554	24319	90	2764	88.5
Nosema ceranae	PA08 1199 (ASM98816v1)	5690748	0	536	42592	35	N/A	N/A	N/A	3209	100.0

3.3 Additional Acknowledgements

Chapter 3, in full, is reprinted from Luallen RJ, Reinke AW, Tong L, Botts MR, Félix M-A, Troemel ER (2016) Discovery of a Natural Microsporidian Pathogen with a Broad Tissue Tropism in *Caenorhabditis elegans*, PLoS Pathogens 12(6): e1005724, doi:10.1371/journal.ppat.1005724 with permission from Public Library of Science (PLoS). The dissertation author was the primary investigator and author of this material. Author contributions to manuscript are as follows: Luallen, R contributed the research for Figures 1-6, except Figure 5b, and the supplemental information in S1-S13 Figures; Reinke, A contributed the genome sequencing and analysis of *N. displodere* represented in Figure 7 and supplemental information in S14 Figure and S1-S3 Tables, Tong, L in conjunction with Luallen, R contributed to Figure 1d and S9 Figure; Botts, M contributed Figure 5b. Félix, M-A co-discovered the new species *N. displodere* and initial work with this new species was conducted in her laboratory at École Normale Supérieure, Institut de Biologie de l'ENS (IBENS), Paris, France thanks to NSF Graduate Research Opportunities Worldwide Fellowship to Luallen, R.

4. Cell-to-cell spread of microsporidia causes *C. elegans* organs to form syncytia.

4.1 Summary

The growth of pathogens is dictated by their interactions with the host environment. Many obligate intracellular pathogens undergo several cellular decisions as they progress through their life cycles inside of host cells. We studied this process for several species of microsporidia in the genus *Nematocida* in their co-evolved animal host *Caenorhabditis elegans*. We found that microsporidia can restructure multicellular host tissues into a single contiguous multinucleate cell. In particular, we found that all three *Nematocida* species we studied were able to spread across the cells of *C. elegans* tissues before forming spores, with two species causing syncytial formation in the intestine, and one species causing syncytial formation in the muscle. We also found that the decision to switch from replication to differentiation in *N. parisii* was altered by the density of infection, suggesting that environmental cues influence the dynamics of the pathogen life cycle. These findings show how microsporidia can maximize the use of host space for growth, and that environmental cues in the host can regulate a developmental switch in the pathogen.

4.2 Introduction

Intracellular pathogens are a diverse category of microbes that rely on the space and resources of their host organisms for replication. After invasion of a single host cell, it is beneficial for intracellular pathogens to spread to other cells to maximize the use of host space for replication before exiting and spreading to new hosts. Several strategies that aid pathogen dissemination within a host have been described for bacterial and viral pathogens. For example, bacterial pathogens in the genera *Listeria*, *Shigella*, and *Rickettsia* have been shown to utilize host actin to move between host

cells by inducing the uptake of a bacterium-containing host cell protrusion into a neighboring cell, thereby avoiding contact with the extracellular space during dissemination [1-3]. Vaccinia viruses have been shown to use host actin in a comparable fashion to spread between host cells [4]. In contrast, several other viruses avoid the extracellular space during spreading by coordinating the fusion of infected host cells with neighboring uninfected host cells to form syncytia [5]. The Gram-negative bacteria *Burkholderia* can also cause host cell fusion as a means for spreading, and fusion is independent of host actin [6]. In addition to spreading through an irreversible fusion of host cells, a recent study found that the bacterial pathogens *Francisella tularensis* and *Salmonella enterica* can be transferred to uninfected cells through an exchange of host cytoplasmic material during partial and temporary fusions of host cells in a process termed trogocytosis [7]. These *in vitro* studies outline a set of growth strategies used by intracellular pathogens to expand their access to host space while remaining inside of host cells, although pathogen dissemination *in vivo* can involve alternative mechanisms. For example, *L. monocytogenes* can cross the barrier of intestinal epithelial cells without host actin via transcytosis into the basal extracellular space [8]. Because animals are composed of diverse and dynamic cells with complex structure, *in vivo* investigations are necessary to understand the relevant mechanisms utilized by intracellular pathogens to grow and spread within the host.

In vivo studies are particularly important for studying infection by eukaryotic pathogens, which have especially complex growth dynamics often involving various stages of differentiation that can take place in several specific host environments [9]. Apicomplexan parasites in the genus *Plasmodium*, the causative agents of malaria, require both a Dipteran insect and vertebrate host to complete their life cycle, which

has several stages and takes place in many tissues of both hosts. One example of an intracellular strategy used by *Plasmodium* pathogens to spread into uninfected cells involves replicating in large multinucleate structures called merozoites that bud off from liver cells in compartments surrounded by host membrane in transit to a new tissue [10]. Growing and spreading throughout the *Plasmodium* life cycle likely involves several host- and tissue-specific strategies, most of which are not currently understood. Indeed, little is known about dissemination strategies for any eukaryotic pathogen. This gap in our understanding is in part due to the complex nature of the life cycles of eukaryotic pathogens and the host tissues in which they grow.

Microsporidia comprise a large phylum of eukaryotic obligate intracellular pathogens that have multi-stage life cycles. There are more than 1400 species of microsporidia, and they can infect animals ranging from single-celled ciliates to humans [11,12]. The life cycles of microsporidia can be broadly categorized into a replication phase and a spore phase, although various subdivisions of the life cycle have been inferred from diverse morphological data [13]. To initiate infection, a unique microsporidian infection apparatus called a polar tube is thought to pierce the host cell membrane and inject spore contents directly into the host cytoplasm [14]. Replication by many species of microsporidia is carried out in direct contact with the host cytoplasm, and is characterized by nuclear duplication without cell division yielding multinucleate structures called meronts [13]. The final stage of the microsporidia life cycle involves differentiation from meronts into spores, which can exit the host cell and transmit infection. Our understanding of microsporidia growth comes from studies of cells or animals with constant exposure to relatively high levels of pathogen. As such,

we currently lack an understanding of the progression that a single microsporidia cell takes as it grows within a single host cell of an intact animal to complete its life cycle.

Caenorhabditis elegans is a powerful model system for studying infection by intracellular pathogens in a whole-animal host [15]. Several species of microsporidia in the genus *Nematocida* have been isolated from wild-caught nematodes around the world [16-18]. *Nematocida* species appear to have a life cycle that is generally similar to other microsporidia: after invasion of host cells, *Nematocida* cells replicate in the form of meronts and then differentiate into spores to exit the host cell and propagate infection [17-20]. The best-characterized species is *Nematocida parisii*, which invades and replicates exclusively in the intestine [18]. We recently identified another species of *Nematocida* called *N. displodere*, which invades several tissues including the intestine, muscle, epidermis, and nervous system [17]. *C. elegans* and *Nematocida* species can impart selective pressure on each other, suggesting that these host/pathogen pairs likely co-evolve in the wild [21]. The transparency and invariant cellular topology of *C. elegans* together with a collection of their natural microsporidian pathogens provides an ideal system for studying how microsporidia have evolved to grow in dynamic hosts with complex structure.

Here, we characterize the dynamics of the microsporidia life cycle *in vivo* by inoculating *C. elegans* animals with a single pathogen cell in a single host cell. We find that there is a lag phase after invasion, after which growth and replication continues exponentially until sporulation. Surprisingly, *N. parisii* spreads across more than half of the host intestinal cells during the replication phase of growth. By imaging live animals we find that *N. parisii* spreads across host intestinal cell boundaries, causing them to fuse into syncytia that share cytoplasmic space. Growth across host cells before

sporulation is a shared property for *Nematocida* species that infect distinct tissues, suggesting that this strategy is conserved for microsporidia. While growth by inducing host cell fusion is shared between *Nematocida* species, there is variation in the tissues that are fused, the speed of growth, and the fitness effects these species have in the host. *N. parisii* and *N.* sp. 1 both grow in the intestine, but *N.* sp. 1 grows faster, spreads more, forms spores sooner, and has a larger negative effect on host fitness than *N. parisii*. Additionally, we find that the pathogen decision to differentiate into spores happens sooner in smaller and denser growth environments. These experiments identify a novel and conserved growth strategy for microsporidia not seen before among eukaryotic pathogens, and illustrate how the host environment influences microsporidia growth and differentiation.

4.3 Results

4.3.1 Intracellular infection by a single microsporidian cell grows to occupy most of the *C. elegans* intestine

To characterize the *in vivo* growth dynamics of microsporidia, we measured the progression of infection in hosts by generating populations of synchronized infections consisting of a single parasite cell in a single intestinal cell. We pulse-inoculated *C. elegans* with a low dose of *N. parisii* spores to obtain infected populations where most animals were either uninfected, or infected with a single microsporidian cell in a single intestinal cell (Table 4-S1). To visualize infection, we fixed a fraction of the population at various hours post-inoculation (hpi) and stained using a fluorescence *in situ* hybridization (FISH) probe that targets the *N. parisii* small subunit rRNA. At 3 hpi, we

found that *N. parisii* cells are small and irregularly shaped, with a single nucleus (Figure 4-1a). *N. parisii* cells with two nuclei were not observed until 18 hpi (Figure 4-1b), indicating that replication only occurs after a significant lag time post-infection. By 36 hpi *N. parisii* had grown to spread across several host intestinal cells (Figure 4-1c). No spores had formed at this time, indicating that *N. parisii* was able to grow across the lateral cell boundaries of neighboring intestinal cells before differentiating into what was previously thought to be the only stage of the microsporidia life cycle able to escape a host cell. New spores were first observed to form at 52 hpi, and by this time *N. parisii* had grown to fill a large fraction of the intestine (Figure 4-1d). We observed what appeared to be different stages of sporulation, indicated by morphological transitions from tubular meronts to budding rounded structures, rod-shaped forms surrounded by diffuse chitin, and smaller rod-shaped cells that stained brightly for chitin, which we loosely define as late meronts, immature spores, and mature spores, respectively (Figure 4-1e). In addition to defining the transitions that single *N. parisii* cells took through the life cycle as they grew, we observed that meronts grew roughly contiguously in large interconnected structures (Figure 4-1c-e). We quantified the growth in size of single microsporidia cell infections, and found that initially *N. parisii* took up a miniscule fraction of one *C. elegans* intestinal cell but grew rapidly to take up more than half the space of the entire intestine by the time new spores were formed (Figure 4-1f).

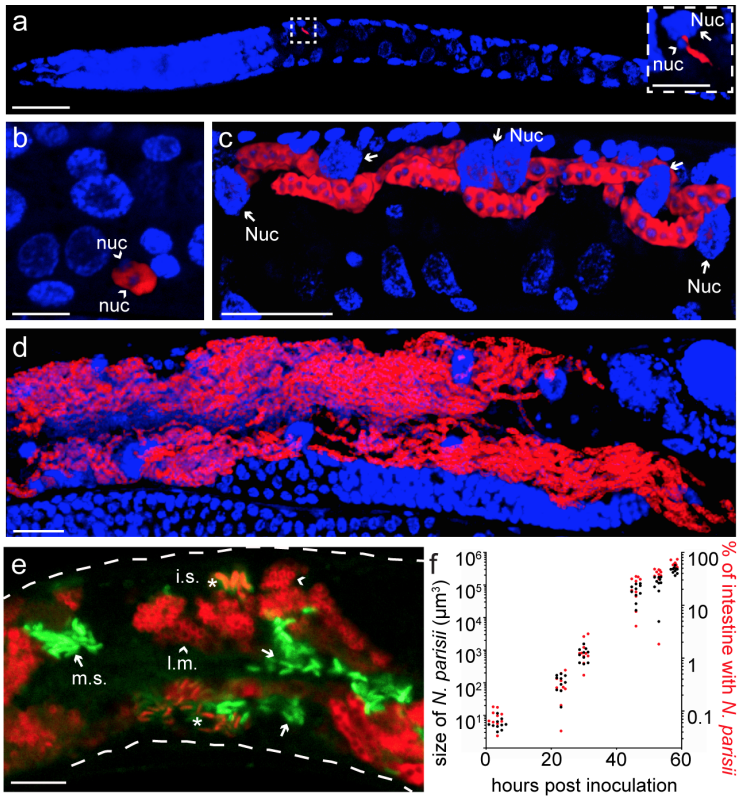

Figure 4-1 . A single *N. parisii* cell can grow to fill most of the *C. elegans* intestine.

(a-d) Animals infected by a single N. parisii cell, then fixed and stained for DNA with DAPI (blue) and for *N. parisii* with an rRNA FISH probe (red). Images are 3D renderings of confocal z-stacks, and all images are oriented with the anterior of the animal to the left. (a) An animal infected by a single microsporidia cell 3 hpi. Scale bar spans 20 μm. The dashed box encloses a magnified region containing the microsporidia cell and its single nucleus (arrowhead, nuc) next to a larger host nucleus (arrow, Nuc). Scale bar within the box spans 5 μm. (b) Image of infection 18 hpi, marking the beginning of replication by the presence of two pathogen nuclei (arrowheads, nuc). Scale bar spans 5 μm. (c) Image of infection 36 hpi, in which the pathogen has replicated and grown across several intestinal cells (host nuclei indicated by arrows, Nuc). Scale bar spans 20 μm. (d) Image of infection 54 hpi, with extensive growth throughout the intestine and marking the beginning of sporulation. Scale bar spans 20 μm. (e) Magnified image of sporulation 54 hpi in an animal stained with an *N. parisii* rRNA FISH probe (red) and DY96 to label chitin (green). Microsporidia meronts begin to form rounded structures enclosing single nuclei (late meronts indicated by arrowheads, l.m.), rod-shaped cells bearing chitin (immature spores indicated by asterisks, i.s.), and fully formed spores that exclude FISH staining (mature spores indicated by arrows, m.s.). The dashed white line outlines the animal. Scale bar spans 10 μm. (f) Quantification of microsporidia growth from single cells over time. Each dot represents measurement of a single animal. Black dots correspond to measurements of microsporidia volume (left yaxis), and red dots correspond to those same measurements expressed as a fraction of the total intestinal volume (right y-axis).

4.3.2 *N. parisii* infection spreads across host cell boundaries by fusing neighboring intestinal cells

The growth of single *N. parisii* cells across the host intestine indicated that the boundaries between neighboring host cells might be restructured during infection. To visualize host cell boundaries during single microsporidia cell infections, we infected transgenic animals expressing an intestinal GFP-tagged version of LET-413, a highly conserved protein that localizes to the basolateral membrane of polarized cells [22]. We observed deformation of intestinal cell boundaries as *N. parisii* grew laterally (Figure 4-2a). Imaging live transgenic animals at this stage of infection demonstrated that *N. parisii* can appose an intact intestinal cell boundary and then grow across that boundary coincident with localized loss of lateral LET-413 (Figure 4-2b-c, and Video S1). We quantified this growth and found that *N. parisii* infections had spread into one neighboring host cell on average by 27 hpi, and by the time of sporulation the parasite had spread across 12 on average of the 20 total host intestinal cells (Figure 4-S1).

The results above indicate that *N. parisii* spreads across cell boundaries during growth, leading to the question of whether these microsporidia-induced modifications cause neighboring intestinal cells to join together and share cytoplasmic space. To address this question, we generated transgenic animals that express the green-to-red photoconvertible fluorescent Dendra protein in the cytoplasm of their intestinal cells. After infecting these animals, we photoconverted Dendra in a single cell from green to red and then recorded the diffusion of the red signal. When we photoconverted uninfected cells within an infected animal, we found that the red signal remained restricted to the cell in which it was converted (Figure 4-2d), indicating that the boundaries of host intestinal cells not yet reached by *N. parisii* were intact. In contrast,

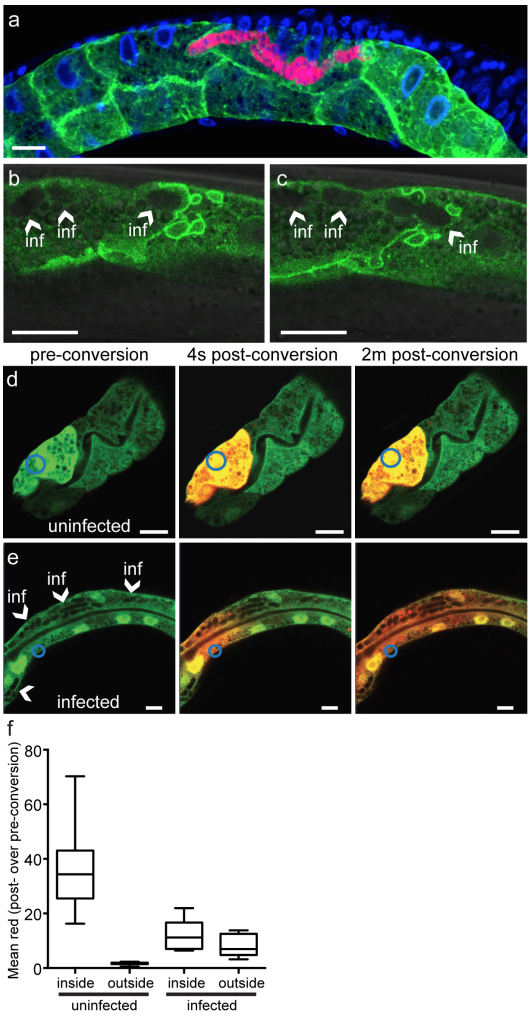

Figure 4-2. *N. parisii* can spread across and fuse intestinal cells into a syncytia
(a) Image at 31 hpi in a fixed transgenic animal expressing GFP-labeled basolateral LET-413 in the intestine (green), stained for DNA with DAPI (blue) and *N. parisii* rRNA with FISH (red). (b) Image of a live infected GFP::LET-413 animal. *N. parisii* is observable as oval-shaped clearings (arrowheads). (c) Image of the same animal as in (b) but captured 1 minute later. (d-e) Images of a live uninfected (d) or infected (e) transgenic animal expressing the photoconvertible Dendra protein under an intestinal-specific promoter before conversion (left panel), four seconds after conversion (middle panel), and two minutes after conversion (right panel). Blue circle indicates the region that was targeted for photoconversion. Arrowheads in (e) point to areas in which *N. parisii* can be seen based on the absence of fluorescence. Scale bars are 10 µm. (f) Quantification of red Dendra signal diffusion in 10 uninfected cells of infected animals, or 10 infected cells. The amount of red signal was measured before and 2 minutes after conversion within the targeted cell and outside of the targeted cell (>30 µm from cell boundary into neighboring cell). Box plots show the fold change in red signal post- over preconversion. The labels for inside and outside indicate the cell that was measured with respect to the cell targeted for photoconversion.

when Dendra was photoconverted in an infected cell, we found that the red signal diffused across all neighboring cells where infection was present (Figure 4-2e). When quantifying this diffusion we found little red signal outside of photoconverted uninfected cells, but large amounts of red signal outside of photoconverted infected cells (Figure 4-2f). These data show that *N. parisii* is able to spread across the boundaries of neighboring host cells, and in so doing cause intestinal cells to join together into syncytia and share cytoplasmic space. Thus, we show that a eukaryotic pathogen causes what appear to be abnormal cell fusion events in the host to allow for intercellular spread.

4.3.3 Infection by different *Nematocida* species causes syncytia formation within distinct host tissue

Microsporidia species vary in the host tissues where they can infect and replicate. We investigated whether infection-induced fusion of host cells is a conserved growth strategy for microsporidia by characterizing the growth of two other *Nematocida* species from single cells. Like *N. parisii*, *N.* sp. 1 only invades and replicates in the intestine of *C. elegans,* while *N. displodere* invades and replicates within several tissues [17,18]. To compare the ability of different microsporidia species to cause host-tissue syncytia formation, we performed single-cell infections of animals with these three *Nematocida* species (Table 4-S1) and quantified the number of host cells with infection after growth to the point of spore formation. Of note, these experiments were performed at 15°C to facilitate *N. displodere* replication, while other experiments were performed at 20°C. First we analyzed infections in the intestine, and here we found that both *N. parisii* and *N.* sp. 1 always spread across several host intestinal cells by the

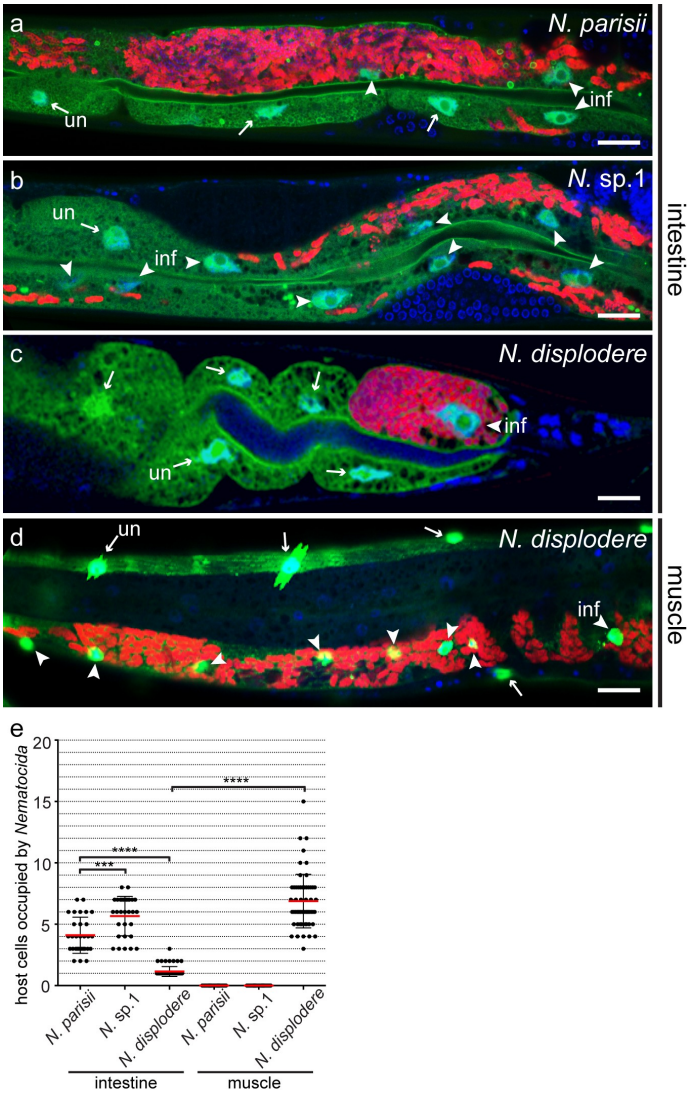

Figure 4-3. Spreading is a conserved microsporidia growth strategy with distinct host cell fusion patterns caused by different *Nematocida* species
Images of single-cell infections by *N. parisii* (a), *N.* sp. 1 (b), or *N. displodere* (c) in the intestine at the time of sporulation. Transgenic animals with GFP expressed in the cytoplasm and nuclei of intestinal cells (green) were fixed and stained for DNA with DAPI (blue) and *Nematocida* rRNA with FISH (red). Arrowheads point to host nuclei of cells with infection (inf), arrows point to host nuclei of cells without infection (un). Scale bars are 20 μm. (d) Image of a single-cell infection by *N. displodere* in a transgenic animal with GFP expressed in the cytoplasm and nuclei of muscle cells. (e) Quantification of the number of host cells occupied by parasite at sporulation (76 hpi for *N. parisii* and *N. displodere*, 120 hpi for *N. displodere*, all at 15°C). Data are combined from two independent experiments with at least 15 animals measured per condition. Each dot is a measurement from a single animal. Red bars show averages, black bars show SD, with p-values from one way ANOVA at ***≤0.001, and ****≤0.0001.

time of spore formation (76 hpi), but that *N. displodere* was most often restricted to a single intestinal cell at its time of spore formation (120 hpi) (Figure 4-3a-c,e). Next, we analyzed spread in the muscle. Unlike skeletal and somatic muscle cells in other animals, the 95 body wall muscle cells of *C. elegans* do not fuse into syncytia during normal development [23]. However, we observed that single-cell *N. displodere* infections grew across many host muscle cells before forming spores, while *N. parisii* and *N.* sp. 1 did not invade or replicate in the muscle (0/60 animals analyzed) (Figure 4-3d-e). Furthermore, we observed four cases of single *N. displodere* cell infections that appeared to have spread out of the large hypodermal syncytium of *C. elegans* (hyp7) and into the anterior epidermal cells (Figure 4-S2) [24]. These data demonstrate that at least among natural pathogens of nematodes, intercellular spread through host cell syncytia formation is a conserved growth strategy for microsporidia determined by species- and tissue-specific interactions.

4.3.4 Microsporidia species vary in their intestinal growth dynamics and effects on host fitness

While both *N. parisii* and *N.* sp. 1 grow in the intestine of *C. elegans*, we found that single *N.* sp. 1 cells spread into more host intestinal cells on average than single *N. parisii* cells by the time of spore formation (Figure 4-3e). This observation indicated that there could be differences in the dynamics of growth between species of microsporidia despite the fact that they start off in the same environment. To compare the dynamics of intestinal pathogen growth between species of microsporidia, we

infected animals with single *N. parisii* or *N.* sp. 1 cells and measured their rates of growth and spore formation over time. Both species grew from a single cell to replicate

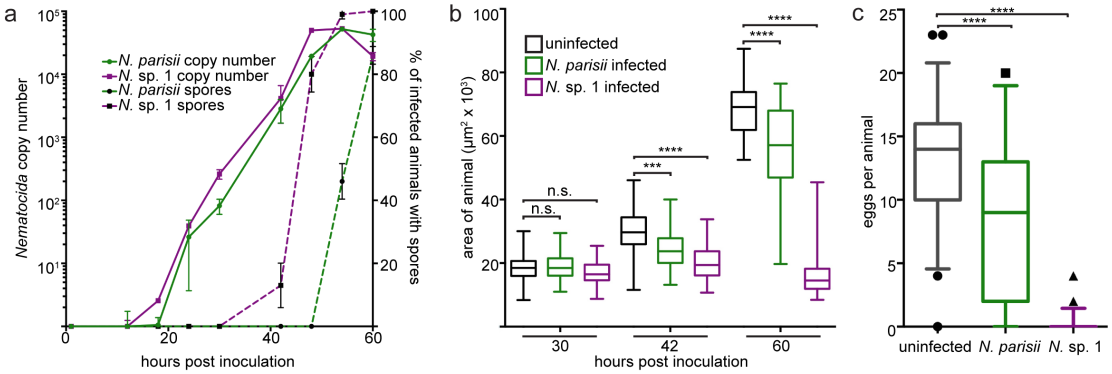

Figure 4-4. *Nematocida* sp. 1 completes its lifecycle faster and impairs fitness of *C. elegans* more than *N. parisii*

(a) Growth kinetics of single-cell *N. parisii* and *N.* sp. 1 infections. Purple lines correspond to *N.* sp. 1 kinetics, green lines correspond to *N. parisii* kinetics. Solid lines show the kinetics of microsporidia replication, dashed lines show the kinetics of spore formation in the same populations of animals. Averages of two biological replicates are shown with standard deviation. (b) Sizes of animals infected by single *N. parisii* cells (green boxes) or *N.* sp. 1 cells (purple boxes) compared to uninfected animals (black boxes) over time. Box-and- whisker plots include data from 50 animals per condition. (c) Eggs in animals infected by single *N. parisii* cells (green boxes) or *N.* sp. 1 cells (purple boxes) compared to uninfected animals (black boxes) at 60 hpi. Box-and-whisker plots include 95% of the data from measurements of 50 animals per condition; dots represent the remaining 5%. Significance was tested by one-way ANOVA, p-values indicated by asterisks with ***≤0.001, and ****≤0.0001.

50,000 times before forming spores (Figure 4-4a). Interestingly, *N.* sp. 1 grew slightly faster and formed spores much earlier than *N. parisii*. Rates of growth were non-uniform over the course of infection, but the average doubling times during the exponential stages of growth (18 hpi – 48 hpi) for *N. parisii* and *N.* sp. 1 were 2.4 h and 2.1 h, respectively. In addition to completing its lifecycle more rapidly, *N.* sp. 1 infection had a much stronger negative effect on host fitness than *N. parisii* infection. Single *N. parisii* cell infections slightly reduced the growth of developing animals compared to uninfected animals, while single *N.* sp. 1 cell infections stunted practically all host

growth (Figure 4-4b). Furthermore, *N. parisii* infection decreased host egg production at 60 hpi compared to uninfected animals while *N.* sp. 1 infection essentially eliminated host egg production (Figure 4-4c). These observations reveal that related microsporidia species can have distinct growth dynamics in the same niche and can differentially exploit host space with varied effects on host fitness.

4.3.5 Host body size and infection density affect the timing of microsporidia sporulation

Based on the kinetics of microsporidia growth (Figure 4-1f and Figure 4-4a), at least two major transitions are apparent: a lag phase during which pathogen cells are not replicating after invasion of host intestinal cells, and a sporulation phase in which some pathogen cells stop replicating and form new spores to complete the life cycle. We noticed that infection by *N.* sp. 1 caused animals to be smaller than infection by *N. parisii* (Figure 4-4), and therefore hypothesized that differences in host size might influence the timing of the decision to form new spores. To test this possibility, we infected body size mutants with single *N. parisii* cells and compared spore formation timing to wild-type animals. The *sma-6* and *lon-1* mutations occur in members of the transforming growth factor (TGF) beta signaling pathway that lead to shorter or longer animals, respectively [25,26]. Animal size is positively regulated by *sma-6*, which encodes a TGF beta-like type I receptor, while *lon-1* encodes a downstream factor that is negatively regulated by signaling through SMA-6. Somewhat surprisingly, we found that both the *sma-6* and the *lon-1* mutant strains were smaller in total area than wild-type animals, providing a useful set of strains for testing the hypothesis that body size

could affect the growth dynamics of microsporidia (Figure 4-5a). Interestingly, we found that single pathogen cell infections in these small mutant animals had formed spores

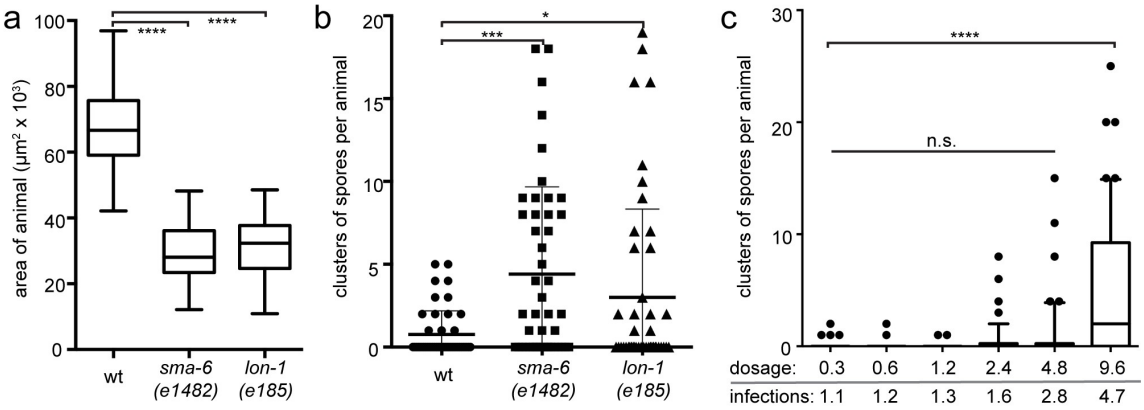

Figure 4-5. *N. parisii* forms spores faster in denser growth environments
(a) Sizes of wild-type and size mutant animals infected by single *N. parisii* cells 53 hpi. Box-and-whisker plots include data from 50 animals per condition. (b) Spore clusters per animal measured in the same animals as in (a). Dots represent measurements of individual animals; bars show averages with standard deviations. (c) Spore clusters per animal 52 hpi in populations that were pulse-infected with different dosages of *N. parisii* spores. Dosages of spores (x106) are shown underneath the graph, along with the average number of infections per animal at each dosage. Box-and-whisker plots include 95% of the data from measurements of 50 animals per dosage; dots represent the remaining 5%. Significance was tested by one-way ANOVA, p- values indicated by asterisks with *≤0.05, ***≤0.001, and ****≤0.0001.

earlier than wild-type animals (Figure 4-5b). These differences could result from a decrease in the time it takes for *N. parisii* to fill the host intestine, potentially providing a density-dependent cue to transition into the spore formation stage of the life cycle. We tested for the influence of infection density on the timing of spore formation by increasing the initial multiplicity of infection, which would increase the rate at which *N. parisii* fills the host tissue. In this experiment, we pulse-infected animals with a range of *N. parisii* spore dosages and measured new spore formation at 52 hpi. Consistent with our hypothesis, we found that more spores formed when we increased the multiplicity of infection (Figure 4-5c). Because all infected animals will eventually be full of spores,

we interpret the increase in spores formed at 52 hpi as evidence that spores form sooner in smaller animals or animals that were infected by multiple microsporidia cells. Furthermore, we found that the growth rate of *N. parisii* was similar in hosts of different sizes and at different multiplicities of infection, demonstrating that infection density affects the timing of spore differentiation, but does not affect the lag phase or rate of replication (Figure 4-S3). Thus, host size and infection density appear to influence the timing of a switch from replication to differentiation into spores for microsporidia.

4.4 Discussion

Like many other eukaryotic intracellular pathogens, microsporidia transition through distinct stages as they progress through the life cycle. These stages are typically defined through analysis of mixed-stage infections in cell culture and histological sections. In this paper, we used a pulse-chase technique to follow the progression of synchronized infections initiated by a single microsporidia cell in a single host cell of an intact animal from invasion until the final stage of the life cycle. With these data we provide a comprehensive view of the growth dynamics for microsporidia in a natural niche, and identify a novel mechanism for the intercellular spread of eukaryotic intracellular pathogens.

The most surprising observation that we made with our experimental approach is that microsporidia spread between host cells by fusing them together into syncytia. Cell-cell fusion is a widespread phenomenon in animal development. *C. elegans* exemplifies this, with more than 30% of all somatic nuclei sharing cytoplasmic space [27]. To our knowledge, this is the first description of a eukaryotic pathogen causing syncytia formation in animal host tissues. Viruses and bacteria have been shown

previously to spread by causing host cell fusions in several animals, including a virus that infects and causes syncytia formation in the intestine of *C. elegans* [28]. Structural and mechanistic distinctions can be made between enveloped viruses that cause host cell fusion through expression of viral entry receptors on the host cell surface that end up binding to and fusing with uninfected cells (e.g. influenza, HIV, and ebola viruses), and non-enveloped reoviruses that fuse host cells solely to spread from an infected into an uninfected host cell [29]. The structural and molecular mechanisms underlying bacterial pathogen-induced host cell fusion have not yet been identified. We do not yet know if there are any structural similarities between the canonical host cell fusion processes and the microsporidia- induced host cell fusions that we describe here. As such, we use the term 'fusion' as a simple way to describe the joining together of cells that are normally separated by membranes. It remains a possibility that *Nematocida* microsporidia cells spread to span several neighboring *C. elegans* cells by breaking down their lateral membranes as opposed to fusing the two lipid bilayers. Further studies on the molecular and structural changes involved in the *Nematocida-C. elegans* interactions we described here will contribute to our understanding of how two separate cells can be joined together.

We observed species-specific patterns in the host cell fusions induced by the microsporidian pathogens of *C. elegans*. Specifically, *N. parisii* and *N.* sp. 1 caused intestinal host cell fusions but did not grow in other tissues, while *N. displodere* grew in several tissues causing host cell fusions in the muscle and epidermis but not the intestine. The failure of *N. displodere* to spread across intestinal cells was not due to an inability to grow within the tissue, as single intestinal cells were filled with pathogen that differentiated and completed its life cycle. These patterns suggest that there is variation

in the factors used by *Nematocida* to cause host cell fusion in *C. elegans*. The general consistency of *Nematocida*- induced syncytia formation in distinct tissues raises the question of why a pathogen would evolve to grow by causing host cell fusion. A common hypothesis for why intracellular pathogens remain in the host cytoplasm during cell-cell spread is to limit the exposure to potentially harmful factors in the extracellular space, such as immune cells. While *C. elegans* does not have any known professional immune cells, other extracellular factors such as antimicrobials including C-type lectins, lysozymes and lipases might be detrimental to microsporidia in this host. Another possibility involves the rate of access to host resources. In the case of microsporidia, we have previously shown that *N. parisii* can escape host intestinal cells by differentiating into spores and exiting through the exocytic pathway [30]. Spores are specialized structures that can withstand harsh environmental conditions but must invade host cells and progress through a lag phase before growth. These limitations imply that microsporidia growth might occur more rapidly by accessing additional host space and resources through spreading before differentiating into spores. The shared features of intercellular spread among species of *Nematocida* also raises the question of how conserved this growth strategy is across microsporidia. There have been previous reports on infections of both vertebrates and invertebrates where microsporidia caused the formation of xenomas, which are described as hypertrophic host cells that increase in size and number of nuclei [31-33]. Given the potential difficulties in distinguishing hypertrophy from cell fusion events in histological sections, we speculate that some of the host cell changes in these microsporidia infections may reflect the kind of host cell syncytia formation that we observed for *Nematocida* during intercellular spread. Identifying the factors involved in *Nematocida*-induced host cell

fusion will allow us to search for factors that may be important for other microsporidia-host cell interactions.

The experimental approaches taken in this paper allowed us to identify several features of *Nematocida* growth. Despite the lower temperatures used in this study, we measured a similar *N. parisii* doubling time compared to our previous estimates at a higher temperature (2.4 h at 20°C vs 2.9 h at 25°C, respectively) [20]. Thus, microsporidia grow faster than previously estimated, which may be accounted for in part by differences between the two studies in the synchronicity of infections. Additionally, we found that the doubling rate was uneven over time. The changes in the rate of growth occurred over distinct phases with similarities to other microbes including a lag phase without replication, exponential growth and replication phase, and a slowing to stationary phase at the time of spore differentiation. There are several definitions for the lag phase of microbial growth, but it can be generally described as the time it takes for a microbe to begin growing in biomass and replicating after inoculation in growth media [34]. A recent study identified transcriptional signatures of two distinct sub-phases in the *E. coli* lag phase: one in which there is metabolic activity without an increase in biomass, and a second in which there is an increase in biomass but not yet cell number [35]. While there have been advances in our understanding of the lag phase for bacteria, virtually nothing is known about the lag phase for eukaryotic pathogens. As the timing of the lag phase of growth can profoundly alter the outcome of interactions with a host [36], it will be important to determine how comparable the lag phases are among pathogenic microbes. Studying the lag phase of obligate intracellular pathogens like microsporidia will require strategies for overcoming the

challenge of extracting signal from the extremely low ratios in pathogen to host material during this stage of infection.

Genetic variation can be a strong determinant of host-pathogen interactions [37]. We previously showed that there is variation among *C. elegans* strains in their resistance to microsporidia infection, which is a complex genetic trait [21]. Here we show that there is genetic variation among microsporidia in their ability to grow and affect the fitness of *C. elegans*. Through our observations of the differences between microsporidia species in their rates of growth, we were pointed towards factors that influence the kinetics of the microsporidia life cycle. We found that increasing the density of infection by decreasing the host body size or increasing the number of infectious events sped up the development of spores. Neither of these modifications changed the growth rate of *N. parisii*, indicating that the transition from replication to spore differentiation is regulated by environmental factors in the host. Our experiments lead us to speculate that the cue for transitioning from replication to spore formation in microsporidia may be related to the sensing of host resource availability and/or the sensing of self, both of which are related to the density of infection. There is precedent for eukaryotic organisms making developmental decisions based on density, which is exemplified by several fungal species that undergo developmental switches in response to high density and nutrient availability [38]. As has been shown for many other developmental switches in pathogens [39], the specific factors that regulate transitions in the microsporidia life cycle likely involve responses made by both host and pathogen to changes in their shared metabolic pool. Our finding that microsporidia can grow across a substantial portion of the cells comprising an entire animal organ before differentiating opens up a new set of questions regarding the dynamic inputs

that intracellular pathogens interpret from the host environment to optimize growth and transmission.

4.5 Materials and methods

4.5.1 *C. elegans* and *Nematocida* strains

C. elegans strains were maintained on nematode growth media (NGM) seeded with *E. coli* OP50-1 (which is a streptomycin-resistant OP50 strain) as previously described [40]. For simplicity, this strain is referred to as OP50 throughout. To obtain starved and synchronized L1 larvae, gravid adults were bleached to isolate eggs, which then were allowed to hatch overnight at 20°C [41]. The *C. elegans* wild-type N2, small mutant CB1482 *sma-6(e1482)*, long mutant CB185 *lon-1(e185)*, and intestinal GFP transgenic SJ4144 *zcIs18 [ges-1p::GFP(cyt)]* strains were obtained from the Caenorhabditis Genetics Center. ERT351 was derived from SJ4144 by backcrossing to N2 eight times. Transgenic animals with intestinal expression of GFP-labeled LET-413 were generated by injection of pET213 *[vha-6p::GFP::let-413]* and a *myo-2::mCherry* co-injection marker to generate a multi-copy array strain. This strain was treated with UV psoralen at 700μJ to generate the integrated ERT147 *jyIs21[vha-6p::GFP::let-413, myo-2::mCherry]* strain. A cytoplasmic intestinal photoconvertible fluorescent protein construct pET207 was generated using three-part Gateway recombination by fusing the intestinal-specific *vha-6* promoter to Dendra [42] with the *unc-54* 3'UTR. This construct was injected into N2 animals and transgenic progeny were recovered to generate a multi-copy array strain ERT113 *jyEx46[vha-6p::dendra::unc-54 3'UTR]*. Infection experiments were performed with *Nematocida parisii* strain ERTm1,

Nematocida sp. 1 strain ERTm2, and *Nematocida displodere* strain JUm2807 [17,18]. Spores were prepared and quantified as previously described [43].

4.5.2 Single microsporidia cell infections

Synchronized first-larval stage (L1) animals were inoculated with OP50 and a series of spore dilutions on NGM plates at 20°C. These animals were collected two and a half hours after plating, washed three times with PBS containing 0.1% Tween 20 to remove spores, and re-plated with OP50 at 20°C. A fraction of the population was fixed at this time with 4% PFA for 30 minutes, then stained by FISH with the *Nematocida* ribosomal RNA-specific MicroB probe [18] conjugated to a red Cal Fluor 610 dye (Biosearch Technologies). The number of infectious events per animal was quantified in 50 animals per dosage after mounting samples on agarose pads with VECTASHIELD mounting medium containing DAPI (Vector Labs) and imaging using a Zeiss AxioImager M1 upright fluorescent microscope with a 40X oil immersion objective. A limiting dilution of *Nematocida* spores was tested to identify a concentration in which more than 83% of infected animals contained only a single microsporidia cell. The spore dosage that had this characteristic typically yielded a Poisson distribution of infection, in which an average of 72% of the population was uninfected and 28% infected. Infection distributions were measured for all experiments to ensure that the vast majority of infected animals contained a single microsporidia cell (see Table S1).

4.5.3 Measuring microsporidia growth by microscopy

The ERT351 strain was infected at the L1 stage at a dosage following the parameters described above for single microsporidia cell infections. Animals were fixed at various times post-inoculation in 4% PFA for FISH staining and microscopy-based analysis of

growth. Samples were mounted on 5% agarose pads and imaged using a 40X oil immersion objective or a 10X objective on a Zeiss LSM700 confocal microscope run by ZEN2010 software. Z-stacks were acquired of the entire intestinal space with a z-spacing of 1μm (at 400X) or 6μm (100X), collecting GFP signal (expressed in cytoplasm of intestine) and RFP signal (microsporidia signal stained by FISH). Analysis of these images was performed with Fiji software [44]. Briefly, the brightest slice was used to threshold GFP and RFP to binary signals. The 3D objects counter function was used to measure voxels after converting signals, which were used to quantify the volume of intestine (GFP) and pathogen (RFP) in 10 animals per time point.

4.5.4 Analysis of microsporidia growth across host intestinal cells

ERT147 animals were infected with a single microsporidia cell. These animals were imaged at various times post-inoculation either after being fixed and stained as described above or as live animals using a 40X oil immersion objective on a Zeiss LSM700 confocal microscope run by ZEN2010 software. For live imaging, infected ERT147 animals were mounted on 5% agarose pads with microsphere beads and imaged with a 63X oil-immersion objective for 120 cycles at 1.58 μs pixel dwell time for five minutes. GFP was excited with a 488nm laser at 2.1% power, and light was collected with the pinhole set to 44μm. Quantifying growth of microsporidia across intestinal cell boundaries was performed after fixing ERT147 animals and staining by FISH as described above. To measure the diffusion of cytoplasm in intestinal cells, ERT113 animals were infected at the L1 stage and imaged live 48 hours post-inoculation with a 40X oil-immersion objective. A 488 nm laser at 0.5% power was used to excite green Dendra proteins and a 555 nm laser at 14% power was used to excite

red Dendra proteins. Light was collected with a pinhole size of 42 μm and a 3.15 μs pixel dwell time. Dendra proteins were converted in a 4 μm diameter space with a 405 nm laser at 35% power with a pixel dwell time of 50 μs. Infected cells could be distinguished from uninfected cells based on exclusion of fluorescent signal. To quantify the diffusion of converted signal, the mean red signal was measured in a 15 μm2 area within the targeted cell or outside of the targeted cell (at a distance of greater than 30 μm from targeted cell) before and two minutes after conversion.

4.5.5 Comparing *Nematocida* growth across different host tissues

Transgenic animals expressing GFP in the cytoplasm and nuclei of intestinal or muscle cells were infected with single *N. parisii*, *N.* sp. 1, or *N. displodere* cells at 15°C and fixed at the time of spore formation. For the intestinal-GFP strain ERT413 *jySi21[spp-5p::GFP; cb-unc-119(+)] II* [17], 1000 synchronized L1 larvae were grown at 20°C for 48 hours to the young adult stage before being inoculated with 3.7 x 105 *N. parisii* spores, 3.2 x 105 *N.* sp. 1 spores, or 1.25 x 104 *N. displodere* spores for 30 minutes. Spores were washed off and infection progressed at 15°C. For the muscle-GFP strain HC46 *ccIs4251[myo-3::GFP-NLS, myo-3::GFP- MITO] I; mIs11[myo-2::GFP] IV* [45], 1000 synchronized L1 larvae were infected in duplicate at 15°C with 5.0-20.0 x 104 spores of *N. displodere* on a 6 cm plate. A fraction of animals was fixed in 4% PFA diluted in PBS + 0.1% Tween-20 at 24 hpi for FISH to verify infection distributions. At 76 hpi (*N. parisii* and *N.* sp. 1) or 120 hpi (*N. displodere*), animals were fixed for FISH with or without DY96 (10μg/ml) staining to stain infection and spores. *N. displodere* FISH was performed as previously described [17]. All analysis and imaging was conducted on a Zeiss LSM700 confocal microscope with a 40x oil-immersion objective.

The numbers of GFP+ host cell nuclei abutted by pathogen in a 3D stack of confocal images were counted to quantify the number of host cells that infection had spread into by the time of sporulation.

4.5.6 Measuring microsporidia growth by qPCR

The N2 strain was infected at the L1 stage at a dosage following the parameters described above for single microsporidia cell infections. Animals were fixed at various times post- inoculation in Extracta (Quanta Biosciences) to isolate DNA for qPCR-based analysis of growth. Microsporidia copy number was quantified with iQ SYBR Green Supermix (Bio- Rad) on a CFX Connect Real-time PCR Detection System (Bio-Rad). We measured the relative abundance of *Nematocida* and *C. elegans* DNA in 30 ng of DNA with the following primer sets: Np_rDNAF1: aaaaggcaccaggttgattc, Np_rDNAR1: agctctctgacgcttccttc, Ce_snb- F1: ccggataagaccatcttgacg, Ce_snb-R1: gacgacttcatcaacctgagc. Microsporidia copy number was measured by normalizing to samples infected by single microsporidia cells at early stages of growth when only a single nucleus is observed. We validated qPCR measurements of microsporidia copy number by taking a microscopy-based method of manually counting the average number of microsporidia nuclei per infection during growth from a single nucleus to 100 nuclei. Copy number measurement discrepancies between qPCR and manual count analyses were within 11%. Primer efficiencies were measured, and fold difference was calculated using the Livak comparative Ct method ($2^{-\Delta\Delta Ct}$).

4.5.7 Measuring animal size, egg number, and microsporidia spores

Animals were fixed and stained by FISH as described above, then imaged using a Zeiss AxioImager M1 upright fluorescent microscope with a 40X oil immersion

objective. 50 animals per condition were manually outlined with Fiji software to calculate size (in μm2). The number of eggs per animal was measured at 60 hpi by adding DY96 (4ng/ml with 0.1% SDS) to FISH-stained samples for 30 minutes before imaging. DY96 stains chitin [46], which is a component of the eggshell. The 60 hpi time point was chosen because it is when uninfected animals first consistently contain eggs. Eggs were counted in 50 animals per condition. Microsporidia spores also contain chitin, and were stained with DY96. Spore clusters per infected animal in 50 total animals per condition were counted. Each cluster of spores contained approximately 50 spores. Spore clusters (which we define as regions within meronts that contain approximately 30 spores with bright chitin staining) were counted at 52 hpi, which is the time at which single microsporidia cell infections begin to differentiate in to spores in N2 animals as described above.

4.6 Supplemental Figures and Tables

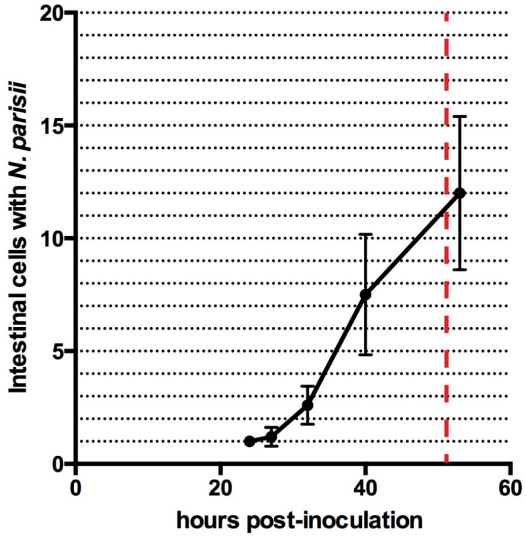

Figure 4-S1. Quantification of *N. parisii* spreading across host intestinal cells over time

Transgenic GFP-labeled LET-413 animals were infected with single *N. parisii* cells and fixed at several time points to stain for infection by FISH and count the number of host intestinal cells that infection had spread to by confocal microscopy. 10 animals were counted per time point. Averages with standard deviations are plotted over time. The horizontal dashed black lines show where each of the 20 total host intestinal cells fall on the y-axis, the vertical dashed red line shows to time at which spores begin to form in some infected animals on the x-axis.

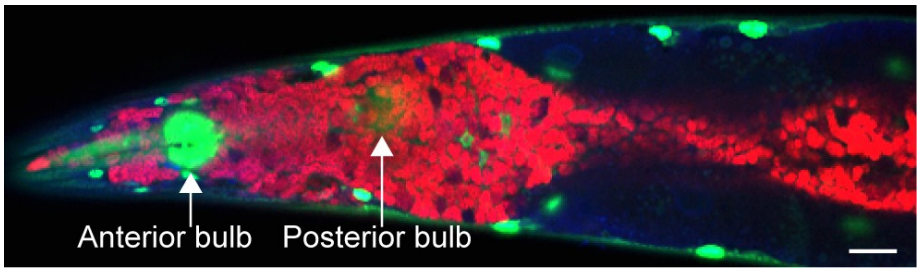

Figure 4-S2. *N. displodere* causes syncytia formation in the anterior hypodermal cells of *C. elegans*

Image of a single-cell infection by *N. displodere* in a transgenic animal with GFP expressed in the cytoplasm and nuclei of muscle cells (see infection distribution for muscle measurements in TableS1). Transgenic animals were fixed and stained for DNA with DAPI (blue) and *Nematocida* rRNA with FISH (red). Infection can be seen spreading across from the hyp7 hypodermal syncytium into the anterior hypodermal cells. Hypodermal cells around and to the left of the anterior bulb in this image are normally separated from the hyp7 syncytium, which encompasses the posterior bulb and continues to the right.

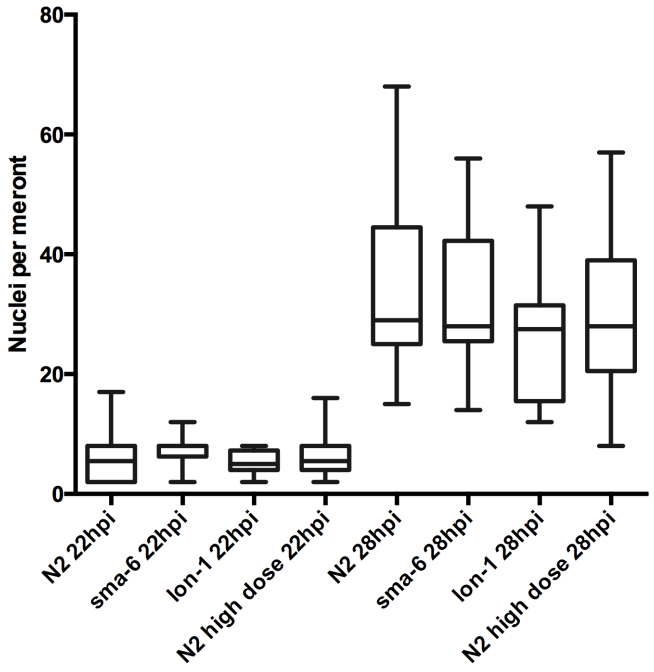

Figure 4-S3. Quantification of *N. parisii* growth rate in size mutants and at high multiplicity of infection

Animals were infected with single *N. parisii* cells or an average of 5 *N. parisii* cells (N2 high dose) and fixed at 22 hpi or 28 hpi. *N. parisii* was stained by FISH, nuclei were stained with DAPI, and nuclei per meront were counted in 10 meronts per condition by confocal microscopy.

Table 4-S1. Quantification of infection distributions
Measurements of the number of infections per animal across experiments

Samples	# of animals counted	% infected with 0	% infected with 1	% infected with 2	% infected with 3	% infected with >3
Figure 1	100	79	19	2	0	0
Figure 3 (*N. parisii*) (intestine)	100	66	23	10	1	0
Figure 3 (*N.* sp.1) (intestine)	100	84	15	1	0	0
Figure 3 (*N. displodere*) (intestine)	100	62	30	7	1	0
Figure 3 (*N. displodere*) (muscle)	100	86	13	1	0	0
Figure 4 (*N. parisii*)	100	60	34	4	2	0
Figure 4 (*N.* sp. 1)	100	50	42	6	2	0
Figure 5A (wt)	50	82	18	0	0	0
Figure 5A (*sma-6*)	50	80	20	0	0	0
Figure 5A (*lon-1*)	50	82	18	0	0	0
Figure 5C (0.3x10^6)	50	78	20	2	0	0
Figure 5C (0.6x10^6)	50	64	28	6	2	0
Figure 5C (1.2x10^6)	50	38	46	16	0	0
Figure 5C (2.4x10^6)	50	14	54	20	8	4
Figure 5C (4.8x10^6)	50	8	24	18	30	20
Figure 5C (9.6x10^6)	50	0	2	16	12	70

4.7 Acknowledgements

We thank Michael Botts, Kirthi Reddy, and Aaron Reinke for helpful comments on the manuscript, and the *Caenorhabditis* Genetics Center for *C. elegans* strains.

Chapter 4, in full, has currently been resubmitted and accepted for publication, Balla KM, Luallen RJ, Bakowski MA, Troemel ER (2016) Cell-to-cell spread of microsporidia causes *C. elegans* organs to form syncytia, Nature Microbiology (*accepted*) with permission from Nature Publishing Group. The dissertation author was the second author of this material. Author contributions to manuscript are as follows: Luallen, R contributed to the data for Figure 4-3c-e and Figure 4-S2, Balla, K contributed to the data for all remaining figures and tables, and Bakowski, M generated the ERT147 transgenic strain.

4.8 References

1. Bernardini ML, Mounier J, d'Hauteville H, Coquis-Rondon M, Sansonetti PJ (1989) Identification of icsA, a plasmid locus of *Shigella flexneri* that governs bacterial intra- and intercellular spread through interaction with F-actin. Proc Natl Acad Sci U S A 86: 3867-3871.

2. Heinzen RA, Hayes SF, Peacock MG, Hackstadt T (1993) Directional actin polymerization associated with spotted fever group *Rickettsia* infection of Vero cells. Infect Immun 61: 1926-1935.

3. Tilney LG, Portnoy DA (1989) Actin filaments and the growth, movement, and spread of the intracellular bacterial parasite, Listeria monocytogenes. J Cell Biol 109: 1597-1608.

4. Cudmore S, Cossart P, Griffiths G, Way M (1995) Actin-based motility of vaccinia virus. Nature 378: 636-638.

5. Ciechonska M, Duncan R (2014) Reovirus FAST proteins: virus-encoded cellular fusogens. Trends Microbiol 22: 715-724.

6. French CT, Toesca IJ, Wu TH, Teslaa T, Beaty SM, Wong W, Liu M, Schröder I, Chiou PY, Teitell MA, Miller JF. (2011) Dissection of the *Burkholderia* intracellular life cycle using a photothermal nanoblade. Proc Natl Acad Sci U S A 108: 12095-12100.

7. Steele S, Radlinski L, Taft-Benz S, Brunton J, Kawula TH (2016) Trogocytosis-associated cell to cell spread of intracellular bacterial pathogens. Elife 5: e10625.

8. Nikitas G, Deschamps C, Disson O, Niault T, Cossart P, Lecuit M. (2011) Transcytosis of *Listeria monocytogenes* across the intestinal barrier upon specific targeting of goblet cell accessible E-cadherin. J Exp Med 208: 2263-2277.

9. Swann J, Jamshidi N, Lewis NE, Winzeler EA (2015) Systems analysis of host-parasite interactions. Wiley Interdiscip Rev Syst Biol Med 7: 381-400.

10. Sturm A, Amino R, van de Sand C, Regen T, Retzlaff S, Rennenberg A, Krueger A, Pollok JM, Menard R, Heussler VT. (2006) Manipulation of host hepatocytes by the malaria parasite for delivery into liver sinusoids. Science 313: 1287-1290.

11. Stentiford GD, Becnel JJ, Weiss LM, Keeling PJ, Didier ES, Williams BA, Bjornson S, Kent ML, Freeman MA, Brown MJ, Troemel ER, Roesel K, Sokolova Y, Snowden KF, Solter L. (2016) Microsporidia - Emergent Pathogens in the Global Food Chain. Trends Parasitol 10.1016/j.pt.2015.12.004.

12. Stentiford GD, Feist SW, Stone DM, Bateman KS, Dunn AM (2013) Microsporidia: diverse, dynamic, and emergent pathogens in aquatic systems. Trends Parasitol 29: 567-578.

13. Cali A, Takvorian PM (2014) Developmental Morphology and Life Cycles of the Microsporidia. Microsporidia: John Wiley & Sons, Inc. pp. 71-133.

14. Xu Y, Weiss LM (2005) The microsporidian polar tube: a highly specialised invasion organelle. Int J Parasitol 35: 941-953.

15. Balla KM, Troemel ER (2013) Caenorhabditis elegans as a model for intracellular pathogen infection. Cell Microbiol 10.1111/cmi.12152.

16. Felix MA, Duveau F (2012) Population dynamics and habitat sharing of natural populations of *Caenorhabditis elegans* and *C. briggsae*. BMC biology 10: 59.

17. Luallen RJ, Reinke AW, Tong L, Botts MR, Felix M-A, Troemel, ER. (2016) Discovery of a Natural Microsporidian Pathogen with a Broad Tissue Tropism in *Caenorhabditis elegans*. PLoS Pathog 12: e1005724.

18. Troemel ER, Felix MA, Whiteman NK, Barriere A, Ausubel FM (2008) Microsporidia are natural intracellular parasites of the nematode *Caenorhabditis elegans*. PLoS Biol 6: 2736-2752.

19. Bakowski MA, Desjardins CA, Smelkinson MG, Dunbar TL, Lopez-Moyado IF, Rifkin SA, Cuomo CA, Troemel ER. (2014) Ubiquitin-mediated response to microsporidia and virus infection in *C. elegans*. PLoS Pathog 10: e1004200.

20. Cuomo CA, Desjardins CA, Bakowski MA, Goldberg J, Ma AT, Becnel JJ, Didier ES, Fan L, Heiman DI, Levin JZ, Young S, Zeng Q, Troemel ER. (2012) Microsporidian genome analysis reveals evolutionary strategies for obligate intracellular growth. Genome research 22: 2478-2488.

21. Balla KM, Andersen EC, Kruglyak L, Troemel ER (2015) A wild *C. elegans* strain has enhanced epithelial immunity to a natural microsporidian parasite. PLoS Pathog 11: e1004583.

22. Legouis R, Gansmuller A, Sookhareea S, Bosher JM, Baillie DL, Labouesse M. (2000) LET-413 is a basolateral protein required for the assembly of adherens junctions in *Caenorhabditis elegans.* Nat Cell Biol 2: 415-422.

23. Altun Z.F. HDH (2009) Muscle system, somatic muscle. WormAtlas.

24. Altun Z.F. HDH (2009) Epithelial system, hypodermis. WormAtlas.

25. Krishna S, Maduzia LL, Padgett RW (1999) Specificity of TGFbeta signaling is conferred by distinct type I receptors and their associated SMAD proteins in *Caenorhabditis elegans.* Development 126: 251-260.

26. Maduzia LL, Gumienny TL, Zimmerman CM, Wang H, Shetgiri P, Krishna S, Roberts AF, Padgett RW. (2002) lon-1 regulates *Caenorhabditis elegans* body size downstream of the dbl-1 TGF beta signaling pathway. Dev Biol 246: 418-428.

27. Podbilewicz B (2006) Cell fusion. In: Community TCeR, editor. WormBook: WormBook.

28. Felix MA, Ashe A, Piffaretti J, Wu G, Nuez I, Bélicard T, Jiang Y, Zhao G, Franz CJ, Goldstein LD, Sanroman M, Miska EA, Wang D. (2011) Natural and experimental infection of *Caenorhabditis nematodes* by novel viruses related to nodaviruses. PLoS Biol 9: e1000586.

29. Sapir A, Avinoam O, Podbilewicz B, Chernomordik LV (2008) Viral and developmental cell fusion mechanisms: conservation and divergence. Dev Cell 14: 11-21.

30. Szumowski SC, Botts MR, Popovich JJ, Smelkinson MG, Troemel ER (2014) The small GTPase RAB-11 directs polarized exocytosis of the intracellular pathogen *N. parisii* for fecal-oral transmission from *C. elegans*. Proc Natl Acad Sci U S A 10.1073/pnas.1400696111.

31. Leitch GJ, Shaw AP, Colden-Stanfield M, Scanlon M, Visvesvara GS (2005) Multinucleate host cells induced by *Vittaforma corneae* (Microsporidia). Folia Parasitol (Praha) 52: 103-110.

32. Lom J, Dykova I (2005) Microsporidian xenomas in fish seen in wider perspective. Folia Parasitol (Praha) 52: 69-81.

33. Maurand J (1973) Recherches biologiques sur les microsporidies des larves de simulies. CNRS A: Academie de Montpellier.

34. Monod J (1949) The Growth of Bacterial Cultures. Annual Review of Microbiology 3: 371-394.

35. Madar D, Dekel E, Bren A, Zimmer A, Porat Z, Alon U. (2013) Promoter activity dynamics in the lag phase of *Escherichia coli*. BMC Syst Biol 7: 136.

36. Stepanyan K, Wenseleers T, Duenez-Guzman EA, Muratori F, Van den Bergh B, Verstraeten N, De Meester L, Verstrepen KJ, Fauvart M, Michiels J. (2015) Fitness trade-offs explain low levels of persister cells in the opportunistic pathogen *Pseudomonas aeruginosa*. Mol Ecol 24: 1572-1583.

37. Persson J, Vance RE (2007) Genetics-squared: combining host and pathogen genetics in the analysis of innate immunity and bacterial virulence. Immunogenetics 59: 761-778.

38. Sprague GF, Jr., Winans SC (2006) Eukaryotes learn how to count: quorum sensing by yeast. Genes Dev 20: 1045-1049.

39. Olive AJ, Sassetti CM (2016) Metabolic crosstalk between host and pathogen: sensing, adapting and competing. Nat Rev Microbiol 14: 221-234.

40. Brenner S (1974) The genetics of *Caenorhabditis elegans*. Genetics 77: 71-94.

41. Stiernagle T (2006) Maintenance of *C. elegans*. In: Community TCeR, editor. WormBook: WormBook.

42. Gurskaya NG, Verkhusha VV, Shcheglov AS, Staroverov DB, Chepurnykh TV, Fradkov AF, Lukyanov S, Lukyanov KA. (2006) Engineering of a monomeric green-to-red photoactivatable fluorescent protein induced by blue light. Nat Biotechnol 24: 461-465.

43. Estes KA, Szumowski SC, Troemel ER (2011) Non-lytic, actin-based exit of intracellular parasites from *C. elegans* intestinal cells. PLoS Pathog 7: e1002227.

44. Schindelin J, Arganda-Carreras I, Frise E, Kaynig V, Longair M, Pietzsch T, Preibisch S, Rueden C, Saalfeld S, Schmid B, Tinevez JY, White DJ, Hartenstein V, Eliceiri K, Tomancak P, Cardona A. (2012) Fiji: an open-source platform for biological-image analysis. Nat Methods 9: 676-682.

45. Winston WM, Molodowitch C, Hunter CP (2002) Systemic RNAi in *C. elegans* requires the putative transmembrane protein SID-1. Science 295: 2456-2459.

46. Hoch HC, Galvani CD, Szarowski DH, Turner JN (2005) Two new fluorescent dyes applicable for visualization of fungal cell walls. Mycologia 97: 580-588.

5. *N. displodere* displays a broad host tropism but limited temperature range compared to other *Nematocida* species.

5.1 Summary

As obligate intracellular pathogens, the majority of microsporidia evolution is likely due to selective pressure from their host organism, with some pressure coming from the environment and competition with other microbial pathogens and parasites. The discovery of numerous *Nematocida* microsporidian species that infect the nematode *C. elegans* allows for a convenient, tractable system to study the evolution of host/pathogen interactions of closely related, but distinct pathogens infecting the same host. As described earlier, *Nematocida displodere* displays a broad tissue tropism in *C. elegans* compared to other closely related *Nematocida* species, *N. parisii* and *N.* sp. 1, which exclusively infect and proliferate in the intestine. Here, we show that in addition to this broad tissue tropism, *N. displodere* displays a broad host range, able to infect every species of *Caenorhabditis* nematode tested, along with *Pristionchus pacificus* and *Panagrellus redivivus.* By contrast, *N. parisii* and *N.* sp. 1 showed a narrower host range. However, in all tested species, *N. displodere* showed a limited temperature range, with optimal proliferation occurring at 15°C and no growth at 25°C. This temperature specificity is in stark contract to *N. parisii* and *N.* sp. 1 that can infect and proliferate well at all temperatures from 15 to 25°C. Furthermore, *N. displodere* infection shows a minor effect on *C. elegans* thermotaxis behavior, causing early larval stages of the animal to prefer lower temperatures which might facilitate pathogen growth. Altogether, these observations shed light on some of the growth capabilities and restrictions displayed by *N. displodere* in many host nematode species.

5.2 Introduction

Obligate intracellular pathogens are dependent on their host organisms for the proliferative stages of their life cycles, and therefore likely evolve under maximal selective pressure from their hosts. For example, the microsporidia lifecycle begins with a non-replicative spore stage that must survive the natural environment until a new host is found, and for the most part this spore is thought to be protected from desiccation, UV damage, and other environmental insults by a distinct set of spore coat proteins (1). After infection of a host cell through use of the polar tube, all replicative stages of microsporidia, from sporoplasm to newly formed spores, occur inside the host cell where the majority of selective pressure on the pathogen genome would occur. However, complex interactions in the wild complicate the simple model that microsporidia evolution is dependent on interactions with intracellular factors of a single host. For example, there could be multiple competent hosts, interactions with other pathogens in a host, and interactions with environmental factors faced by the host.

The sampling of wild *Caenorhabditis* nematodes from the wild has opened up new research into the natural habitat of these genetic model organisms and their interactions with the environment (2-3). Among one of the most phenotypically striking aspects of these wild nematodes is that they regularly harbor extracellular and intracellular microbes, with microsporidia infection being commonplace (4-6). To date, three published species of microsporidia in the *Nematocida* genus have been described, *N. parisii* and *N.* sp. 1 which infect and proliferate in the intestine of *C. elegans*, and *N. displodere* which infects and proliferates in multiple tissues. Another four unpublished species of *Nematocida* microsporidia have been discovered in wild

nematodes, *N. major*, *N. minor*, *N. ciargi*, and *N. homosporus*, all of which only appear to infect and proliferate in the intestine (7). We previously proposed that the potential competition between microsporidia species and other intestinal pathogens like the Orsay virus (6) could be an explanation for the evolution of a broad, non-intestinal tissue tropism by *N. displodere* (4).

However, another phenotype that was originally noticed when *N. displodere* was discovered is that a mixed population of wild *C. elegans* infected with various stages of *N. displodere* would become uninfected at 25°C and 20°C over time. For this reason, the original study characterizing *N. displodere* infection was conducted at 15°C, a temperature which was capable of maintaining proliferating populations of *N. displodere* for numerous generations (4). This restricted temperature range seen in *N. displodere* is another major divergence point with *N. parisii* and *N.* sp.1, which actually have faster infection progression at 25°C compared to 20°C (5, 8). In fact, an analysis of over 4800 fungal strains from 144 genera showed that the majority grew well between 12-30°C, with a decline for most at temperatures above 35°C (9), suggesting that the limited temperature range of *N. displodere* may be anomalous. Altogether, these observations raise a point that *N. displodere* infection progression is limited by an environmental factor that theoretically could be controlled by a host behavior, the choice of a temperature niche.

The sampling wild nematodes has also found that different *Caenorhabditis* and other nematodes are commonly isolated from the same sampling location (2-3). Additionally, isolates of *N. parisii* and *N.* sp. 1 were found in both *C. briggsae* and *C. elegans* (5, 7). Therefore, it is likely that *Nematocida* microsporidia can infect a number of different nematode hosts (6). In fact many microsporidian species have been found

that have a broad host range, including *Vavraia culici* and *Nosema ceranae* which infect mosquitos and honey bees, respectively (10-11). The microsporidian *Anncallia algerae* has been shown to infect both insects and mammals (12). Therefore, the selective pressure on *Nematocida* evolution would be coming from the intracellular environment of any number of hosts that can be encountered and infected in the wild.

Here, we further investigate the low temperature phenotype displayed by *N. displodere* infection. We find that not only is *N. displodere* incapable of proliferating at 25°C, but the intermediate meront stage of infection is actually cleared at the higher temperature. However, *N. displodere* can invade *C. elegans* at higher temperatures without proliferation, but then proliferate when the host is moved to a permissive lower temperature. Furthermore, we show that *N. displodere* displays a broad host tropism, able to infect every species of *Caenorhabditis* nematode tested, along with *Pristionchus pacificus* and *Panagrellus redivivus.* Yet, *N. displodere* continues to display an decreasing ability to proliferate in all tested species as the temperature is increased from 15° to 25°C, suggesting that the low temperature phenotype of *N. displodere* is specific to the pathogen and likely not due to the host. Finally, *N. displodere* infection shows a minor effect on *C. elegans* thermotaxis behavior, causing early larval stages of the thermotax to lower temperatures which might facilitate pathogen growth. Altogether, these observations show that *N. displodere* has both a broad tissue tropism and a broad host range, but is limited to proliferation at lower temperatures, suggesting a complex interaction of selective pressures acting on this phenotypically divergent species in the *Nematocida* genus.

5.3 Results

5.3.1 *N. displodere* proliferates at 15°C but fails to grow at a higher temperature

After the original sampling of *N. displodere* (strain JUm2807) in Paris, France, at the lab of Dr. Marie-Anne Félix, we found that we could not maintain this strain of *N. displodere* at 20°C and 25°C in the wild *C. elegans* strain in which it was found. As a result, all pathogen characterizations and host phenotypes after infection were conducted at 15°C, a temperature that resulted in nearly 100% of animals displaying the different microsporidia infection stages (4). To further characterize the extent of this phenomenon, we tested whether *N. displodere* had a defect in proliferation at higher temperatures. Wild type N2 *C. elegans* was infected with enriched *N. displodere* spores (using a dose that results in 100% of animals with sporoplasms at 24 hours post infection, hpi) at 15°C for 1 day. This population of infected animals (T_0) was split to either 15°C or 25°C and sampled at 2, 3, and 4 dpi. Using fluorescent in situ hybridization (FISH) staining to track pathogen infection over time, we found that infection with *N. displodere* increased over time at 15°C, while it failed to progress at 25°C (Fig. 5-1a). Infection of these animals was quantified by counting the percent of animals that displayed infection (any amount of rRNA FISH signal), and while 100% of animals were infected at 15°C at all time points, infection was cleared by 4 dpi at 25°C (Fig. 5-1b). We next conducted the reverse of this experiment, infecting N2 with *N. displodere* at 25°C for 1 day and splitting to 15°C and 25°C and looking at infection 48 hours later. Animals maintained at 25°C showed no progression to meronts and a steep drop in any signs of infection, while nearly 100% of animals transferred to 15°C progressed to meronts (Figure 5-1c). These data indicate that *N. displodere* can invade

C. elegans at 25°C and survive for at least 24 hours, as invaded sporoplasms can progress to meronts when the host is moved to 15°C.

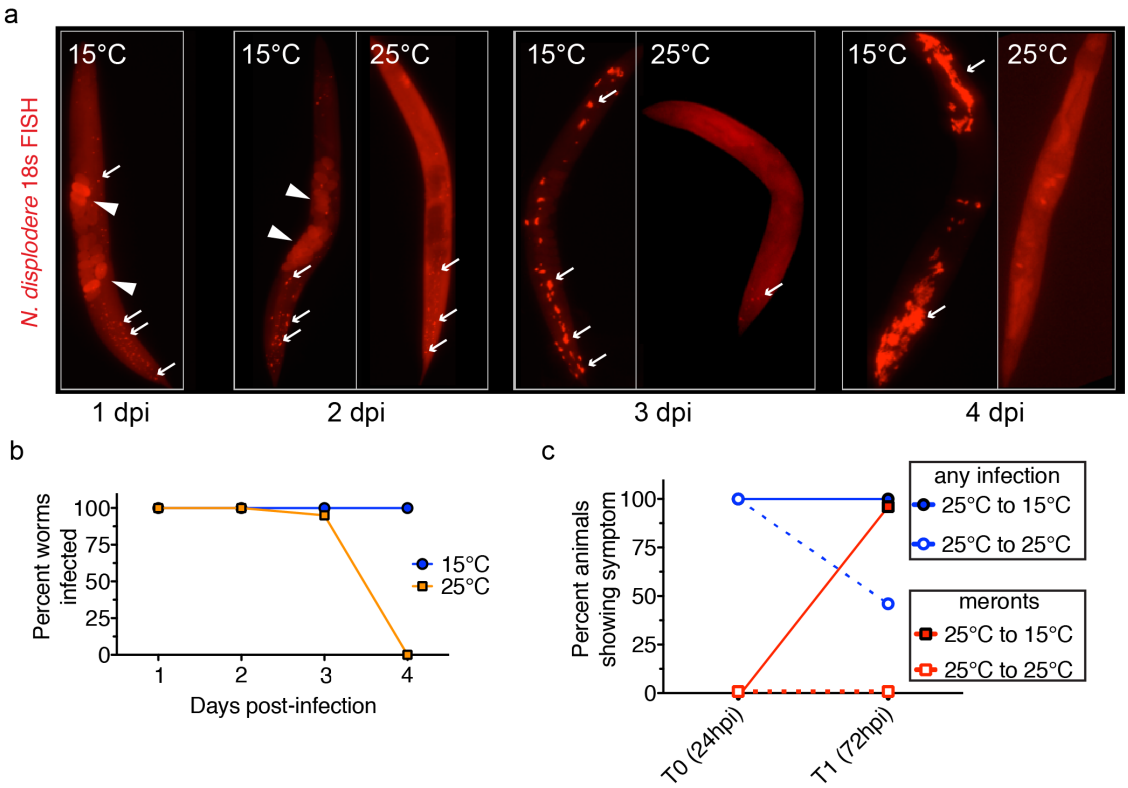

Figure 5-1 *N. displodere* proliferates at 15°C but fails to proliferate at 25°C
(a) Representative micrographs of N2 *C. elegans* infected with *N. displodere* at 15°C for 1 day (left, 1 dpi), then split to either 15°C or 25°C and monitored for three additional days of infection (2-4 dpi). Animals were stained by FISH to *N. displodere* rRNA. Arrows indicate *N. displodere* infection, while large arrowheads indicate *C. elegans* eggs. (b) Quantification of animals from (a) with 10 animals analyzed for any sign of infection (18s FISH signal) at each time point and temperature. (c) N2 *C. elegans* were infected at 25°C for 24 hours (T_0, 24 dpi), then split and placed at both 15°C and 25°C for an additional 48 hours (T_1, 72 dpi). Animals were fixed at both time points and analyzed for any signs of infection (blue lines) or for multinucleate meronts (red lines).

5.3.2 *N. displodere* meronts are cleared at higher temperatures

We next tested whether later stages of *N. displodere* infection could proliferate or were cleared at higher temperatures. N2 animals were infected with *N. displodere* at 15°C for 72 hours until all of the animals were at the meront stage, and then split to 15°C and 25°C. FISH staining of animals showed that meronts were present in animals infected at 15°C after 3 days which increased in size after an additional 48 hours at 15°C (Fig. 5-2a). However, these meronts were cleared after 48 hour incubation at 25°C (Fig. 5-2a). A quantification of these results showed that the total area of infection increased over time at 15°C, but decreased at 25°C (Fig. 5-2b).

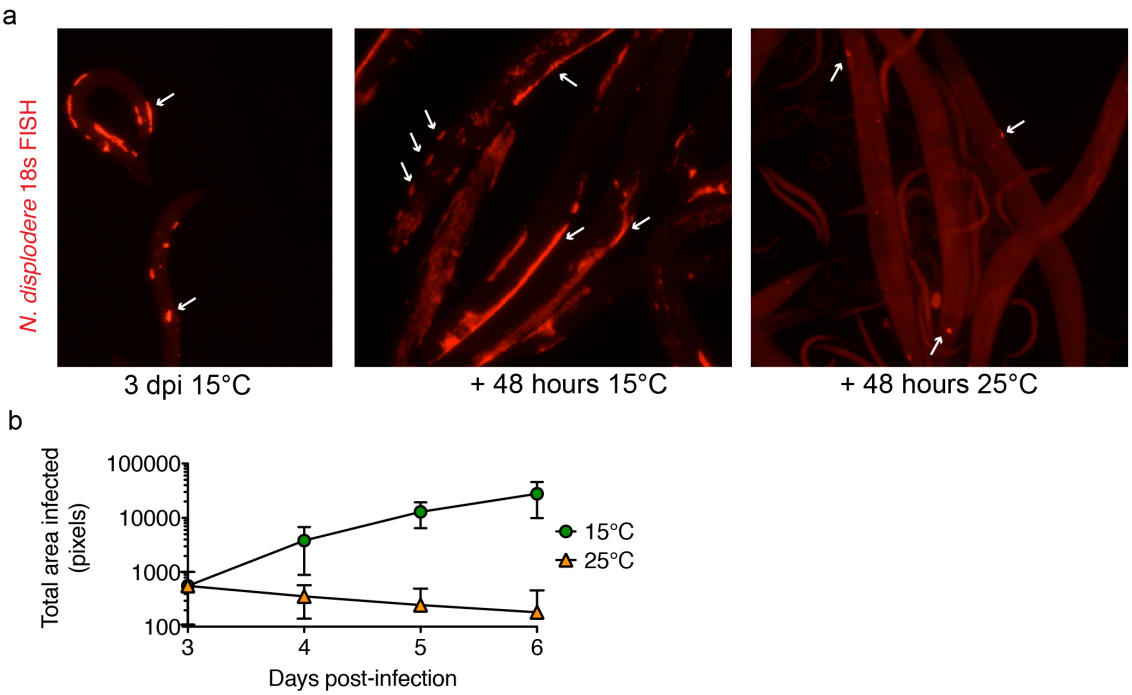

Figure 5-2 *N. displodere* meronts are cleared at 25°C
(a) Representative micrographs of N2 *C. elegans* infected with *N. displodere* at 25°C for 3 day with meronts (left, 3 dpi), then split to either 15°C or 25°C for an additional 48 hours of infection (middle and right, respectively). Animals were stained by FISH to *N. displodere* rRNA (indicated by arrows). (b) Quantification of infection area in a single plane by red fluorescence using ImageJ. Thirty animals were measured for total infection area over time after animals were split at 3 dpi with meronts at 15°C (T_0) to 15°C and 25°C and measured at 4, 5, and 6 dpi.

5.3.3 *N. displodere* displays a broad host range

Since *N. displodere* growth appears to be limited to lower temperatures (below 20°C), we wanted to know if there were other host species that could sustain *N. displodere* growth at higher temperatures. We tested *N. displodere* infection in 9 different species at 15°C, 20°C, and 25°C, including *Caenorhabditis angaria*, *C. brenneri*, *C. briggsae*, *C. japonica*, *C. sinica*, *C. remanei*, *C. tropicalis*, *Pristionchus pacificus* and *Panagrellus redivivus*. Animals were monitored for intracellular pathogen growth at 3 dpi as the percent animals containing meronts, and all nine species were able to sustain *N. displodere* replication at 15°C. This percentage dropped steeply at 20°C for all species, and absolutely no growth was seen in any species at 25°C (Fig 5-3a). This result indicates that *N. displodere* has a broad host range, but is limited a limited temperature tolerance. By contrast, other *Nematocida* species show a more limited host range when looking at proliferation to the spore stage, with *N. parisii*, *N.* sp. 1, and *N. ironsii* showing relatively limited growth in the hosts *C. elegans* and *C. briggsae*. Furthermore, *N. parisii* and *N.* sp. 1 have previously shown competence to complete their entire life cycles in *C. elegans* at 15°C, 20°C, and 25°C, indicating a broader temperature range than *N. displodere* (4-5, 8).

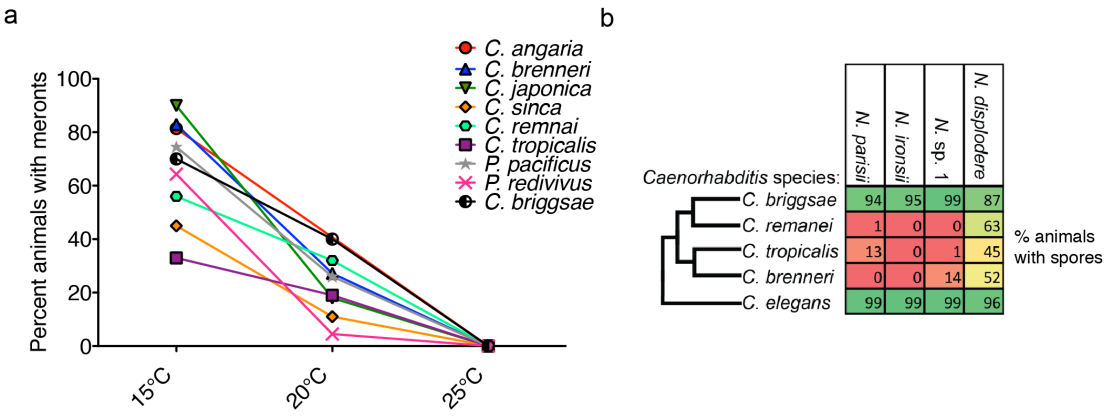

Figure 5-3 *N. displodere* growth is restricted to lower temperature in every host species tested.
(a) Multiple nematode species (seven *Caenorhabditis* species, *P. pacificus,* and *P. redivivus*) were infected with *N. displodere* at 15°C, 20°C, and 25°C. The percent of 100 animals (unless otherwise indicated, see Materials and Methods) with meronts as assessed by pathogen rRNA FISH were quantified at 3 dpi. (b) Five species of *Caenorhabditis* were infected with four species of *Nematocida* at the permissive temperature for the pathogen species and the percent animals with spores present was quantified by direct yellow 96 (DY96) staining of fixed animals. This data is courtesy of Aaron Reinke.

5.3.4 *N. displodere* infected animals show a minor cryophilic behavior phenotype

The limitation of *N. displodere* to only proliferate at lower temperatures in multiple species of nematodes suggests that *N. displodere* infection might affect *C. elegans* behavior towards different temperatures. For example, infection by *N. displodere* could provoke a 'fever' type response, whereby *C. elegans* might show a preference for higher temperature in order to help clear a pathogen (13). Conversely, *N. displodere* could affect *C. elegans* behavior with a preference for lower temperature to promote pathogen growth, as many parasite have been shown to co-opt host behavior for their own benefit (14-15). To test these two models, we tested whether *N. displodere* infection had an effect on *C. elegans* thermotaxis behavior to colder temperatures (15-19°C) versus warmer temperatures (20-24°C). Well-fed *C. elegans*

normally display thermotaxis to the temperature in which they were raised, i.e. 20°C-raised animals preferentially thermotax to 20°C and 15°C-raised animals preferentially thermotax to 15°C (16). Taking advantage of this behavior, we first infected L1 larvae raised for multiple generations at 20°C and tested the effect infection had on their behavior. While mock-infected animals showed a general preference for the warmer half of the plate (as expected), *N. displodere* infected animals showed a significantly higher cryophilic behavior (Fig. 5-4a). *N. parisii*-infected animals also showed a trend toward cryophilic behavior, although this trend was not significant. However, when this experiment was repeated with L3/L4 staged larvae under the same conditions, the effect was lost with animals under all conditions showing more non-cryophilic behavior (Fig. 5-4b). Similarly, we tested L3/L4 larvae that were raised for multiple generations at 15°C for cryophilic behavior. While mock-infected samples looked as expected (showing a more cryophilic behavior), both *N. displodere* and *N. parisii* infection had no significant effect on this behavior (Fig. 5-4c). Altogether, this result suggests that if *N. displodere* is causing *C. elegans* behavior to move to lower temperatures, it may only occur during early larval stages of development.

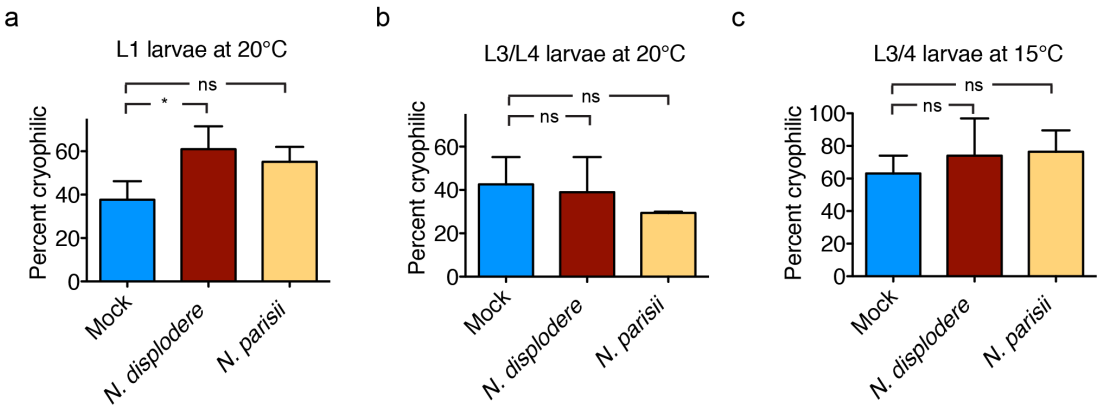

Figure 5-4 *N. diplodere* infection leads to a cryophilic thermotaxis by L1 larvae
(a) L1 larvae maintained at 20°C were mock, *N. diplodere*, or *N. parisii* infected for 24 hours and tested on radial thermotaxis plates at a population level. The percent animals displaying cryophilic taxis (crawling toward the cooler center of the plate) were quantified for each condition. (b) L3/L4 larvae maintained at 20°C were infected for 24 hours and tested as in (a). (c) L3/L4 larvae maintained at 15°C were infected for 24 hours and tested as in (a). Data are represented as the mean and SD for n=4 replicates across two independent experiments for (a) and (c), and n=2 replicates in one experiment for (b) (* p = 0.029, ns = not significant, two-tailed Mann Whitney test).

5.4 Discussion

Here, we further characterize a temperature-dependent phenotype seen by *N. displodere* infection in *C. elegans*, where *N. displodere* is consistently cleared from the host when incubated at higher temperatures. We found that *N. displodere* is incapable of growing at 25°C in ten different nematode species, despite showing the capacity for proliferative infection in all of these same species at 15°C. Interestingly, *N. displodere* is able to infect and invade *C. elegans* at 25°C, but proliferation of the pathogen does not occur unless the host is moved to a permissive temperature. We hypothesized that this limited temperature range for *N. displodere* might result in a behavioral change in host temperature preference and found a small effect on *C. elegans* thermotaxis behavior, such that early larval stages of the animal to prefer lower temperatures. This finding should be pursued further to see if *N. displodere* infection is capable of coopting host behavior to facilitate its own growth.

The limited capacity of *N. displodere* to grow at temperatures above 20°C and inability to grow at 25°C sets it apart from other species in the *Nematocida* genus (5, 8). In fact, an analysis of over 4800 fungal strains (the closest related group to microsporidia) showed that the vast majority could grow between 12-30°C regardless of whether they were from the soil or pathogens of plants or animals (9). As such, *N. displodere* might be classified as a psychrotroph, a term given to microorganisms unable to grow above 20°C (17). Given that the host *C. elegans*, is found in temperate regions of the globe and can be cultivated between 8-27°C (18-19), *N. displodere* might be limited in its global or seasonal distribution to cooler spatiotemporal points. This could be true for any host, as *N. displodere* shows the same temperature restriction in every species tested. However, it is important to note that only one isolate of *N.*

displodere has been found and studied (JUm2807), and this isolate could be anomalous compared to the species as a whole, which necessitates further sampling for other *N. displodere* isolates. Additionally, it is possible that this temperature phenotype of *N. displodere* is a laboratory-restricted phenomenon, perhaps due to interactions with OP50 *E. coli* bacteria used as a food source for the host or due to inauthentic incubation at a single continuous temperature (as temperatures would fluctuate widely in the wild). Further studies are needed to rule out some of these potential laboratory-induced phenomena.

To date, sampling of wild nematodes has found eight species of *Nematocida* microsporidia (4-5, 7, 20). Phylogenetic analysis of the 18s rDNA sequence of these species places *N. homosporus* as the closest sister species to *N. displodere*, which are likely the two earliest branching members of the genus. Interestingly, *N. homosporus* also displays a broader host range compared to other *Nematocida* species (*N. parisii*, *N.* sp. 1*,* and *N. major*), and it shares with *N. displodere* the phenotype of having only a single spore size after infection (hence the name *N. homosporus*) (7). This observation raises the possibility that *N. homosporus* might also display a lower limited temperature range similar to *N. displodere.* Most interestingly, although *N. displodere* and *N. homosporus* share certain phenotypes as sister species, they differ in their tissue tropism. *N. homosporus* infection is limited to the intestine in *C. elegans* while *N. displodere* infection occurs in many non-intestinal tissues, but is relatively poor in the intestine*.* Further analysis of these two species, including genome sequencing of *N. homosporus*, could shed light on host and pathogen mechanisms important growth in the intestine and other tissues.

5.5 Materials and methods

5.5.1 *N. displodere* infection at 15°C and 25°C.

Synchronized N2 L4 larvae were infected with a standard dose of *N. displodere* spores (3.5×10^4 spores per cm^2 of a plate) at 15°C for 30 hours. Animals were pooled at T_0 and split to 7 x 6 cm OP50 plates with 1 plate immediately harvested for FISH (T_0 at 1 day post infection, dpi), 3 plates placed at 15°C, and 3 at 25°C. At 24 hour intervals, 1 plate was harvested for FISH from each temperature, with T_1 at 2 dpi, T_2 at 3 dpi, and T_4 at 4 dpi. Animals were washed to new OP50 plates each day to remove L1 larvae. FISH was conducted as described previously (4), and 10 animals per condition were binned as infected or uninfected based on amount of infection seen.

5.5.2 *N. displodere* clearance at higher temperatures

Synchronized N2 L1 larvae were infected with a standard dose of *N. displodere* spores at 15°C for 72 hours until the meront stage. Animals were pooled at T_0 and split to 7 x 6 cm OP50 plates with 1 plate immediately harvested for FISH (T_0 at 4 dpi), 3 plates placed at 15°C, and 3 at 25°C. At 24 hour intervals, 1 plate was harvested for FISH from each temperature, with T_1 at 5 dpi, T_2 at 6 dpi, and T_4 at 7 dpi. FISH was conducted as described above, and 50 animals per condition were binned as infected or uninfected based on amount of infection seen. Additionally, 30 images per condition were taken on a Zeiss AxioImager M1 upright microscope and FISH infection was quantified as by total area of red using ImageJ (NIH).

5.5.3 *N. displodere* infection at higher temperatures

Synchronized N2 L4 larvae were infected with a standard dose of *N. displodere* spores (3.5×10^4 spores per cm^2 of a plate) at 25°C for 24 hours. Animals were pooled at T_0 and split to 3 x 6 cm OP50 plates with 1 plate immediately harvested for FISH (T_0 at 1 dpi), 1 plate placed at 15°C, and 1 at 25°C. After 48 hours, animals were harvested for FISH (72 hpi). FISH was conducted as described above, and 50 animals per condition were binned as infected or uninfected with sporoplasms, and binned as infected or uninfected with meronts.

5.5.4 Comparison of *N. displodere* infection in several nematode species

Mixed stages of *Caenorhabditis angaria* (PS1010), *C. brenneri* (PB2801), *C. briggsae* (AF16), *C. japonica* (DF5081), *C. sinica* (JU800), *C. remanei* (PB4641), *C. tropicalis* (JU1373), *Pristionchus pacificus* (PS312) and *Panagrellus redivivus* (MT8872) were grown on 10 cm OP50 plates at 15°C. All strains were obtained from the *Caenorhabditis* Genetics Center. Animals were split to 3 x 6 cm OP50 plates, infected with a standard dose of *N. displodere* spores, and incubated at 15°C, 20°C, or 25°C for 3 days. Animals were harvested and processed for FISH as above. Adult animals were analyzed on a Zeiss AxioImager M1 for meront infection, with at least 100 animals per condition analyzed unless otherwise noted (due to poor growth). These are 70 animals for *C. brenneri* at 15°C, 14 for *P. redivivus* at 15°C and 44 at 20°C, and 55 for *P. pacificus* at 15°C. There is no data point for *C. angaria* at 20°C because the animals failed to grow.

5.5.5 *Nematocida* host range for spore production

Synchronized L1 larvae after bleaching of *C. elegans*, *C. briggsae*, *C. remanei*, *C. tropicalis*, and *C. brenneri* were infected with $2.0x10^6$ spores per 6 cm plate at 20°C for 3 days all *Nematocida* species, except for *N. displodere* which was used at $1.0x10^6$ spores at 15°C for 6 days. Animals were fixed and stained for spores with DY96 as previously described (4). At least 100 animals per condition were analyzed for spores for analysis.

5.5.6 Thermotaxis assay

Populations of N2 *C. elegans* were maintained at 20°C by plating 3 x L3 larvae on fresh 6 cm OP50 plates or at 15°C by picking 3 x L4 larvae and removing the gravid adults 2 days later. For L1 larvae experiments the F_1 generation were infected with a standard dose of *N. displodere* or *N. parisii* on the same day gravid adults were removed, for L3/L4 larvae at 15°C experiments the F_1 generation were infected two days after P_0 removal, and for L3/L4 larvae at 20°C experiments the F_1 generation were infected one day after P_0 removal. Animals were infected for 24 hours, then washed off plates with 1 ml of 25 mM potassium phosphate buffer (pH 6.0), 0.3% NaCl and washed 3 times in 500 µl of the same buffer. Animals (100-200) were tested on radial thermotaxis plates as described previously (21). Briefly, fresh, sterile 9 cm plates of 2% agar-agar, 0.3% NaCl and 25 mM potassium phosphate buffer (pH 6.0) were pre-chilled with a vial of frozen glacial acetic acid (warmed at room temperature for 10 minutes) placed in the center of an upside-down plate for 15 minutes to create a radial temperature gradient from ~15°C at the center to room temperature (22-24°C) at the outer edges. Animals were placed at a marked point 1.5 cm from the edge of the plate and allowed to

thermotax for one hour. A continuous radial line is marked on the plate at 1.5 cm from the edge, and the number of animals are counted in the inner circle and outer circle, with animals that did not move from the origin excluded from the count. Percent cryophilic is measured as:

Number of inner circle animals / total number of animals.

5.6 Acknowledgements

The dissertation author was the primary investigator and author of the material in Chapter 5. Author contributions to the manuscript are as follows: Luallen, R contributed the research for Figures 5-1, 5-2, 5-3a, and 5-4. Thank you to Aaron Reinke for allowing use of his data in Figure 5-3b.

5.7 References

1. Weiss LM, Delbac F, Haymann JR, Pan G, Dang X, Zhou Z in *Microsporidia: Pathogens of Opportunity* (eds L. M. Weiss & J. J. Becnel) Ch. 10, 261-306 (Wiley-Blackwell, 2014).

2. Félix MA, Jovelin R, Ferrari C, Han S, Cho YR, Andersen EC, Cutter AD, Braendle C (2013) Species richness, distribution and genetic diversity of *Caenorhabditis* nematodes in a remote tropical rainforest. BMC Evol Biol 13: 10.

3. Félix MA, Duveau F (2012) Population dynamics and habitat sharing of natural populations of *Caenorhabditis elegans* and *C. briggsae*. BMC Biology 10: 59.

4. Luallen RJ, Reinke AW, Tong L, Botts MR, Felix M-A, Troemel, ER. (2016) Discovery of a Natural Microsporidian Pathogen with a Broad Tissue Tropism in *Caenorhabditis elegans*. PLoS Pathog 12: e1005724.

5. Troemel ER, Felix MA, Whiteman NK, Barriere A, Ausubel FM (2008) Microsporidia are natural intracellular parasites of the nematode *Caenorhabditis elegans*. PLoS Biol 6: 2736-2752.

6. Félix MA, Ashe A, Piffaretti J, Wu G, Nuez I, Belicard T, Jiang Y, Zhao G, Franz CJ, Goldstein LD, Sanroman M, Miska EA, Wang D (2011) Natural and experimental infection of *Caenorhabditis* nematodes by novel viruses related to nodaviruses. PLoS Biology 9: e1000586.

7. Zhang G, Sachse M, Prevost MC, Luallen RJ, Troemel ER, Félix MA, Microsporidian infection diversity and specificity among wild rhabditid nematodes (manuscript in preparation).

8. Balla KM, Luallen RJ, Bakowski MA, Troemel ER (2016) Cell-to-cell spread of microsporidia causes *C. elegans* organs to form syncytia, Nature Microbiology (*accepted*).

9. Robert V, Casadevall A (2009) Vertebrate Endothermy Restricts Most Fungi as Potential Pathogens. J Infectious Diseases 10: 1623-6.

10. Desjardins CA, Sanscrainte ND, Goldberg JM, Heiman D, Young S, Zeng Q, Madhani HD, Becnel JJ, Cuomo CA (2015) Contrasting host-pathogen interactions and genome evolution in two generalist and specialist microsporidian pathogens of mosquitoes. Nat Commun 6: 7121.

11. Maside X, Gómez-Moracho T, Jara L, Martín-Hernández R, De la Rúa P, Higes M, Bartolomé C. (2015) Population Genetics of *Nosema apis* and *Nosema ceranae*: One Host (*Apis mellifera*) and Two Different Histories. PLoS One 10:e0145609.

12. Panek J, El Alaoui H, Mone A, Urbach S, Demettre E, Texier C, Brun C, Zanzoni A, Peyretaillade E, Parisot N, Lerat E, Peyret P, Delbac F, Biron DG (2014) Hijacking of host cellular functions by an intracellular parasite, the microsporidian *Anncaliia algerae*. PLoS One 9:e100791.

13. Singh V, Aballay A (2006) Heat-shock transcription factor (HSF)-1 pathway required for *Caenorhabditis elegans* immunity. PNAS 103: 13092-7.

14. Webster JP (2007) The effect of Toxoplasma gondii on animal behavior: playing cat and mouse. Schizophr Bull 33: 752-6.

15. Hughes DP, Andersen SB, Hywel-Jones NL, Himaman W, Billen J, Boomsma JJ (2011) Behavioral mechanisms and morphological symptoms of zombie ants dying from fungal infection. BMC Ecology 11: 13–22.

16. Hedgecock EM, Russell RL (1975) Normal and mutant thermotaxis in the nematode *Caenorhabditis elegans*. PNAS 72: 4061-5.

17. Cavicchioli R. (20160) On the concept of a psychrophile. ISME J 10:793-5.

18. Félix MA, Braendle C (2010) The natural history of *Caenorhabditis elegans*. Curr Biol 20:R965-9

19. Frézal L, Félix MA. (2015) *C. elegans* outside the Petri dish. Elife 2015 Mar 30: 4.

20. Reinke AW, Balla KM, Bennett EJ, Troemel ER (2016) Identification of microsporidia host-exposed proteins reveals a repertoire of large paralogous gene families and rapidly evolving proteins. BioRXiv 056788; doi: http://dx.doi.org/10.1101/056788

21. Mori I, Ohshima Y (1995) Neural regulation of thermotaxis in Caenorhabditis elegans. Nature 376: 344-8.

6. Appendix

6.1 *C. elegans* growth in axenic media

C. elegans is regularly grown in the lab under monoxenic conditions (in the presence of a single organism), with a particular strain of *E. coli* being used as the sole food source. However, under some circumstances it is advantageous to grow the animals under axenic, or sterile, conditions. For example, in our lab, we used axenic media to make sterile spore preparations of *N. parisii* and conduct a preliminary test for a *C. elegans* transcriptional response to bacteria, bacterial lipopolysaccharide, and peptidoglycan. There are generally two means to grow *C. elegans* axenically, with a defined or an undefined media. Defined media uses exact concentrations of nucleotides, amino acids, minerals, and cofactors, as has been described previously (1). Undefined media uses bovine milk, yeast extract, and peptone to grow animals, where the exact concentrations of each constituent nutrient are unknown (2, 3). Both of these methods define the ingredients needed to grow *C. elegans* axenically, but it is still not trivial to make them work in the laboratory (Patrick Phillips and Emily Troemel, personal communications). We were successful at using undefined media to grow *C. elegans* in the lab, with the capacity to maintain animals in axenic media for several generations, although a large proportion of adults retained embryos and died of internal hatching.

To prepare undefined *C. elegans* axenic media (CAX), make sure to have ultrahigh sterilized skim milk (UHS). We used Organic Valley Fat Free Milk from Whole Foods Market, and prepared 15 ml aliquots stored at -80°C using sterile technique. Additionally, it is important to use soybean peptone; we used DifcoSelect Phytone (BD Biosciences #210931). Make a 50 mg/ml solution of hemoglobin (Sigma, #H3760) in 0.1 N KOH and autoclave at 121°C for 9 minutes. To make the CAX media, make the

base for the media by mixing 3% yeast extract (Fisher, #BP1422) and 3% soy peptone in dH_2O and autoclave at 125°C for 20 min. Store at 4°C for no more that 1 month. Right before adding *C. elegans*, mix in 0.5 mg/ml hemoglobin, 5 µg/ml cholesterol, and 20% non-fat milk to make the full CAX media.

To grow *C. elegans* in CAX media, chunk N2 worms from a starved plate to a 10 cm NGM plate with 1 ml superfood. Grow worms for 3-4 days at 20°C. Bleach the gravid adults under more stringent conditions by using 800 µl chlorox bleach and 200 µl 5M NaOH incubating for 3 min with monitoring to verify the majority adults have ruptured. Wash animals four times with 15 ml of M9 buffer and incubate the eggs overnight. Spin down the hatched L1s and add 5 ml fresh M9 to remove any starvation pheromones. Count the L1s and plate ~3000 L1s to 10 ml of freshly prepared CAX media in a 10 cm plate. Make sure the CAX media depth is no more than 2 mm, and grow the animals at 15°C, 20°C, or 25°C without shaking.

6.2 Making polyclonal antibodies to *N. parisii* spores

Microsporidian spores express a distinct set of proteins on their external surface to protect them from environmental insults and desiccation (4). As a means to distinctly visualize the different pathogen stages that express these proteins in *C. elegans*, we made an antibody to *N. parisii* spores (ERTm1). A preparation of spores (lot #2, 1.65 x 10^9 spores total) was incubated with 50 µg/ml Gentamicin for 30 minutes, purified under a 50% Percoll gradient, and washed extensively in sterile H_2O. Spores were fixed in PBS containing 4% paraformaldehyde, 0.1% glutaraldehyde for 20 min, and washed with PBS. Then spores were lysed by boiling for 15 min and flash frozen in liquid N_2 for a total of ten cycles. This antigen was resuspended into 4.2 ml PBS for a

total of four injections in two rabbits (final concentration of spores was 2.0 x 10^8 spores/injection). Antibody production and protein A purification was conducted by ProSci Inc.

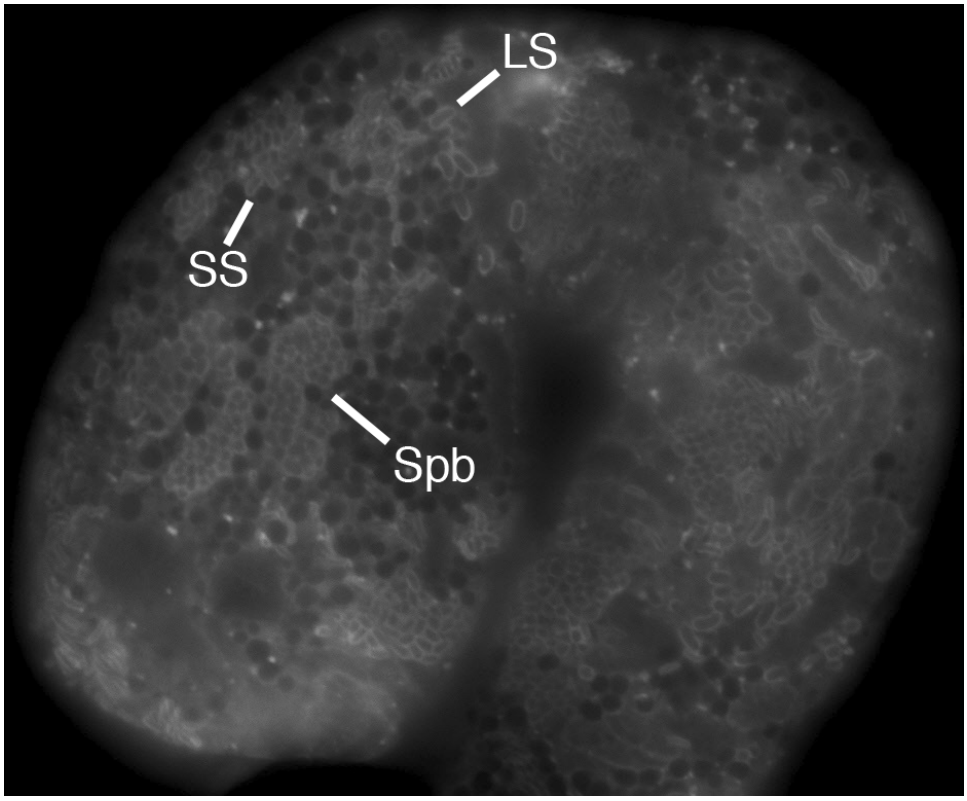

Figure 6-1. Confocal image of *N. parisii*-infected *C. elegans* intestine stained with anti-*Np* spore antibody.
Dissected *C. elegans* intestine stained by anti-*Np* spore antibody and anti-rabbit-Cy3. Numerous internal stages of *N. parisii* infection are seen, including large spores (LS), small spores (SS), and sporoblasts (Sbp).

We verified the specificity of the protein A-purified anti-*N. parisii* (*Np*) spores by immunohistochemistry of infected *C. elegans* intestines. Mixed staged N2 infected with *N. parisii* for 2 days at 25°C were decapitated on a glass dish (at least 50 animals) and fixed in 4% paraformaldehyde in M9 + 0.1% Tween-20 for 2 hours. Samples were blocked overnight in 1 ml block buffer (PBS, 0.5% Triton X-100, 1 mM EDTA, 5% BSA,

and 0.05% NaN_3) at 4°C. Samples were incubated with 10 μg/ml of anti-*Np* spores in 1 ml of block buffer at room temperature and washed with PBS + 0.1% Tween-20. Samples were incubated in 2 μg/ml goat anti-rabbit-Cy3 in 1 ml block buffer for 1 hour at room temperature. Samples were washed as before and mounted with Vectasheild + DAPI and visualized on a Zeiss LSM700 confocal microscope with a 40x objective (Fig 6-1).

6.3 Pulldown of RAB-11 associates proteins after *N. parisii* infection

Suzy Szumowski in the lab has shown that the *C. elegans* endocytic recycling pathway is required for *N. parisii* spore exit via exocytosis, with the small GTPase *rab-11.1* being required for this exit (5). She showed that RAB-11 protein colocalized with newly-formed spores near the apical plasma membrane of infected intestines (5). In order to identify new host and pathogen factors that might be important for *N. parisii* trafficking to and exit from the apical surface of intestinal cells, we conducted co-immunoprecipitation (IP) pulldowns of tagged *rab-11.1* in infected and uninfected transgenic *C. elegans* strains. We have made two transgenic lines expressing *rab-11* with a N-terminal StrepII-3xFlag tag, downstream from one of two intestinal-specific promoters (ERT411 *jySi21[spp-5p::rab-11; cb-unc-119(+)] II* and ERT410 *jySi21[vha-6p::rab-11; cb-unc-119(+)] II*). As controls, we created two additional lines expressing a similarly tagged GFP under control of the same promoters (ERT413 *jySi21[spp-5p::GFP; cb-unc-119(+)] II* and ERT412 *jySi21[vha-6p::GFP; cb-unc-119(+)] II*), as described previously (6). All of these lines are inserted into the same genomic locus on Chr. II using Mos-mediated single copy insertion (MosSCI). Immunohistochemistry of dissected intestines using anti-Flag shows Flag-tagged RAB-11 colocalizes with spores

near the apical membrane, and this signal can also be knocked-down with *rab-11.1* RNAi (Fig. 6.2). This suggests that the tagged RAB-11 shows similar localization as

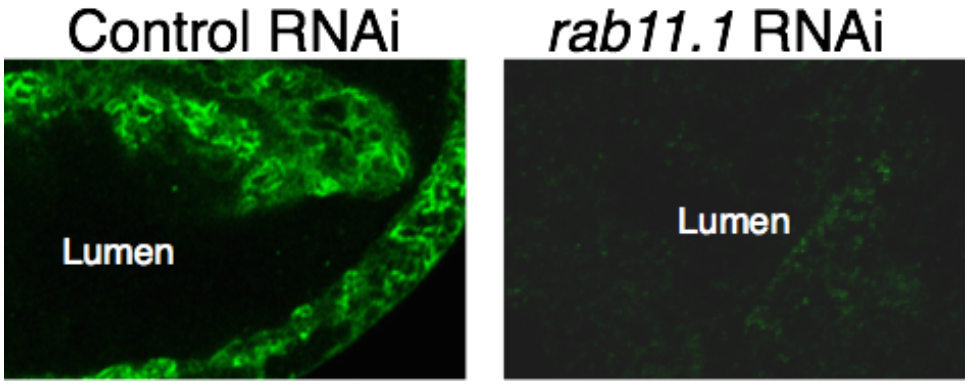

Figure 6-2. Flag-RAB-11 colocalizes with *N. parisii* spores.
Immunohistochemisty of dissected intestines of the transgenic line ERT411 *spp-5p::StrepII::3xFlag::rab-11.* Flag-RAB-11 colocalizes with spores at the apical side of the intestine near the lumen (left) and this signal is lost on *rab-11.1* RNAi (right). Staining was conducted with anti-Flag and anti-mouse-FITC.

physiologically-relevant protein interactions in infected and uninfected *C. elegans* intestines. To identify these proteins, we conducted the following co-IP pulldown protocol with strains ERT411 and ERT413:

1. Chunk worms strains onto 4 x 10 cm OP50 plates with 1ml superfood. Grow 25°C, 3 d.
2. Bleach strains in 15 ml tubes at 2 plates per tube. Grow ON at RT in 5 ml M9.
3. Combine similar L1 strains and count the number of L1s in 5 ul.
4. Add 20,000 L1s per 10 cm plate onto 12x 10 cm plates per strain. Dry in hood. Incubate 20°C for 24 hrs.
5. Infect 5 plates of each strain with 2.4 x 10^7 spores per plate in 2 ml superfood. Mock infect 6 plates of each strain with M9. Dry in hood.
6. Infect at 25°C for 44 hrs. Add 1.5 ml more super food after 24 hrs so worms don't starve.
7. Harvest worms w/ 5 ml M9. Let settle on ice for 5 min. Combine 5x plates from similar conditions.
8. Wash worms 2x with 50 ml ice-cold M9. Let settle on ice.
9. Transfer to 1.5 ml tubes and spin to remove all but ~100 ul of liquid. (Total 400 ul worms + 100 ul M9)
10. Freeze in 50 ml conical tubes containing ~25 ml liquid N2 as below:

a. Get liquid N2 in fewer and prepare 50 ml conicals on a styrofoam rack.
b. Add 25 ml liquid N2 to each tube by pouring.
    i. c. Add 1 ml fresh lysis buffer (50 mM HEPES, pH7.4, 1mM EGTA, 1mM MgCl2, 100 mM KCl, 1% glycerol, 0.05% NP40, 0.5mM DTT, 1x protease inhibitor from tablet, 1 mM additional PMSF) to the worms and then add worms dropwise to 50 ml tubes.
c. Put in -80°C w/ caps un-tightened. Wait 1 hr for N2 to evaporate and tighten the caps.

11. Test infected strains for localization of RAB-11.
12. Prepare worm extract as below:
    a. Pre-chill mortar, pestle, and spatulas with liquid N2 for 5 min. (fill 1/3 full).
    b. Pour worm pellets into mortar and tap lightly to break to pellet size.
    c. Grind 100x with increasing force.
    d. Add liquid N2 and wait to evaporate.
    e. Repeat 100 x grinding 2 more times, adding liquid N2 in between.
    f. Scrape pestle with spatula then scrape lysate into 50 ml conical.
    g. Add lysis buffer to 1.5 ml and spin 20,000g 10 min, 4°C. Save 20 ul for analysis.
13. Conduct IP as below (immediately after lysis):
    a. Aliquot 4 x 50 ul of anti-flag gel suspension (25 ul gel per sample) - total 200 ul suspension.
    b. Centrifuge 8000g, 30 sec. Remove the supernatant.
    c. Wash pellet 2x with 1 ml wash buffer (50 mM HEPES, pH7.4, 1mM MgCl2, 100 mM KCl)
    d. Pre-elute with 1ml of 100 mM glycine pH 3.5. Discard the supernatant.
    e. Wash pellet 3 x 1 ml lysis buffer. Split beads into 4 x 50 ul (total 100 ul slurry).
    f. Mix beads with 1 ml worm lysate from step 12g. Incubate 1 hr at 4°C with rotation.
    g. Wash beads with 2 x 1 ml lysis buffer.
    h. Wash beads 2 x 5min with 1 ml lysis buffer in the cold room.
    i. Wash beads 3 x 1ml wash buffer. Store at -30°C for mass spec.
    j. Elute 2.5 ul of each pulldown with 10 ul of 2xSDS sample buffer without DTT for SDS_PAGE. Boil 3 min.
    k. Add 1.1 ul of 1M DTT to each and load onto a gel.

After SDS-PAGE of a small fraction of the proteins on the anti-Flag beads, the gel was stained with Oriole gel stain for 90 minutes and destained in water for 1 hour. The bait proteins RAB-11 and GFP can be seen in both the infected and uninfected

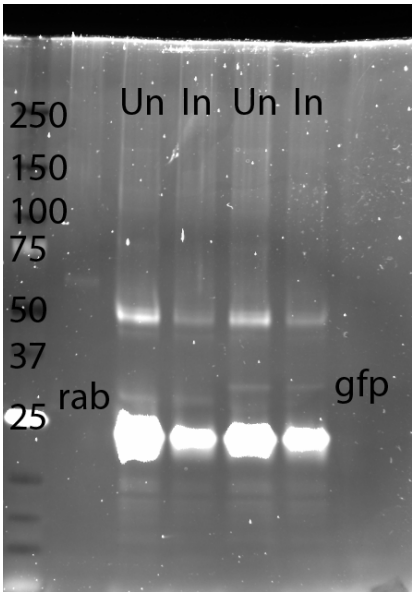

Figure 6-3. SDS-PAGE of Flag-RAB-11 pulldowns.
RAB-11 (left lanes) and GFP protein (right lanes) detected after anti-FLAG pulldowns of ERT413 and ERT411 lysate of uninfected (un) and infected (in) samples. SDS-PAGE gel was stained with Oriole gel stain. Protein markers are shown in the leftmost lane with sizes in kilodaltons.

samples (Figure 6-3). The RAB-11 and control pulldown samples on anti-Flag beads were trypsin digested and analyzed by mass spectrometry by the UCSD Biomolecular/Proteomics Mass Spectrometry Facility. First, we annotated the RAB-11 pulldown sample lists (ERT411) by removing all proteins found in both infected and uninfected GFP samples (ERT413), as these would be considered background binding. After this, a total of 61 *C. elegans* proteins were found to have least 1 significant peptide hit in uninfected ERT411 (rab-11::Flag) animals (Table 6-1) and 12 *C. elegans* proteins were found in *N. parisii* infected ERT413 (Table 6-2). This includes the bait protein RAB-11.1. Among these uninfected/infected datasets, there were 9 proteins common to both sets, giving 52 unique proteins found in uninfected conditions and 3 unique protein in infected conditions. This stark difference in total proteins between uninfected and infected conditions is reflected in the number of peptide hits found

Table 6-1 Mass spectrometry hits of putative RAB-11 interactors in uninfected conditions.

Accession	Name	Species	Peptides (95%)	Overlap infected
gil156400	myosin heavy chain	*C. elegans*	315	No
gil25150354	Non-muscle MYosin family member (nmy-1)	*C. elegans*	98	No
gil71983975	Non-muscle MYosin family member (nmy-2)	*C. elegans*	60	No
gil6624	actin	*C. elegans*	112	Yes
gil6799	myosin heavy chain 3	*C. elegans*	48	No
gil6786	myosin 1	*C. elegans*	50	No
gil55584154	RecName: Full=Myosin-2; AltName: Full=Myosin heavy chain C	*C. elegans*	56	No
gil71992941	LEVamisole resistant family member (lev-11)	*C. elegans*	47	Yes
gil405831	rabGDI	*C. elegans*	36	No
gil72000718	hypothetical protein T25F10.6	*C. elegans*	47	No
gil17561652	MYOsin heavy chain structural genes family member (myo-5)	*C. elegans*	38	No
gil485116	Myosin light chain protein 3, isoform a	*C. elegans*	29	Yes
gil3024760	RecName: Full=Troponin T	*C. elegans*	24	No
gil71983406	UNCoordinated family member (unc-87)	*C. elegans*	22	No
gil2088715	Rab family protein 11.1	*C. elegans*	27	Yes
gil17569077	Myosin Light Chain family member (mlc-2)	*C. elegans*	19	No
gil7503999	hypothetical protein F53A9.10 - Caenorhabditis elegans	*C. elegans*	24	No
gil21431922	RecName: Full=Uncharacterized protein C53C9.2	*C. elegans*	11	No
gil89179497	Uncoordinated protein 27	*C. elegans*	12	No
gil3878776	C. elegans protein R01H10.3a, confirmed by transcript evidence	*C. elegans*	8	No
gil5541648	troponin C	*C. elegans*	9	No
gil71992969	LEVamisole resistant family member (lev-11)	*C. elegans*	22	No
gil17554322	Myosin Light Chain family member (mlc-4)	*C. elegans*	6	No
gil3879795	C. elegans protein T12D8.6, confirmed by transcript evidence	*C. elegans*	7	No
gil3880219	C. elegans protein T25C8.2, confirmed by transcript evidence	*C. elegans*	41	No
gil71988317	hypothetical protein K08E3.10	*C. elegans*	6	No
gil71995565	Rab Escort Protein homolog family member (rep-1)	*C. elegans*	4	Yes
gil74955935	RecName: Full=Tropomodulin	*C. elegans*	4	No
gil17509391	UNCoordinated family member (unc-15)	*C. elegans*	6	No
gil193208140	KETtiN (Drosophila actin-binding) homolog family member (ketn-1)	*C. elegans*	4	No
gil59798922	RecName: Full=Troponin I 1; Short=CeTNI-1; Short=TnI 1	*C. elegans*	4	No
gil3879474	C. elegans protein T04C12.5, confirmed by transcript evidence	*C. elegans*	109	No
gil7496020	hypothetical protein C14F5.3	*C. elegans*	3	No
gil59798921	RecName: Full=Troponin I 4; Short=CeTNI-4; Short=TnI 4	*C. elegans*	3	No
gil9755517	Histone protein 22	*C. elegans*	2	Yes
gil9755509	Histone protein 21	*C. elegans*	2	No
gil133904197	hypothetical protein F40F8.5	*C. elegans*	2	No
gil6688	capping protein alpha subunit	*C. elegans*	2	No
gil414640	myosin IA	*C. elegans*	2	No
gil9755510	Histone protein 18	*C. elegans*	2	No
gil17569207	Elongation FacTor family member (eft-4)	*C. elegans*	2	Yes
gil74963152	RecName: Full=Heat shock protein 90; AltName	*C. elegans*	1	No
gil71992964	LEVamisole resistant family member (lev-11)	*C. elegans*	45	No
gil71993109	hypothetical protein K04C1.4	*C. elegans*	1	No
gil71983779	DIsorganized Muscle family member (dim-1)	*C. elegans*	1	No
gil71982026	TuBulin, Alpha family member (tba-2)	*C. elegans*	1	No
gil3873972	C. elegans protein C04F12.4, confirmed by transcript evidence	*C. elegans*	1	No
gil3924793	C. elegans protein K01G5.7, confirmed by transcript evidence	*C. elegans*	2	No
gil46576384	RecName: Full=Intermediate filament protein ifb-1	*C. elegans*	1	No
gil17558264	GRound-Like (grd related) family member (grl-10)	*C. elegans*	1	No
gil3878255	C. elegans protein K06A4.3, confirmed by transcript evidence	*C. elegans*	1	No
gil156482	polyubiquitin	*C. elegans*	2	No
gil7507340	hypothetical protein T07A9.11 - Caenorhabditis elegans	*C. elegans*	1	No
gil3877650	C. elegans protein F56A8.6, confirmed by transcript evidence	*C. elegans*	1	Yes
gil3876374	C. elegans protein F28D1.7, confirmed by transcript evidence	*C. elegans*	1	No
gil17539540	hypothetical protein D2096.8	*C. elegans*	1	No
gil59798977	RecName: Full=Troponin I 3; Short=CeTNI-3; Short=TnI 3	*C. elegans*	2	No
gil71991097	VITellogenin structural genes (yolk protein genes) member (vit-6)	*C. elegans*	1	No
gil3150491	Hypothetical protein F56C3.3	*C. elegans*	1	No
gil3879244	C. elegans protein T01C3.7, confirmed by transcript evidence	*C. elegans*	1	Yes

Table 6-2 Mass spectrometry hits of putative RAB-11 interactors after infection with *N. parisii*.

Accession	Name	Species	Peptides (95%)	Overlap uninfected
gil405831	rabGDI	*C. elegans*	43	Yes
gil2088715	Rab family protein 11.1	*C. elegans*	32	Yes
gil71995565	Rab Escort Protein homolog family member (rep-1)	*C. elegans*	9	Yes
gil829164	actin	*C. elegans*	5	Yes
NEPG_01228T0 l	NEPG_01228 l Nematocida parisii ERTm1 actin	*N. parisii*	2	No
gil3877650	C. elegans protein F56A8.6, confirmed by transcript evidence	*C. elegans*	2	Yes
gil485116	Myosin light chain protein 3, isoform a	*C. elegans*	2	Yes
gil17569207	Elongation FacTor family member (eft-4)	*C. elegans*	2	Yes
gil71984942	Myosin Light Chain family member (mlc-1)	*C. elegans*	1	No
gil3879244	C. elegans protein T01C3.7, confirmed by transcript evidence	*C. elegans*	1	Yes
gil482806	14-3-3 protein	*C. elegans*	1	No
gil9755517	Histone protein 22	*C. elegans*	1	Yes
gil71994052	hypothetical protein Y37E3.17	*C. elegans*	1	No

in each of the conditions, as uninfected conditions yielded far more significant peptide hits than infected. This could be due to the extended infection time (44 hours at 25°C) by *N. parisii* depleting a large amount of host resources and space relative to uninfected (see Fig. 4-1 above). An interesting finding, however, is that although *C. elegans* actin was a hit in both infected and uninfected conditions, unique peptides to ACT-5 were pulled down in the uninfected conditions, but were absent after infection. Unique peptides to the other actin isoforms were found in both infected and uninfected samples. This fits with prior descriptions of ACT-5 protein being redirected from the apical to the basolateral side of the intestine after *N. parisii* infection to promote gaps in the apical terminal web (7). Intriguingly, unique peptides to *N. parisii* actin (the only parasite protein found in the dataset) were pulled down with RAB-11 in infected animals but were absent in uninfected. This data could support further investigations to a role for *N. parisii* actin playing a positive role in RAB-11 localization to spores or infection progression, perhaps by displacing ACT-5 at the apical side of the intestine.

6.4 References

1. Szewczyk NJ, Kozak E, Conley CA (2003) Chemically defined medium and *Caenorhabditis elegans.* BMC Biotech 3:19.

2. Brock TJ, Browse J, Watts JL (2006) Genetic Upregulation of Unsaturated Fatty Acid Composition in *C. elegans*. PLoS Genetics 2: e108.

3. Houthoofd K, Braeckman BP, Lenaerts I, Brys K, De Vreese A, Van Eygen S, Vanfleteren JR (2002) Axenic growth up-regulates mass-specific metabolic rate, stress resistance, and extends life span in *Caenorhabditis elegans.* Exper Gerontol 37: 1369-76.

4. Weiss LM, Delbac F, Haymann JR, Pan G, Dang X, Zhou Z in *Microsporidia: Pathogens of Opportunity* (eds L. M. Weiss & J. J. Becnel) Ch. 10, 261-306 (Wiley-Blackwell, 2014).

5. Szumowski SC, Botts MR, Popovich JJ, Smelkinson MG, Troemel ER (2014) The small GTPase RAB-11 directs polarized exocytosis of the intracellular pathogen *N. parisii* for fecal-oral transmission from *C. elegans*. Proc Natl Acad Sci U S A 10.1073/pnas.1400696111.

6. Luallen RJ, Reinke AW, Tong L, Botts MR, Felix M-A, Troemel, ER. (2016) Discovery of a Natural Microsporidian Pathogen with a Broad Tissue Tropism in *Caenorhabditis elegans*. PLoS Pathog 12: e1005724.

7. Estes KA, Szumowski SC, Troemel ER (2011) Non-lytic, actin-based exit of intracellular parasites from *C. elegans* intestinal cells. PLoS Pathog 7: e1002227.